University of Alberta

Study of Magnesium effect on Lead induced Stress Corrosion Cracking (PbSCC) of UNS N08800 (Alloy 800)

by

Anandakumaran Palani

©

A thesis submitted to the Faculty of Graduate Studies and Research
in partial fulfillment of the requirements for the degree of

Master of Science

in

Chemical Engineering

Department of Chemical and Materials Engineering

Edmonton, Alberta
Fall 2008

Library and Archives Canada

Published Heritage Branch

395 Wellington Street
Ottawa ON K1A 0N4
Canada

Bibliothèque et Archives Canada

Direction du Patrimoine de l'édition

395, rue Wellington
Ottawa ON K1A 0N4
Canada

Your file Votre référence
ISBN: 978-0-494-47384-9
Our file Notre référence
ISBN: 978-0-494-47384-9

NOTICE:
The author has granted a non-exclusive license allowing Library and Archives Canada to reproduce, publish, archive, preserve, conserve, communicate to the public by telecommunication or on the Internet, loan, distribute and sell theses worldwide, for commercial or non-commercial purposes, in microform, paper, electronic and/or any other formats.

The author retains copyright ownership and moral rights in this thesis. Neither the thesis nor substantial extracts from it may be printed or otherwise reproduced without the author's permission.

AVIS:
L'auteur a accordé une licence non exclusive permettant à la Bibliothèque et Archives Canada de reproduire, publier, archiver, sauvegarder, conserver, transmettre au public par télécommunication ou par l'Internet, prêter, distribuer et vendre des thèses partout dans le monde, à des fins commerciales ou autres, sur support microforme, papier, électronique et/ou autres formats.

L'auteur conserve la propriété du droit d'auteur et des droits moraux qui protège cette thèse. Ni la thèse ni des extraits substantiels de celle-ci ne doivent être imprimés ou autrement reproduits sans son autorisation.

In compliance with the Canadian Privacy Act some supporting forms may have been removed from this thesis.

While these forms may be included in the document page count, their removal does not represent any loss of content from the thesis.

Conformément à la loi canadienne sur la protection de la vie privée, quelques formulaires secondaires ont été enlevés de cette thèse.

Bien que ces formulaires aient inclus dans la pagination, il n'y aura aucun contenu manquant.

Canada

ABSTRACT

The effect of magnesium on lead induced stress corrosion cracking (PbSCC) of UNS N08800 was studied in neutral crevice at 300°C. Lead reduces ultimate tensile stress (UTS), elongation and reduction area (RA) of UNS N08800, whereas magnesium increases the UTS, elongation and RA. Fracture morphologies were studied using SEM. In order to understand the process of PbSCC, experiment was conducted using different Mg/Ca ratio solutions at room temperature and in different magnesium concentration solutions at 300°C. Polarization experiments using UNS N08800 at room temperature and at 300°C indicate that anodic peak and passive current density increase in lead containing solution whereas they decrease in magnesium containing solutions. The repassivation behavior of passive films on UNS N08800 has been studied using scratch technique and it is significantly reduced when lead is present in the solution whereas magnesium increases repassivation. Pure Cr and Ni repassivation behavior is not affected by lead in alkaline condition, but Fe repassivation is affected by lead. Electronic properties of passive films studied at room temperature indicate that donor densities increase on addition of PbO whereas an increase in Mg/Ca ratio decreases donor density. At high temperatures the addition of magnesium decreases donor density. XRD analysis was carried out to study the spinel oxide formation in passive film.

Key words: UNS N08800, Repassivation, donor density, SEM, lead, XRD, SSRT

Acknowledgements

I am indebted to Prof. Jingli Luo for her trust, support, excellent guidance and encouragement throughout my course of this study.

I would like acknowledge Dr. Baotong Lu and Dr. Lianpeng Tian for their helpful suggestions and discussions during the course of my research.

This work would not have been possible without the financial support of the Natural Sciences and Engineering Research Council and Atomic Energy of Canada Limited.

Table of contents

Chapter 1– INTRODUCTION 1

Chapter 2– LITERATURE REVIEW 4

2.1 Introduction 4

2.2 Stress corrosion cracking 5

2.3 Mechanisms of SCC 6

2.3.1 Film rupture model 7

2.3.2 Hydrogen embrittlement model 8

2.4 Thermodynamic framework of PbSCC 8

2.5 Sources of lead 10

2.6 PbSCC 11

2.6.1 Potential and pH 11

2.6.2 Lead concentration 12

2.6.3 Alloy composition and structure 13

2.6.4 Temperature 15

2.6.5 Stress 16

2.7 Mechanism of PbSCC 16

2.8 Passivity of metals 18

2.9 Growth of passive film 21

2.9.1 Place exchange model 21

2.9.2 High field ion conduction model 22

2.9.3 Point defect model 25

2.9.4 Double layer model for Ni-Cr-Fe alloy 26

2.10 Overview of passive film on Ni-Cr-Fe alloy 28

2.10.1 Thermodynamic framework for passive film formation 28

2.10.2 Composition of the passive film 29

2.11 Environmental effect on film growth 29

2.11.1 Potential 29
2.11.2 Solution composition 30
2.11.3 Temperature 30
2.12 Effect of lead on electrochemical behavior of UNS N08800 30
2.13 Effect of lead on passive film 33
2.14 Effect of lead on repassivation 37
2.15 Summary 39
Chapter 3- EXPERIMENTAL PROCEDURE 40
3.1 Test materials 40
3.2 Solution composition 40
3.3 Sample preparation 42
3.3.1 Specimen for room temperature measurements 42
3.3.2 Specimen for high temperature measurements 43
3.4 Experimental procedure 44
3.4.1 Electrochemical experiments 44
3.4.2 Scratch test 46
3.4.3 Slow strain rate test (SSRT) 47
3.4.4 Mott-Schottky test 48
3.4.5 X-ray diffraction (XRD) 49
Chapter 4- RESULTS AND DISCUSSION 50
4.1 Effect of magnesium on PbSCC of UNS N08800 50
4.1.1 SSRT test results 50
4.1.2 Side view and fractographic observation 52
4.2 Effect of Mg/Ca ratio and magnesium on lead induced corrosion of UNS N08800 60
4.2.1 Polarization behavior of UNS N08800 61
4.2.1.1 Effect of magnesium and calcium ratio on the polarization behavior .. 61

4.2.1.2 Effect of magnesium on polarization behavior at 300°C 63
4.2.2 Effect of magnesium to calcium ratio on semi conducting properties of passive film 67
4.2.3 Effect of magnesium on semi conducting properties of the passive films formed at 300°C 71
4.2.4 Repassivation kinetics 74
4.2.4.1 Repassivation behavior in acidic crevice chemistries 75
4.2.4.2 Repassivation behavior in alkaline crevice chemistries 78
4.2.4.3 Repassivation time 80
4.3 Transient dissolution of Fe, Cr and Ni at active dissolution potential 81
4.4 Effect of passivation potential on lead induced degradation of film rupture ductility 86
4.5 Morphology of oxide film 90
4.6 XRD analysis 93
Chapter 5- CONCLUSIONS AND FUTURE WORK 99
5.1 Conclusions 99
5.2 Future work 101
References 102

List of figures

Figure 1-1 Total electricity generation in Canada (584.4 TWh), 2006 with break down of contributions from individual source (Data from canelect) 1

Figure 1-2 Lead concentration in sludge samples from steam generators at BNGS A. (Reproduced from King et al.) 2

Figure 2-1 Schematic diagram of parameter's interactions to cause SCC 5

Figure 2-2 Schematic diagram of crack growth (Jones et al.) 6

Figure 2-3 Schematic representation of crack propagation by the film-rupture model. (a) Crack tip stays bare. (b) Crack tip passivates and is ruptured repeatedly (reproduced from Jones et al.) 8

Figure 2-4 Potential as a function of pH for Ni (solid lines) and Pb (dotted lines) at 300°C. (Reprinted from Staehle 2003) 9

Figure 2-5 Ratio of concentration of species in deposits from 340 failed SG tubes (Cattant et al.) 10

Figure 2-6 Depth penetration determined metallographically and polarization current density for UNS N08800 and UNS N06690 TT exposed to 1 M NaOH at 300°C (Reproduced from Kilian et al.) 12

Figure 2-7 Concentration ratio of Cr vs. Fe for Ni-Cr-Fe alloys tested in pure water at 316°C with 10 g of Pb powder added to the autoclave and specimens stressed as single U-bends and tested for 8 weeks. (Reproduced from Staehle 2005) 15

Figure 2-8 Crack growth rate vs. 1000/T for water and water +PbO determined by CERT at 10^{-7} s^{-1} (Reproduced from Staehle 2003) 16

Figure 2-9 Schematic Evans diagram of passivation. (a) Thick film passivation. (b) Thin film passivation (Reproduced from Kelly et al.) 20

Figure 2-10 Schematic diagram of place exchange model (Reproduced from Sato et al. 1964) 22

Figure 2-11 Schematic process of high field ion conduction model passive film growth. (a) Passive film growth layer by layer. (b) Simultaneous hydroxide layer and oxide layer growth (Reproduced from Marcus et al. 2001) 24

Figure 2-12 Schematic of physico- chemical processes that occur within a passive film according to point defect model (Reproduced from Macdonald 1992) 25

Figure 2-13 Model for the mechanism of the formation of the passive film on Ni-Cr-Fe alloys (Reproduced from Machet 2004) 27
Figure 2-14 (a) Polarization diagram of UNS N08800 SG tube in neutral crevice chemistry. (b) Specimen treated for 24 h near active peak without PbO. (c) Specimen treated near active peak in PbO solution for 24 h (Reproduced from Staehle 2005, courtesy Lu 2005) 32
Figure 2-15 The effect of Pb on passive film composition of UNS N06600 at different pH's (Reproduced from Hwang et al. 1997) 34
Figure 2-16 Concentration depth profile of Pb in surface layer of sample passivated at 40 OC in SG alkaline crevice chemistry containing 2.2 mM PbO (Reproduced from Lu et al. 2007) 35
Figure 2-17 Profile of Ni_{OH}^{2+} in passive film formed on UNS N06690 at 40°C (Reproduced from Lu et al. 2007) 36
Figure 2-18 Profile of Cr_{OH}^{3+} in passive film formed on UNS N06690 at 40°C (Reproduced from Lu et al. 2007) 36
Figure 2-19 Current transient plot of UNS N06690 in 90°C , pH 4 water at an applied potential of -100 mV $_{SCE}$ (Reproduced from Ahn et al. 2006 b) 38
Figure 2-20 Current transient plot of UNS N06690 in 90°C , pH 10 water at an applied potential of -100 mV $_{SCE}$ (Reproduced from Ahn et al. 2006 b) 38
Figure 3-1 Diagram and dimension of SSRT test specimen (All dimensions are in mm) 43
Figure 3-2 Schematic diagram of room temperature electrochemical cell setup 45
Figure 3-3 Schematic electrochemical cell setup for high temperature experiment .. 46
Figure 3-4 Schematic diagram of scratch cell setup 47
Figure 3-5 Schematic diagram of SSRT test set up 48
Figure 4-1 Stress-elongation curve of UNS N08800 in neutral crevice solution at 300°C 51
Figure 4-2 Ultimate tensile stress (UTS), reduction area (RA) and elongation of UNS N08800 in neutral crevice solution at 300°C 52

Figure 4-3 SEM fractrographs of fracture surface after SSRT testing in different neutral crevice solution at 300°C (a) N1, (b) N2, (c) N3 and (d) N4 55
Figure 4-4 Higher magnification of fracture surface marked as A in Fig. 4-3 (a) N1, (b) N2, (c) N3 and (d) N4 57
Figure 4-5 Side view of UNS N08800 after SSRT testing in different neutral crevice solution at 300°C (a) N1, (b) N2, (c) N3 and (d) N4 59
Figure 4-6 Higher magnification of N2 fracture surface marked as B in Fig. 4-3 (b) 60
Figure 4-7 Polarization behavior of UNS N08800 in acidic crevice chemistries..... 62
Figure 4-8 Polarization behavior of UNS N08800 in alkaline crevice chemistries ... 63
Figure 4-9 Polarization diagram of UNS N08800 at 300°C in neutral crevice solution 64
Figure 4-10 EDX survey of passive film formed on UNS N08800 at 300°C for 24 hours in different neutral crevice solution (a) N 1, (b) N 2, (c) N 3 and (d) N 4..... 66
Figure 4-11 Mott-Schottky plots for passive films formed on UNS N08800 in the solution at (a) pH 1.6, (b) pH 12.9 69
Figure 4-12 Donor density of passive film formed on UNS N08800 at different pH .. 71
Figure 4-13 Mott-Schottky plots of the passive film formed in neutral crevice solution treated at -490 mV $_{vs\ SHE}$ for 900 s at 300°C 73
Figure 4-14 Donor density of the passive film formed in neutral crevice solution treated at -490 mV $_{vs\ SHE}$ for 900 s at 300°C 74
Figure 4-15 (a) Current transient curves; (b) log i(t) vs. q(t) and (c) log i(t) vs. 1/q(t) plots for the passive films formed on UNS N08800 at pH 1.6 77
Figure 4-16 cBV value measured in different solutions at pH 1.6 78
Figure 4-17 (a) Current transient curves, (b) log i(t) vs. 1/q(t) plots for passive films formed on UNS N08800 at pH 12.9 80
Figure 4-18 cBV values measured in different solutions at pH 12.9..... 80
Figure 4-19 Repassivation time calculated from the current transient plot..... 81
Figure 4-20 (a) Current transient curves, (b) log i(t) vs. 1/q(t) plots for passive films formed on Fe at pH 12.9 83
Figure 4-21 (a) Current transient curves, (b) log i(t) vs. 1/q(t) plots for passive films formed on Cr at pH 12.9 84

Figure 4-22 (a) Current transient curves, (b) log i(t) vs. 1/q(t) plots for passive films formed on Ni at pH 12.9 85
Figure 4-23 Mott-Schottky plots for passive films formed on UNS N08800 at 300°C in neutral lead free solution 88
Figure 4-24 Mott-Schottky plots for passive films formed on UNS N08800 at 300°C in neutral lead contaminated solution 88
Figure 4-25 Donor densities of the passive films formed on UNS N08800 at 300°C at different film form potentials 89
Figure 4-26 Correlation between the donor densities and film rupture ductility for the passive films formed on UNS N08800 at 300°C at different passivation potentials 89
Figure 4-27 SEM Micrograph of oxide film formed on UNS N08800 at 300°C in different solution (a) N1, (b) N2, (c) N3 and (d) N4 92
Figure 4-28 XRD patterns of the passive film formed in neutral solutions at 300°C treated in OCP for 24 h (a) N1, (b) N2, (c) N3 and (d) N4 97

List of tables

Table 3-1 Compositions of materials used in the experiment 40
Table 3-2 Simulated SG crevice acidic and basic solution composition 42
Table 3-3 Simulated SG crevice neutral solution 42
Table 4-1 Potentials used for passivating the sample at 300°C (data from Lu et al. 2008) 87

List of symbols

AcSCC	Acidic SCC
Ag/AgCl	Silver-Silver chloride reference electrode
AkSCC	Alkaline SCC
AVT	All volatile treatment
HPSCC	High potential SCC
IGSCC	Intergranular SCC
LME	Liquid metal embrittlement
LPSCC	Low-potential SCC
MA	Mill annealing
OCP	Open circuit potential
PbSCC	Lead induced SCC
PDM	Point defect model
ppm	Parts per million
ppt	Parts per trillion
PWR	Pressurized water reactor
RA	Reduction area
SCC	Stress corrosion cracking
SCE	Standard calomel electrode
SEM	Scanning electron microscope
SG	Steam generator
SHE	Standard hydrogen electrode
SN	Sensitization
SSRT	Slow Strain Rate test
SR	Stress relief
TT	Thermal treatment
t_r	Repassivation time
UPD	Under potential deposition
UTS	Ultimate tensile stress
XPS	X-ray photoelectron spectroscopy
XRD	X-ray diffraction

Chapter 1– INTRODUCTION

Increasing energy needs around the world and consistent depletion of traditional energy sources like coal and crude oil increases the need for harnessing alternative energy resources. At the same time, alternate energy sources should be clean, renewable and should not worsen the deteriorating global climate. Hydro power and nuclear power each constitute a significant portion of current energy production in Canada (Canelect). Fig. 1-1 shows the break down of contributions from different sources to the total electricity production for the year 2007 (Canelect).

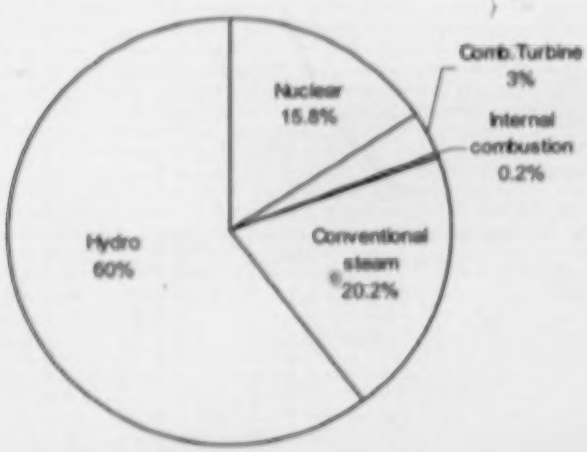

Figure 1-1 Total electricity generation in Canada (584.4 TWh), 2006 with break down of contributions from individual source (Data from canelect)

Nuclear power plants pose serious safety concerns during operation. Existing power plants are licensed to operate over extended life cycles to offset the growing energy demands, which pose a challenge to the safety of plant operation. Economics of plant operation also require the plant to operate without any unscheduled major shutdowns for the entire life cycle of the plant. Environmentally assisted stress corrosion

cracking of nickel based alloys in steam generators (SG) poses one of the major problems for smooth operation of nuclear power plants. Initially UNS N06600 was used as the preferred material for SGs until the advent of UNS N06690. Failure of SGs due to the effects of lead were reported St.Lucie-I (1987), EDF (1990-1993), Doel -4 (1992), Kori-2 (1990) and Oconee plants (1991) (Staehle 2003). In Canada, Ontario Hydro's Bruce Nuclear Generating Station (BNGS) A unit 2 consists of four 760 MW reactor with 8 SGs. Each SG consists of 4200 tubes having 12.7 mm diameter constructed of UNS N06600. One of the four units (unit 2) experienced stress corrosion cracking (SCC) and the problem resulted in shutdown and lay up of the unit in September 1995 (Wright). One of the reasons for severe SCC in unit 2 might be due to introduction of lead blankets during maintenance in 1986; the sludge analysis shown in Fig. 1-2 indicates lead accumulation in all of the SG units. The lead concentration in unit 2 SG sludge was 1000 ppm, whereas sludge from other units showed lesser but significant amounts of lead around 100 ppm. Laboratory studies indicate that lead induced SCC (PbSCC) can be initiated with very low lead concentrations as low as 0.2 ppm in solution (Staehle 2003).

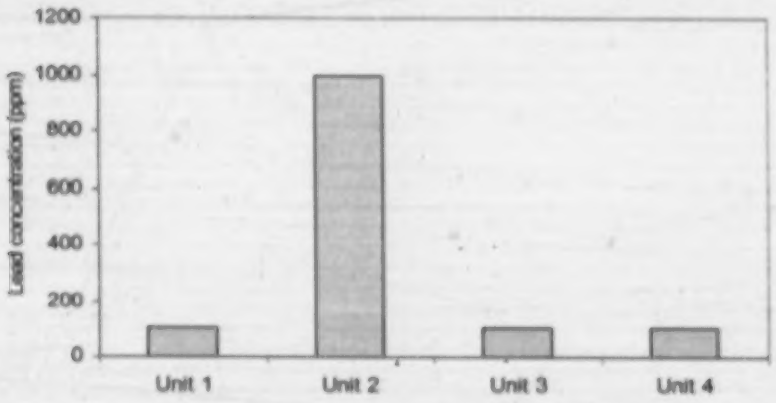

Figure 1-2 Lead concentration in sludge samples from steam generators at BNGS A. (Reproduced from King et al.)

All the failed SGs reported in previous literature were built of UNS N06600 and UNS N06690 was used as replacement materials for SGs in many countries. CANDU* reactors and German power plants use UNS N08800 in the construction of SGs. It is necessary to understand the corrosion susceptibility of UNS N08800 for effective corrosion control management. There are other elements and oxides (Cu, Fe_3O_4, Co_2O_3, ZnO, K, N, Na, TiO_2, As_2O_3, MoO_3, Ca, Al_2O_3, SiO_2 and Mg) present in the pulled SG (Cattant et al.). Some of the elements are present in significant amounts when compared to PbO, and the ratio of magnesium (crevice to adjacent free span) is higher compared to other elements (Cattant et al.). This sparked my curiosity to study the effect of magnesium on lead induced corrosion in UNS N08800. The effect of calcium on lead induced corrosion of UNS N06690 was reported by Lu et al. (2007). It necessitated to study the effect of magnesium to calcium ratio on lead induced corrosion. In this research the effect of magnesium on lead induced corrosion and SCC was studied at high temperature (300°C). Room temperature experiments were conducted to further understand the effect of magnesium to calcium ratio on the PbSCC mechanism.

The following chapter will review the pertinent literature associated with lead induced corrosion in SGs and SCC. Chapter 3 will describe the experimental techniques used in this research, and Chapter 4 will discuss the results. Conclusions and future work in this area are outlined in Chapter 5.

* CANDU is a registered trademark of Atomic Energy of Canada Limited (AECL)

Chapter 2– LITERATURE REVIEW

2.1 Introduction

The premature degradation of SG tubes due to the presence of lead is of great concern in the nuclear industry. PbSCC was first studied by Copson et al. in 1965. UNS N06600 was the most widely used material for the construction of SG tubes in 1960's. It now has been phased out by UNS N06690 and UNS N08800 which are considered to have better corrosion resistant properties compared to UNS N06600. UNS N08800 was the alloy mostly used in German and CANDU nuclear power plants. UNS N08800 is iron based wheras UNS N06600 and UNS N06690 are nickel based. It is important to understand the corrosion behavior of this alloy for better corrosion control management in SG tubes. All of the SG tubing materials, irrespective of their heat treatment before service, show propensity toward PbSCC, with some variance between materials at different pHs.

PbSCC can occur over a wide range of potential and pH and lead is soluble over the full range of operating pH at 300°C. There are a few sub modes of SCC listed by Staehle (2003), namely acidic SCC (AcSCC), alkaline SCC (AkSCC), low-potential SCC (LPSCC), and high-potential SCC (HPSCC). The lead concentration required to induce PbSCC is as low as 0.1ppm (Staehle 2003), and the presence of lead in feed water (ppt) is the main source of lead contamination (Staehle 2005). In this chapter the concept and theory of SCC is discussed initially and the characteristics of PbSCC are discussed in

detail. Since PbSCC mainly happens due to passivity degradation, passivity concepts and lead effect on the passivity of SG tube materials are also discussed.

2.2 Stress corrosion cracking

Stress Corrosion Cracking (SCC) is the combined action of environment, material and stress as shown in Fig. 2-1. Environment is the most critical factor for control of SCC in SG tubes as the other two factors are beyond our control.

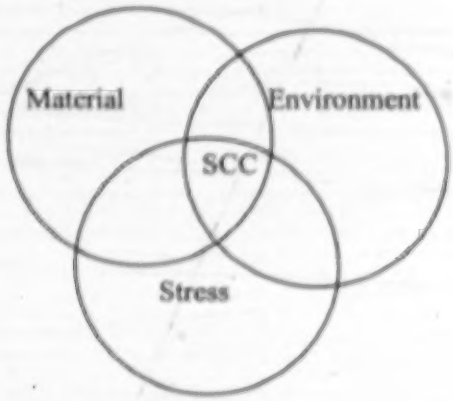

Figure 2-1 Schematic diagram of parameter's interactions to cause SCC

The SCC is alloy-environment specific as specific environments cause SCC of specific alloys, for example SCC of copper alloys occurs in an ammonia environment. Generally speaking, SCC happens in an alloy-environment which forms passive film on the surface. This passive film covers the surface in the corrosive environment, thereby protecting the surface from further general corrosion.

The SCC process consist of three stages as shown in Fig. 2-2,

i) Crack initiation and stage I propagation

ii) Steady state crack propagation

iii) Final failure

Crack initiation occurs during passive film breakdown on the surface. The growth of a crack starts when the threshold stress intensity to initiate SCC is reached. The stage I propagation increases until it reaches the second stage of propagation where the crack growth rate is stable. Stage 3 is called final failure of the material. It occurs when the crack propagation exceeds the steady state and the stress intensity reaches a critical stress intensity leading to mechanical fracture.

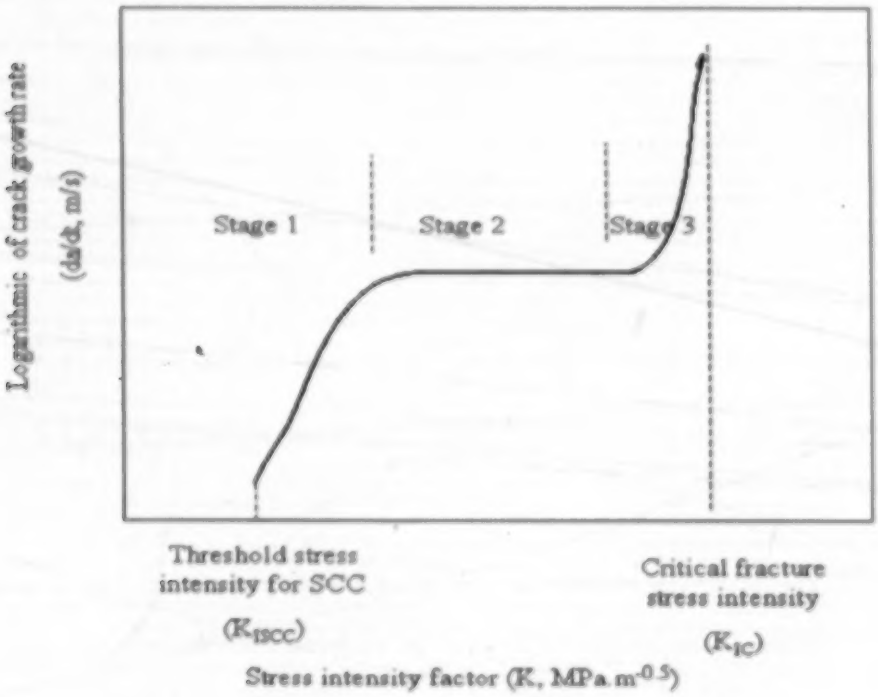

Figure 2-2 Schematic diagram of crack growth (Jones et al.)

2.3 Mechanisms of SCC

Different mechanisms are proposed to explain SCC. These mechanisms can be classified into two categories depending upon the corrosion reaction happening at the crack tip, namely anodic and cathodic mechanisms. In the anodic mechanism the dissolution of crack tips leads to crack growth whereas in cathodic mechanism the

cathodic reaction of hydrogen evolution leads to the crack advance. Most of the prior research concentrated on the propagation of SCC rather than crack initiation due to the difficulty involved in measuring the crack initiation. Usually the crack initiates at surface discontinuities and pits developed on the surface during operation. Two SCC mechanisms will now be described in detail, namely film rupture model and hydrogen embrittlement.

2.3.1 Film rupture model

This model is based on the anodic dissolution at the crack tip that leads to crack growth, wherein crack growth is described related by the following Faradic relationship

$$\frac{da}{dt} = \frac{i_a M}{zF\rho} \qquad 2\text{-}1$$

where i_a is the anodic current density at crack tip, M is the atomic weight , z is the valence , F is the Faraday's constant and ρ is density of the material. This relationship is applicable to many materials (Jones et al.). In this model localized plastic deformation leads to the rupture of the passive film at a crack tip, and the bare metal so exposed to the environment causes dissolution which causes crack propagation. It is believed that once a crack starts it will continuously lead to crack growth as the rate of film rupture is greater than passive film growth at the crack tip, as shown in Fig. 2-3 (a). It is believed that believe that crack growth is not a continuous process as the crack tip repassivates quickly, and so rupture occurs by crack growth as shown in Fig. 2-3 (b).

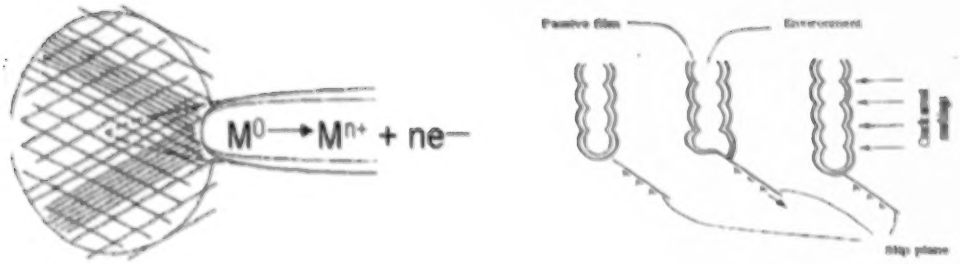

(a) (b)

Figure 2-3 Schematic representation of crack propagation by the film-rupture model. (a) Crack tip stays bare. (b) Crack tip passivates and is ruptured repeatedly (reproduced from Jones et al.)

2.3.2 Hydrogen embrittlement model

The source of hydrogen might be from cathodic reaction, gaseous hydrogen or internal hydrogen. The gaseous molecular hydrogen absorbed on the surface must dissociate to atomic hydrogen whereas cathodic hydrogen will be formed as atomic hydrogen on the surface. This atomic hydrogen will diffuse into the metal and recombine as molecular hydrogen in the micro voids or cracks present in the metal. The accumulated hydrogen molecules will exert pressure to an extent where ductility and tensile stress of the material is reduced and cracks will open. Generally, hydrogen adsorbed on the surface will lead to a crack, and in some cases it will lead to segregation of impurities in the grain boundary which eventually lead to a crack.

2.4 Thermodynamic framework of PbSCC

A thermodynamic framework is used to elucidate the dependence of PbSCC on potential and pH. The reaction of lead with other elements in a range of potential and pH can also be understood from a Pourbaix diagram. Staehle (2003) superimposed the Pb-H_2O and Ni-H_2O diagrams at 300°C having 10^{-6} M concentration of species, as shown in

Fig. 2-4. At low pH (-2 to +4) the equilibrium potentials of Ni^{2+}/Ni and Pb^{2+}/Pb are almost same and are below the equilibrium potential of H_2O/H_2. In the pH range 4 to 7 the equilibrium potential of Ni^{2+}/Ni is slightly higher than the equilibrium potential of $Pb(OH)^+$/Pb. At higher potential (10 to 14) the equilibrium potential of $HNiO_2^-$ /Ni is lower than the equilibrium potential of H_2O/H_2, the equilibrium potential of Pb(OH)/Pb is higher than H_2O/H_2. This behavior indicates that at higher pH the reduction of lead can be coupled with the oxidation of nickel and that lead is soluble over the entire pH range.

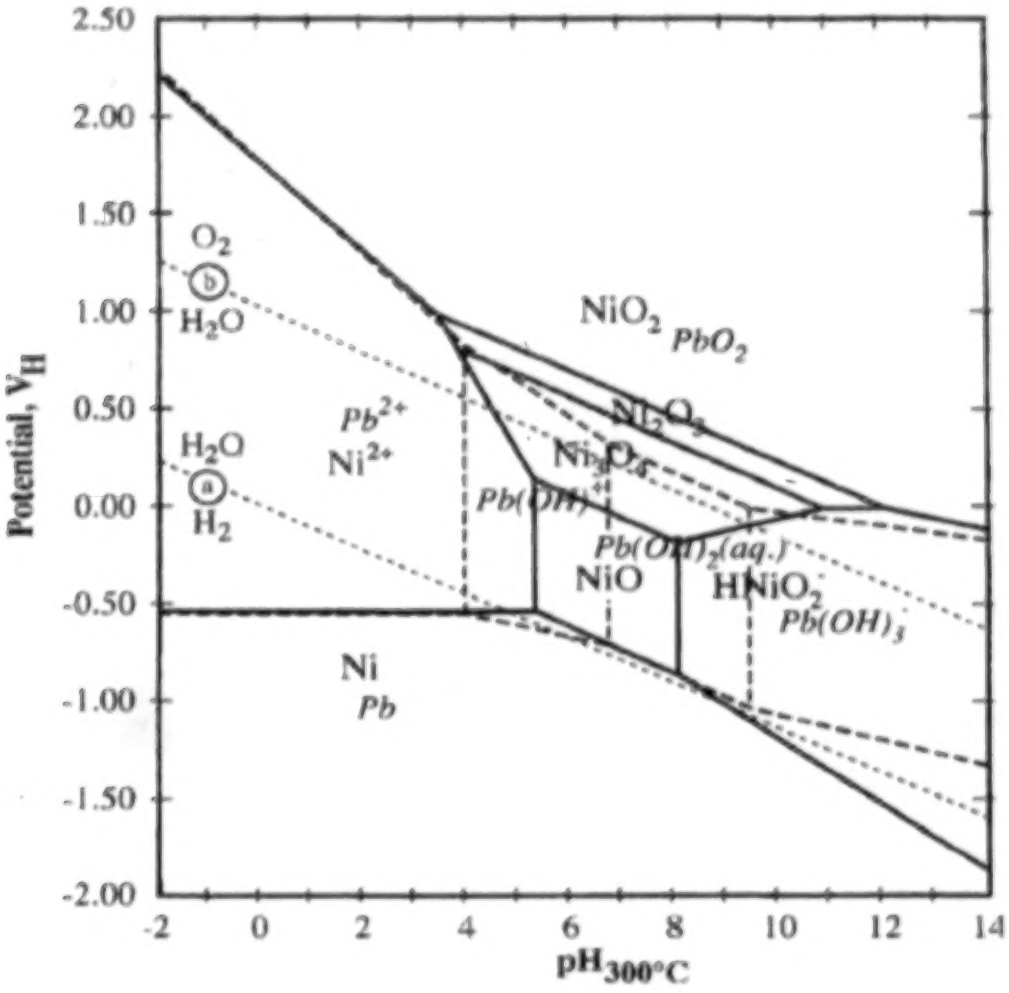

Figure 2-4 Potential as a function of pH for Ni (solid lines) and Pb (dotted lines) at 300°C. (Reprinted from Staehle 2003)

2.5 Sources of lead

The source of lead contamination is feed water, which contains lead in the order of ppt and 10 ppt of lead in feed water leads to 200 to 500 g deposition per year in SG tubes (Staehle 2005). The metallic lead accumulates on the heat transfer crevices and tube supports and adjacent tube supports (Staehle 2003 (a)). Fig. 2-5 shows the concentration ratio of deposit in the heat transfer crevice relative to that in adjacent free span from 340 pulled tubes (Cattant et al.). These values differ between different PWR since dissolved species in feed water are different. From the figure it is clear that lead accumulates on the heat transfer crevice.

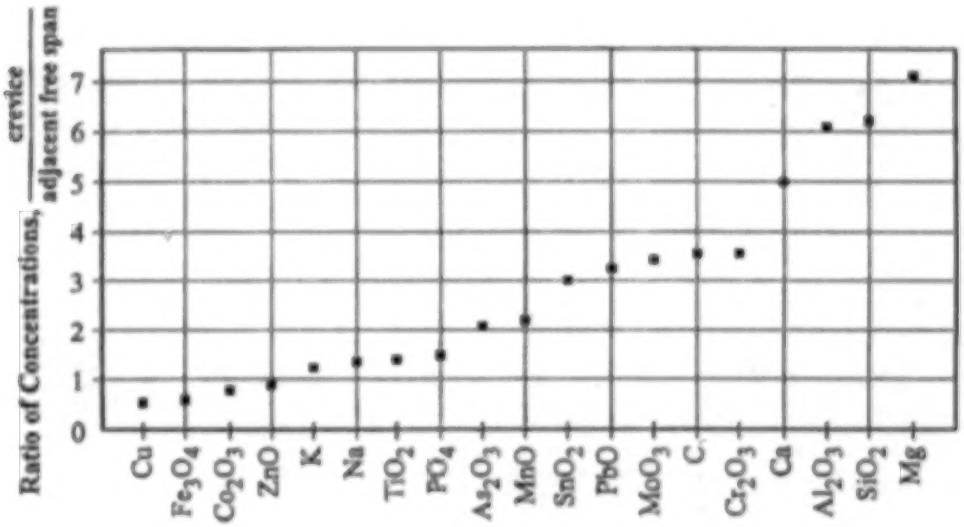

Figure 2-5 Ratio of concentration of species in deposits from 340 failed SG tubes (Cattant et al.)

2.6 PbSCC

PbSCC depends upon seven primary variables (Staehle 2003) namely pH, potential, species, alloy composition, alloy structure, temperature and stress. The effect of each of these variables on PbSCC is discussed in detail below.

2.6.1 Potential and pH

PbSCC plotted against potential and pH at 300°C with significant reaction of Ni and Fe shows that PbSCC occur over the pH range of 4 to 13 and potential range of -1.4 V to -0.1 V (Staehle 2003). Kilian superimposed polarization curves and SCC penetration for UNS N06690 TT and UNS N08800 (Fig. 2-6). In this figure the maximum depth of SCC occurs when the material is in the anodic peak region for UNS N08800. The SCC extending to the passive region indicates that passive film is not stable in UNS N08800. Kilian found that the trend for UNS N08800 was not observed for UNS N06690 TT, quite contradicting with other published results (Staehle 2003, Staehle 2005).

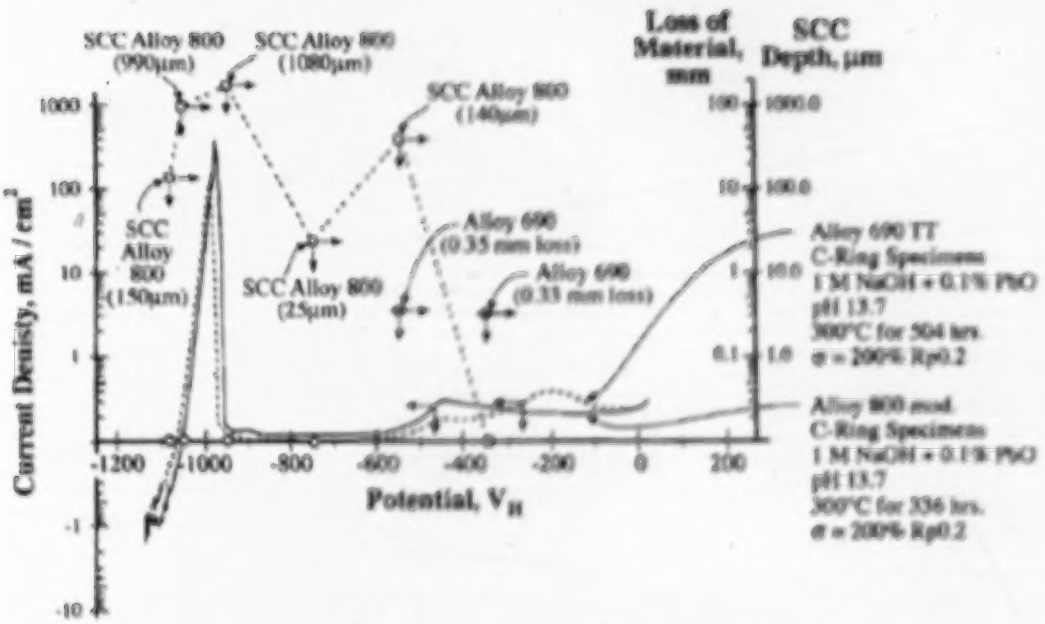
SCC Alloy 800 (990μm)
SCC Alloy 800 (1080μm)
SCC Alloy 800 (140μm)
SCC Alloy 800 (150μm)
SCC Alloy 800 (25μm)
Alloy 690 (0.35 mm loss)
Alloy 690 (0.33 mm loss)
Loss of Material, mm
SCC Depth, μm
Current Density, mA / cm²
Potential, V_H
Alloy 690 TT C-Ring Specimens 1 M NaOH + 0.1% PbO pH 13.7 300°C for 504 hrs. σ = 200% Rp0.2
Alloy 800 mod. C-Ring Specimens 1 M NaOH + 0.1% PbO pH 13.7 300°C for 336 hrs. σ = 200% Rp0.2

Figure 2-6 Depth penetration determined metallographically and polarization current density for UNS N08800 and UNS N06690 TT exposed to 1 M NaOH at 300°C (Reproduced from Kilian et al.)

2.6.2 Lead concentration

PbSCC was studied using PbO (Copson et al., Airey , Hwang 1997, Lu 2005) as the source of lead, but some people also used other compounds of lead namely $PbCl_2$ (Saski 1998), $PbSO_4$ (Costa et al.). Lead was found in the SG sludge as PbO when compared to other lead chemicals. Helie (1993) studied the SCC behavior of UNS N06600, UNS N06690 and UNS N08800 in 10,000 ppm PbO concentration at 325°C and reported that UNS N06600 was severely affected by SCC in lead contaminated solution, while for UNS N06690 and UNS N08800, caustic medium was required to promote SCC. Briceno et al. (1996) studied the SCC susceptibility of UNS N06600 MA, UNS N06600 TT and UNS N08800. In this study the 4% caustic solution with varying concentration of

PbO from 0.2% to 0.001% and AVT water containing 0.01% to 0.001% concentration of PbO were used for the study of lead effect. This study showed that AVT water containing PbO is more aggressive when compared to PbO in caustic solution for UNS N06600 MA and UNS N06690 TT materials, but for UNS N08800 caustic solution containing PbO is more aggressive compared to AVT water containing lead. Hwang et al. (1999) studied the SCC behavior of UNS N06600 MA, TT and UNS N06690 using C-ring specimens in 100 ppm and 5000 ppm PbO containing caustic solutions and the finding for UNS N06600 was consistent with the results reported by Helie and Briceno et al. and showed that UNS N06690 TT is not immune to lead induced corrosion. Lumsden (2005) studied the SCC behavior of UNS N06600 TT and UNS N06690 TT using reverse U-bend specimens in solution with PbO concentrations of 50 ppm and 500 ppm and found that the maximum PbSCC susceptibility in both alloys occurred at 500 ppm PbO solution. All the test results suggest one common factor: that UNS N06600, UNS N06690 and UNS N08800 are susceptible to PbSCC in acidic, neutral and alkaline solutions even at low concentrations of lead.

2.6.3 Alloy composition and structure

Initially, UNS N06600 (Fe-8.5%, Cr-15.5%, Ni-74%) was the main alloy used in SG tubes construction. It was eventually replaced by UNS N06690 (Fe-10%, Cr-30%, Ni-59%) which has higher chromium content. Since both the alloys are susceptible to PbSCC, new materials with increased iron content and decreased nickel content were used as SG tubing material to improve corrosion resistance towards PbSCC. As the nickel content increases in alloys its propensity towards SCC also increases (Stachle 2005). Fig. 2-7 shows effect of PbSCC on the relationship between concentrations of chromium and

iron for Ni-Cr-Fe alloys, with PbSCC interstices based on results from U bend specimen tests under alkaline condition. It can be inferred from the figure that UNS N06600 readily sustains PbSCC, since it is clearly in the PbSCC region, while the compositions of UNS N06690 and UNS N08800 are above the edge of the PbSCC region. Stainless steel is away from the PbSCC region, and so has relative immunity towards PbSCC. However, little research has been done on PbSCC using this material.

The microstructure of an alloy depends upon the nature of the cold work done before the material is put into service. The major cold work done on SG tubes includes mill annealing (MA), thermal treatment (TT), sensitization (SN) and stress relief (SR). Airey studied the effect of heat treatments on PbSCC in neutral AVT environment on UNS N06600. He measured the total time to failure, and found that heat treatment did not have much effect on PbSCC. The fracture mode is TGSCC in SR, SN, TT and IGSCC in MA alloys.

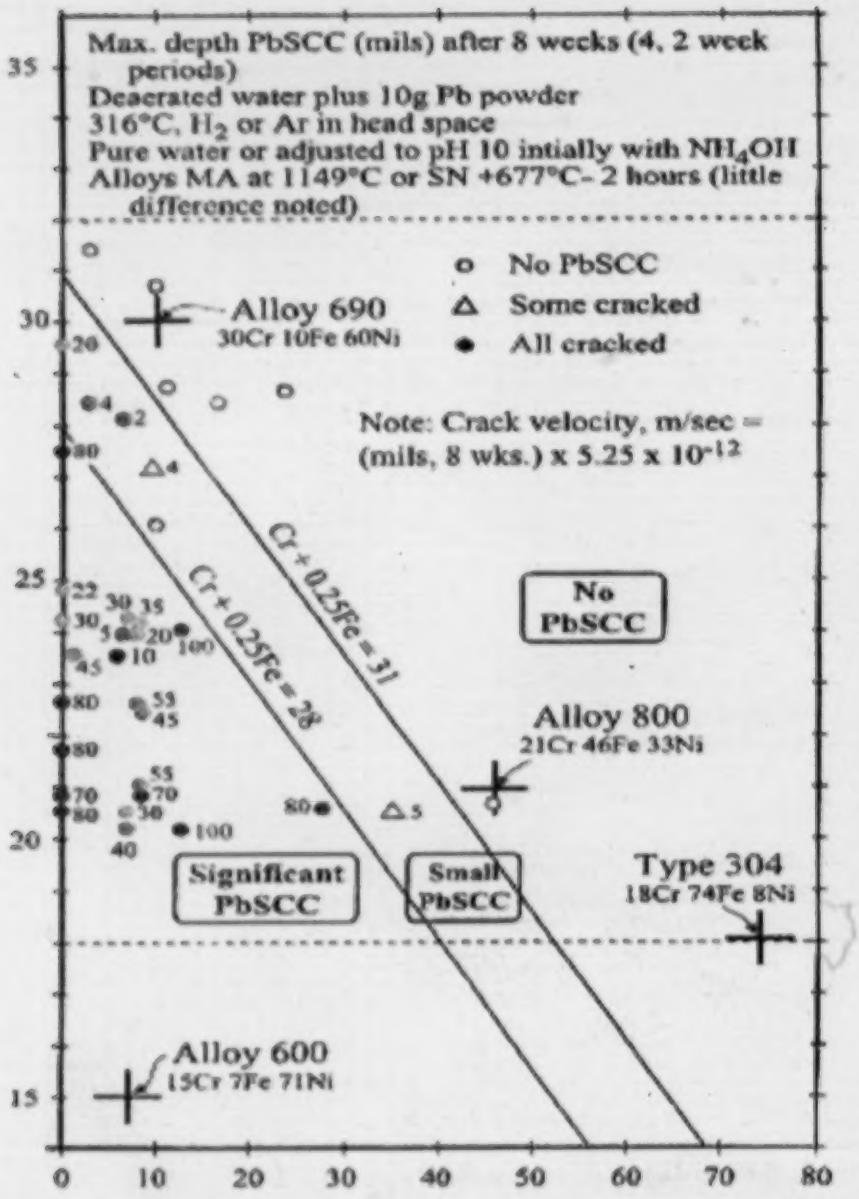

Figure 2-7 Concentration ratio of Cr vs. Fe for Ni-Cr-Fe alloys tested in pure water at 316°C with 10 g of Pb powder added to the autoclave and specimens stressed as single U-bends and tested for 8 weeks. (Reproduced from Staehle 2005)

2.6.4 Temperature

PbSCC was found to increase with temperature of the experiment (Staehle 2003).

Fig. 2-8 shows the crack growth rate as a function of temperature. The activation energy

for crack growth rate in lead contaminated and pure water is almost the same, and in both the solutions the crack growth rate increases with temperature.

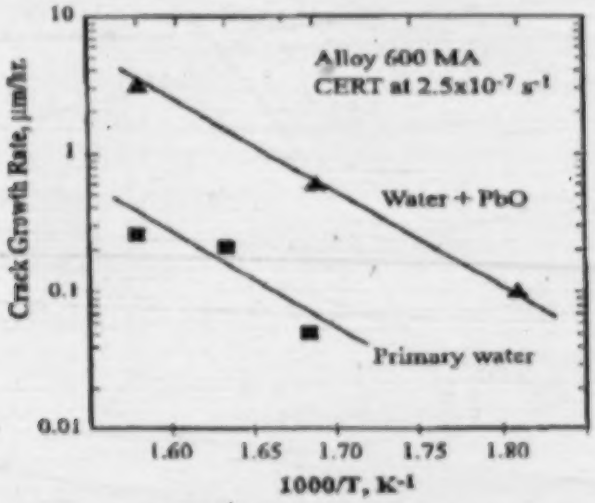

Figure 2-8 Crack growth rate vs. 1000/T for water and water +PbO determined by CERT at 10^{-7} s^{-1} (Reproduced from Staehle 2003)

2.6.5 Stress

Stress is required to initiate and propagate the crack. Application of stress as low as 20% of the room temperature yield strength (RTYS) can produce SCC for samples in lead containing solution (Staehle 2003).

2.7 Mechanism of PbSCC

There is no generally accepted comprehensive mechanism to explain PbSCC. Due to different researchers used different solutions and testing methods, and so correlation of the results is very difficult. Two mechanisms are proposed for the early stages of PbSCC namely, liquid metal embrittlement (LME) and passivity degradation by lead.

SCC of SG tubing material by LME is a plausible mechanism because the operating temperature of SG is close to the melting point of lead. Copson and Dean (1965) conducted experiments using liquid lead at 350°C and could not find any crack after 4000 h in UNS N06600. Helie et al. (1993) conducted experiments on UNS N06600 at two different temperatures, one above the melting point of lead and one below the melting point of lead, to find out whether metallic lead or soluble lead is responsible for SCC. The results showed that in both the testing conditions UNS N06600 shows SCC and confirmed that only soluble lead was responsible for cracking. Briceno et al. (1996) conducted tests at the same temperature as Helie for UNS N06600, and found that the material sustained SCC. These results showed that specimen is not failed due to LME.

SG tube failure due to hydrogen embrittlement was studied by Pasila-Dombrowski (1999). He conducted experiments on UNS N06600 and UNS N06690 in alkaline solutions with and without PbO at 320°C. The alloys did not show a significant increase in the amount of hydrogen uptake due to lead contamination. These results indicated that PbSCC was not due to hydrogen embrittlement.

Interaction between lead in solutions and a passive film formed on SG tubes may decrease the stability of the passive film, this leading to SCC. The effect of lead on passive film formation was studied by Hwang et al. (1997), and the passive film formed in acidic and alkaline condition was analyzed by AES. In caustic solution, Ni was depleted and Cr was enriched in the passive film formed in lead containing solution, but in lead containing alkaline solution Cr was depleted and Ni was enriched. The mechanism of passivity degradation by lead was studied by Lu et al. (2007) using UNS N06690 at 40°C, including the interaction of Ca^{2+} with lead in the solution. During

passive film formation, initially the hydroxides of the matrix elements formed within the solution, and dehydration of the hydroxides led to the oxides. These dehydrations led to the formation of spinel oxides which are highly corrosion resistant. The presence of lead decreased the dehydration reaction which in turn decreased the stability of the passive film. The equilibrium rate constants of the dehydration reaction was compared and the stability of $Cr(OH)_2$, $Fe(OH)_2$ are lower than $Pb(OH)_2$ (Lu et al. 2007).

2.8 Passivity of metals

Passive films play a vital role in corrosion resistance of SG alloys. PbSCC mechanisms are related to the passivity of the alloys, as discussed in section 2-7. Some metals and alloys are used in our industrial society due to its capability to resist corrosion by forming passive films on the surface. Passivity was first described by Keir in 1790 (Keir). When iron was placed in dilute nitric acid, it dissolved at a high rate with evolution of NO2, but the same material was found to be immune to corrosion when placed in concentrated nitric acid. The term passivity was coined by Schonbein in 1836, but it was Faraday's experiment that showed phenomena of passivity (Kelly et al.). Passivity can be expressed in many ways and, according to Kelly (2003) passivity of metals can be classified in to two types.

1) "A metal is passive if it substantially resists corrosion in an environment where there is a large thermodynamic driving force for its oxidation (also known as thick film passivity)"

2) " A metal is passive if, on increasing its potential to more positive values, the rate of dissolution decreases, exhibiting low rates at high potentials (also known as thin film passivity)"

The Evans diagram for materials which have the tendency to type 1 passive film is shown in Fig. 2-9 (a). Examples for the materials of this category are Al in water and Pb in H_2SO_4. These materials will have a high anodic Tafel slope, and an increase in potential will not increase dissolution. The Evans diagram for the materials which form type 2 passive films is shown in Fig. 2-9 (b). The tafel slopes of these materials have strong potential dependence. Examples of this type of passivity are Ni and Cr in H_2SO_4.

The mechanism of passivity can be explained in terms of mixed potential theory. At corrosion potential (E_{corr}), the metal corrodes uniformly and the metal is free of passive film. As the potential increases in the noble direction, dissolution of metal increases until the potential reaches passivation potential (E_{pp}). The current corresponding to E_{pp} is called the critical current density (i_{crit}). Above E_{pp}, the potential is called passive potential. The current density decreases from critical current density and is called passive current density. The dissolution rate of the material is decreased significantly in the passive range, and materials are designed to operate at passive potential dissolution rate. When the potential of the material increases above the passive potential, transpassive dissolution of the material will occur with evolution of oxygen in most of the metals.

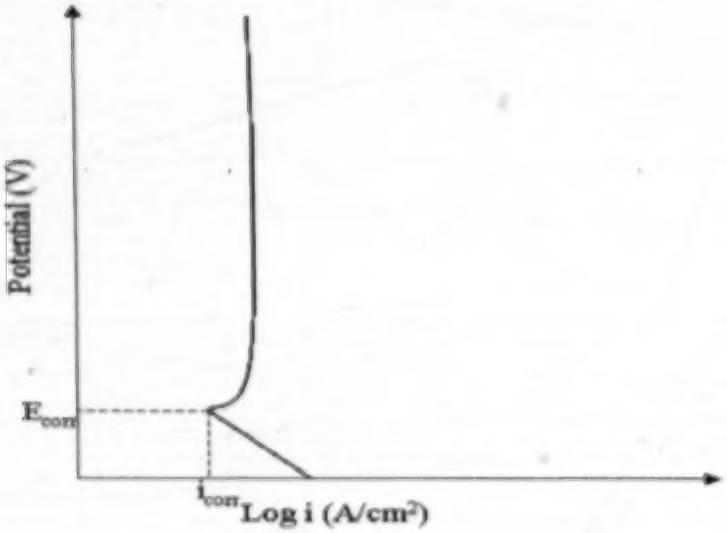

(a)

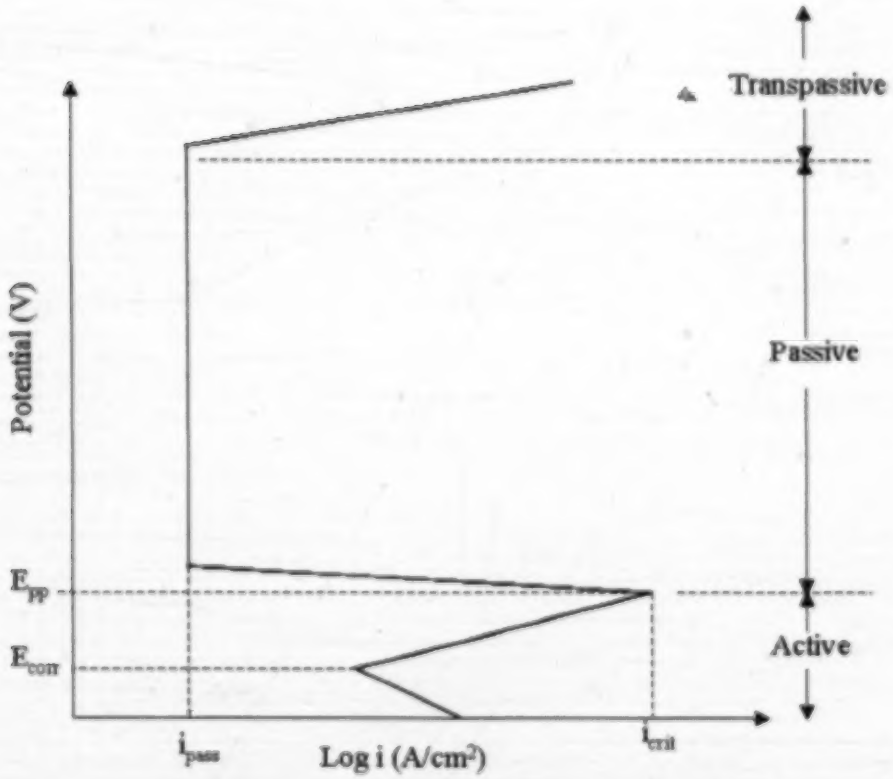

Figure 2-9 Schematic Evans diagram of passivation. (a) Thick film passivation. (b) Thin film passivation (Reproduced from Kelly et al.)

2.9 Growth of passive film

Passive film grows by interaction between metal atoms and solution. Passive films formed on Ni-Cr alloys were studied by Jabs et al. (1998) and Machet et al. (2004) and it was revealed that passive films formed comprise two layers, an inner layer which mostly consists of metal oxide and an outer layer consisting of metal hydroxides. The outer layer of Ni-Cr alloys consists of chromium and nickel hydroxides while the inner layer consists of chromium and nickel oxides. The composition of the passive film mainly depends on the electrochemical behavior of the base metal. Different mechanisms postulated to explain the passive film growth are described in detail in the following section.

2.9.1 Place exchange model

This model for the passive film growth was proposed by Sato and Cohen (1964). Fig. 2-10 shows the schematic process of the place exchange model mechanism. In this model initially a pair of oxygen atoms adsorbs on the surface and exchange with underlying metal atoms by rotation, which causes fresh metal atoms to come into contact with the solution. Then second oxygen atom is adsorbed onto the metal surface, and these second M-O pairs will rotate simultaneously with first M-O pair. Repetitions of these processes enable passive film growth on the surface. According to this model, the logarithm of current density (log i(t)), arising from a scratch is linearly proportional to charge density flowing from the scratch surface.

$$\log i(t) = \log k' + \beta V - \frac{q(t)}{K} \qquad 2\text{-}2$$

where k', β, K are constants, V is the applied voltage and q(t) is charge density.

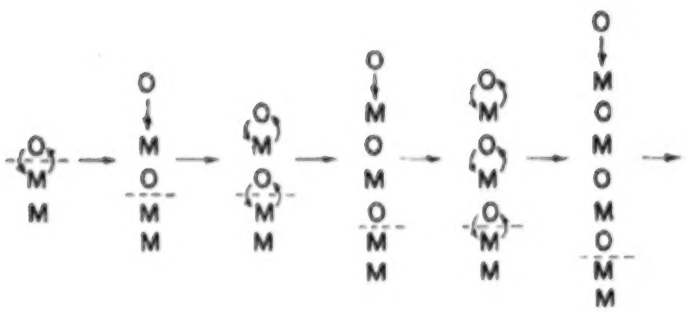

Figure 2-10 Schematic diagram of place exchange model (Reproduced from Sato et al. 1964)

2.9.2 High field ion conduction model

This model was put forward by Cabrera and Mott (1948) and is based on the assumption that the electric field inside the passive film is constant irrespective of the film thickness. The passive film grows by transport of the metal cations produced at the metal/film interface to film/solution interface under high electric field, where the cations react with the solution to form the passive film. Fig. 2-11 is a schematic diagram of passive film formation according to the high field ion conduction model. Repassivation rate is expressed in terms of current density as (Cabrera et al.)

$$i(t) = A\exp\left(\frac{BV}{h(t)}\right) \qquad 2\text{-}3$$

where A and B are constants associated with activation energy, V is the potential drop across the film/electrolyte interface, and h(t) is the thickness of the passive film. The charge density q(t) flowing from the scratch surface vs. film thickness can be expressed using the following expression (Cabrera et al., Burstein et al.)

$$q(t) = \frac{zF\rho\, h(t)}{M} \qquad 2\text{-}4$$

where z is the number of moles of electron transferred in oxidation reaction, F is the Faraday constant, ρ is the film density, and M is molecular mass of the film. Rearranging Equation 4.2 and substituting for h(t) in Equation 4.1 yields (Cabrera et al., Burstein et al., Cho et al.)

$$\log i(t) = \log A + \frac{cBV}{q(t)} \qquad 2\text{-}5$$

where c is a constant and equal to zFρ/2.3M. It has been explained that cBV value is an effective way to characterize the repassivation behavior for a metal (Cho et al., Bernard et al., Ahn et al.2006 b). The lower the cBV value, the faster the metal reforms a protective layer.

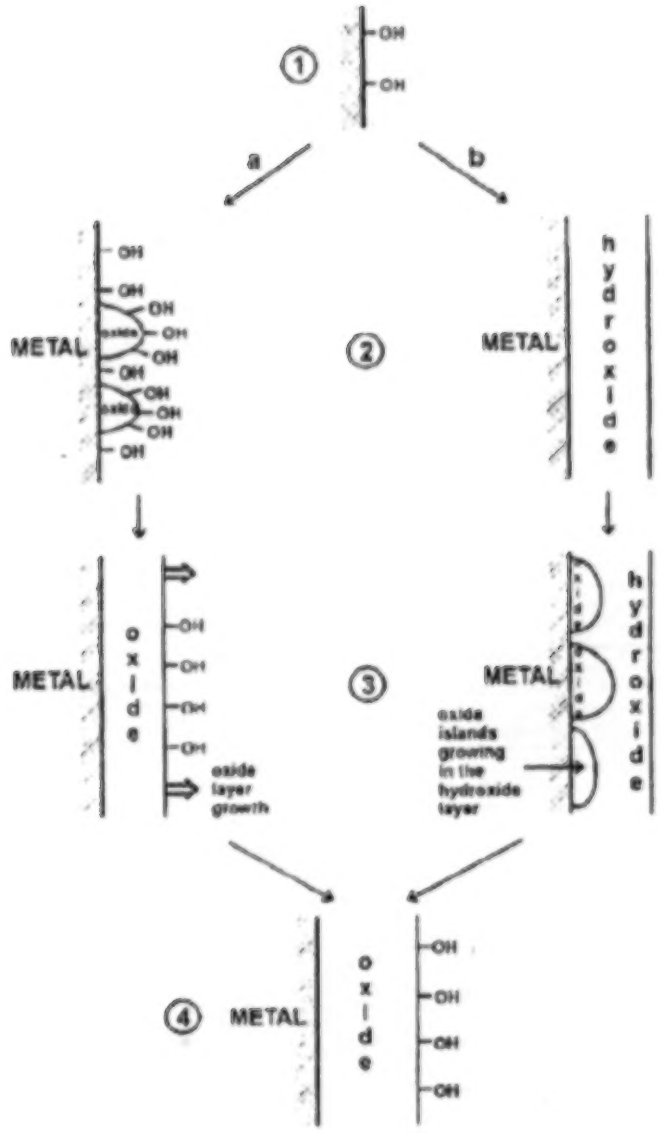

Figure 2-11 Schematic process of high field ion conduction model passive film growth. (a) Passive film growth layer by layer. (b) Simultaneous hydroxide layer and oxide layer growth (Reproduced from Marcus et al. 2001)

2.9.3 Point defect model

A point defect model was proposed by Chao et al. (1981) and later reviewed by Macdonald (1992). PDM was based on the following experimental data

1) The passive film is bilayer in structure, with an inner layer comprising a highly defective barrier layer which is semiconductor in nature.
2) Growth of the barrier layer varies linearly with logarithm of the steady state current when there is no change in oxidation state of the cation in the passive range.
3) The electric field within the passive film is independent of the applied voltage.

A schematic diagram of passive film growth and dissolution of PDM is shown in Fig. 2-12, where m = metal atom, M_M = metal cation in cation site, O_O = oxygen ion in anion site, $V_M^{z'}$ = cation vacancy, V_m = vacancy in metal phase, $V_O^{\cdot\cdot}$ = anion vacancy.

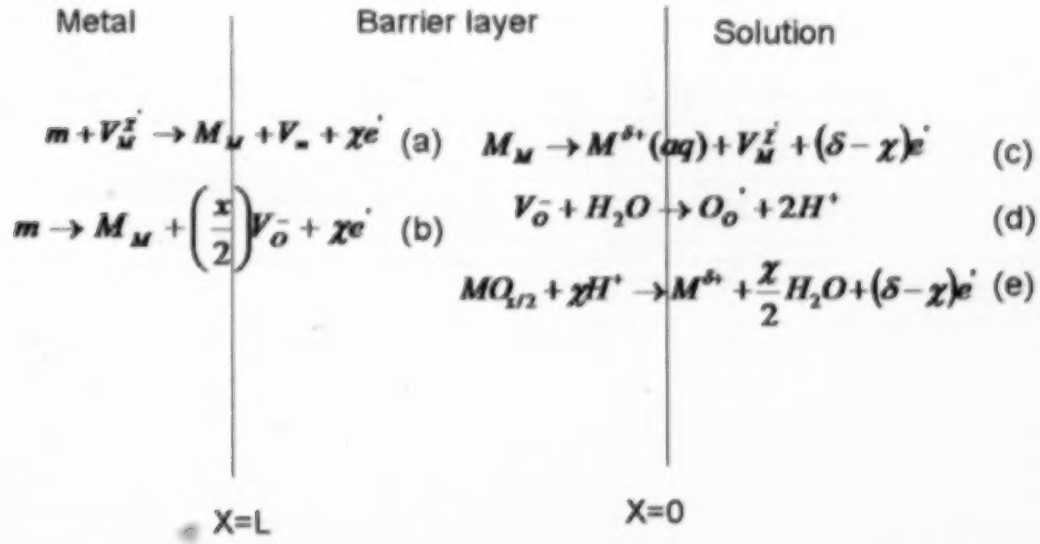
Metal
Barrier layer
Solution
$m + V_M^{z'} \rightarrow M_M + V_m + ze'$ (a)
$m \rightarrow M_M + \left(\frac{x}{2}\right)V_O^{\cdot\cdot} + ze'$ (b)
$M_M \rightarrow M^{\delta+}(aq) + V_M^{z'} + (\delta - z)e'$ (c)
$V_O^{\cdot\cdot} + H_2O \rightarrow O_O^{\times} + 2H^+$ (d)
$MO_{x/2} + zH^+ \rightarrow M^{\delta+} + \frac{z}{2}H_2O + (\delta - z)e'$ (e)
X=L
X=0

Figure 2-12 Schematic of physico- chemical processes that occur within a passive film according to point defect model (Reproduced from Macdonald 1992)

During passive film growth, a metal cation vacancy produced at the film/solution interface moves toward the metal/film interface, whereas an oxygen anion produced at the metal/film interface moves toward the film/solution interface leading to the formation of the passive film. The reactions a, c, d are lattice conservatory and do not have any impact on the passive film growth while reactions b, e are responsible for the passive film growth.

2.9.4 Double layer model for Ni-Cr-Fe alloy

Passive film growth on Ni-16Cr-9Fe poly crystals and Ni-17Cr-7Fe single crystal alloys during early stages (0.4-8.2 min) at 325°C were studied by Machet et al. (2004). Maurice et al. (1998) studied passive film formed on Ni-18Cr-13Fe single crystal after 20 min at room temperature. Fig. 2-13 shows the mechanism of passive film growth on UNS N06600.

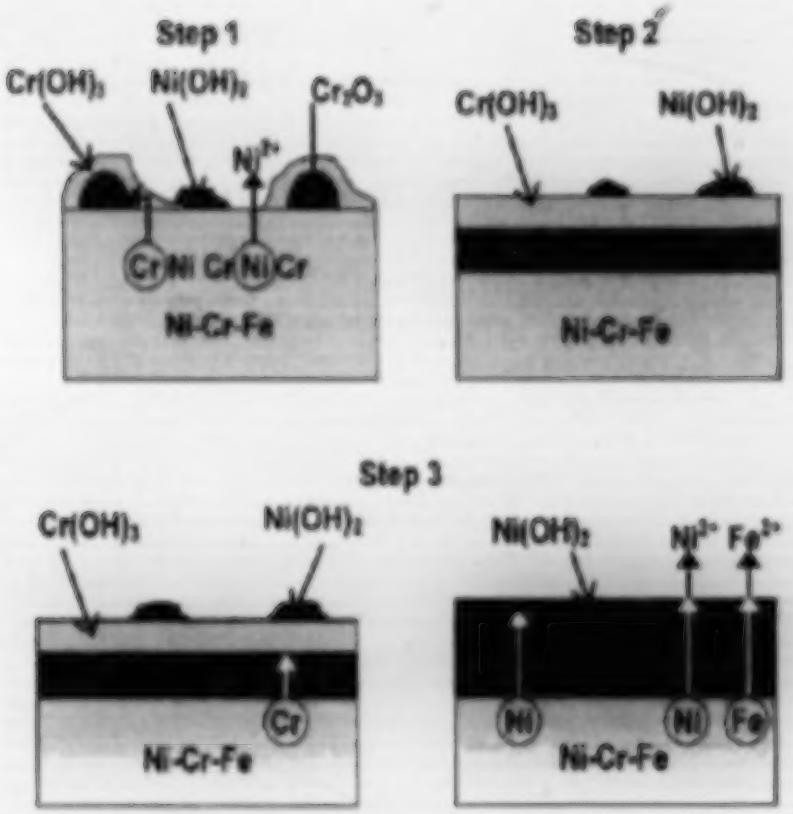

Figure 2-13 Model for the mechanism of the formation of the passive film on Ni-Cr-Fe alloys (Reproduced from Machet 2004)

1) Initial nucleation and growth of chromium oxide inside of $Cr(OH)_3$ on the surface, coupled with the selective dissolution of nickel and iron at the surface.
2) Continuous layer of Cr_2O_3 is formed on the surface by coalescence of Cr_2O_3 islands on the surface. During this stage the growth of Cr_2O_3 is temporarily stopped.
3) Once the surface is covered entirely by Cr_2O_3, the growth of the oxide layer starts by dehydration of $Cr(OH)_3$ to Cr_2O_3.

4) Ni and Fe migrate through the oxide layer, and there is partial dissolution of Ni^{2+} and Fe^{2+}. A portion of the Ni forms $Ni(OH)_2$. Since the Fe concentration is lower compared to Ni in the matrix, the outer layer is enriched with Ni.

2.10 Overview of passive film on Ni-Cr-Fe alloy

Passive films play an important role in corrosion resistance of material at high temperature application in SG tubes. Relatively little prior research has been done on passive films formed on UNS N08800. Since UNS N08800 consists of Ni, Cr and Fe, the passive films formed on related Ni-Cr-Fe alloys, Fe-Cr and Ni-Cr are reviewed here.

2.10.1 Thermodynamic framework for passive film formation

The stability of the various oxides formation in the Ni-Cr-Fe – H_2O system was studied by Cubicciotti and Berverskog et al. (1999). The oxide films formed in pure metal and alloys are of different thermodynamic stability. The thermodynamic stability of the passive region in Ni-Cr-Fe alloy is higher than those of the individual metals. Passive film formed by the ternary system consists of spinel oxides, magnetite (Fe_3O_4), trevorite ($NiFe_2O_4$), chromite ($FeCr_2O_4$) and nichromite ($NiCr_2O_4$). Trevorite shows stability over the entire potential region whereas the chromite stability region is located very close to the hydrogen line. Berverskog et al. (1999) showed that the stability region of nichromite is lower than those of the compared to other bimetallic spinel oxides. The crystal structure of each spinel oxide accommodates the cations in their tetrahedral and octahedral holes, and the presence of non-stoichiometric proportions of oxides leads to the semiconductor properties of the passive film.

2.10.2 Composition of the passive film

The passive film formed on UNS N08800 at high temperature was studied by Albarez (1996 b) using static autoclave methods. The passive film formed at 350°C is duplex in structure with iron enriched crystals on the surface and chromium enriched inner layer. The morphology of the crystals on the surface does not change when the exposure time is increased from 770 h to 1250 h. The composition of the passive film formed on UNS N08800 treated for 770 h at 350°C was determined using XPS. The Ni/Cr ratio decreased as the sputtering time increased. The ratio was lower at the metal/oxide layer interface than in the base metal, indicating that the inner layer was enriched in chromium and depleted of nickel. The analysis of precipitated crystal showed that the outer layer was enriched in iron with nickel but depleted in chromium.

2.11 Environmental effect on film growth

Growth of passive film involves the exchange of ions with the electrolyte and depends on the potential, solution composition, pH and temperature (Olsson 2003).

2.11.1 Potential

Haut et al. studied passive film growth on Fe-15Cr alloy at different applied potentials. The rate of passive film increases linearly with applied potential; however passivation at the same potential for longer time does not significantly increase overall passive film thickness (Maurice 1998). Increase in the passivation time increases the inner oxide layer thickness and decreases the outer hydroxide layer thickness. The film composition varies with the applied potential in Fe-Cr alloys. At lower potentials within the passive region the concentration of chromium in the passive film increases, but at

higher potential the iron concentration is enriched. The composition difference in Fe-Cr alloy is due to the relative stabilities of Fe, Cr at different potentials in the passive region (Olsson 2003).

2.11.2 Solution composition

Anions present in the solution are responsible for the passive film growth. Hydroxyl and oxygen anions are the primary constituents required for passive film growth. Olsson et al. (2000) studied passive film growth on Ni-Cr alloys in acidic and alkaline solution. Thickness of the passive film is higher in alkaline condition compared to acidic solution but the composition of the film is not changed.

2.11.3 Temperature

Passive films formed at room temperature and at 90°C do not show significant thickness difference when formed in 0.5 M NaCl solution (Jin et al.). However the passive films formed at higher temperatures is thicker compared to those at room temperature. The composition of the passive film does not change with temperature. It indicated that passive film composition is not changed, only thickness change with temperature.

2.12 Effect of lead on electrochemical behavior of UNS N08800

Electrochemical behavior of SG tubing material in lead containing solutions were studied by Saski et al. (1992, 1998), Hwang et al. (2002) and Lu (2005). The results suggest that the presence of lead increases the anodic current density and passive current density. Saski studied the electrochemical behavior of alloys UNS N06600 MA, TT and UNS N06690 TT in mildly acidic solution with 300 ppm $PbCl_2$ at 280°C and reported

that lead does not have any effect on OCP; however it increased the anodic current density. In contrast in alkaline AVT solution lead decreased the OCP and increased the passive current density.

Hwang et al. (2002) studied the electrochemical interaction of lead with UNS N06600 and UNS N06690 at 90°C. He studied the polarization behavior of UNS N06600 and UNS N06690 in lead free solution, 100 ppm and 500 ppm PbO under both acidic and alkaline conditions. The study revealed that OCP decreased and passive current density increased with the addition of lead. As the lead concentration increased in solution, the anodic peak increased, and this increase in anodic peak was partly due to anodic dissolution of metallic lead deposited during the cathodic pretreatment before the polarization experiment.

The effect of lead contamination on dissolution of SG tubes was studied extensively by Lu (2005). The polarization behavior of UNS N06690 in alkaline crevice solution at 300°C as a function of different PbO concentrations showed that the lead effect was significant when the PbO concentration was 10 ppm, and anodic peak current density and passive current density both increased as the PbO concentration increased. Potentiostatic experiments were done by Lu (2005) for UNS N08800 at the potential close to the anodic peak region for 24 h in lead free solution and 500 ppm lead contaminated solution to find out whether the anodic peak is due to metal dissolution or oxidation of lead deposited during the cathodic precondition. Fig. 2-14 shows the polarization curve of UNS N08800 and the potential used in potentiostatic condition. The tube which was passivated in lead free solution did not show corrosion on the surface but the tube passivated in lead contaminated solution had significant corrosion product on the surface

which clearly indicated that lead increased anodic dissolution. If the anodic peak was due to the dissolution of metallic lead, it would not show corrosion on the surface as it was in lead free solution.

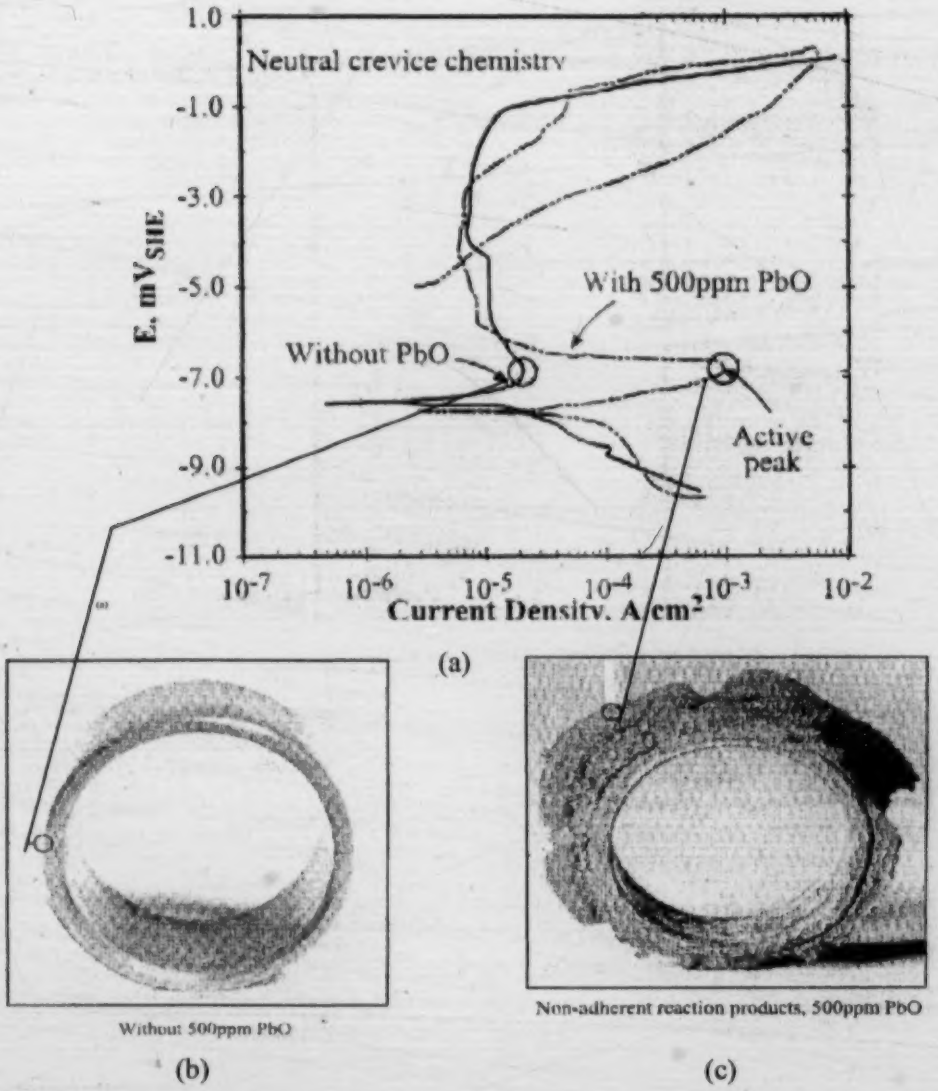

Figure 2-14 (a) Polarization diagram of UNS N08800 SG tube in neutral crevice chemistry. (b) Specimen treated for 24 h near active peak without PbO. (c) Specimen treated near active peak in PbO solution for 24 h (Reproduced from Staehle 2005, courtesy Lu 2005)

2.13 Effect of lead on passive film

The lead effect on passive film of SG tubing alloys has not been studied as extensively as PbSCC. Passive films act as barriers against localized corrosion since the localized corrosion is usually a precursor to SCC. Electrochemical behaviors of SG alloys in lead contaminated solution are reviewed in section 2.6.6, which shows the passive region is reduced, while passive current density and anodic peak are increased by the addition of lead. Interaction of lead with the oxide film formed on UNS N06600 and UNS N06690 was studied in 0.1M $HClO_4$ solution with PbO. To study the effect of lead on passivity, lead was added after the passivation in lead free solution for 30 min. Lead does not increase the passive current. These results show that lead does not interact with fully formed passive films (Radhakrishnan et al.).

Passive film formed on UNS N06600 was studied by Saski (1992) at high temperature in saturated lead solution and lead free solution in acidic and neutral pH. Passive films are characterized by Ni/(Ni+Cr+Fe) at.% (Atomic percentage) and Cr/(Ni+Cr+Fe) at.% vs. depth profile after one week exposure of the samples at 280°C .The average values of Ni/(Ni+Cr+Fe) at.% and Cr/(Ni+Cr+Fe) at.% show that each passive film was depleted in nickel and enriched in chromium. The depletion was higher in acidic solution than in neutral lead free solution. The same trend was seen in passive film formed in lead containing water and the extent of depletion was higher when compared to lead free solution. Hwang et al. (1997) studied the passive film formed at different lead concentrations and his results were comparable with those by Saski (1992). Depth profiles of the passive film explored by AES show similar trends: the atomic ratio of Ni was depleted and Cr was enriched in passive films formed as the lead concentration

increased. Fig. 2-15 shows the schematic film composition of passive film formed at different pH. Outer surface analysis by XPS showed that, irrespective of the solution pH, the passive film was Ni depleted and Cr enriched. However the inner layer of the passive film showed an increase in Ni and decrease in Cr concentration as the lead concentration increased. This trend was more predominant in alkaline solution compared to the acidic solution. It was unknown whether the lead affected only Cr, Ni concentration, or whether lead was incorporated into the passive film? Lu et al. (2007) studied passive film formed on UNS N06690 in alkaline solution at 40°C and found that Pb was incorporated. Fig. 2-16 shows the XPS spectrum of lead peak in the passive film. It suggests that lead existed as lead oxide in the passive film, which might be due to replacement reaction with other matrix elements, especially nickel (Lu et al. 2007).

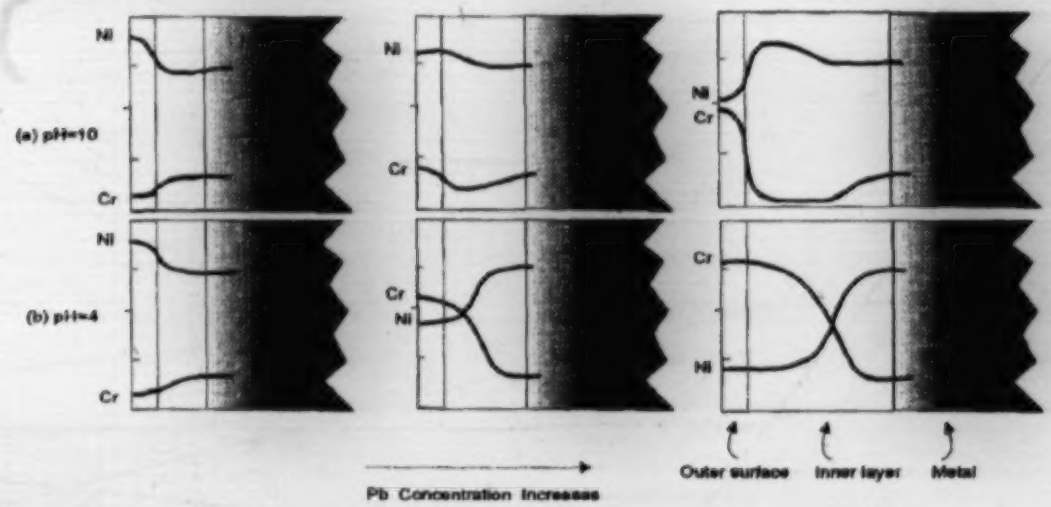

Figure 2-15 The effect of Pb on passive film composition of UNS N06600 at different pH's (Reproduced from Hwang et al. 1997)

Delayed dehydration reaction is one of the possible mechanisms by which lead decreases the stability of the passive film. If the dehydration is delayed, the passive film

contains more hydroxides and less oxide. Fig. 2-17, 2-18 show the $Cr(OH)_3$ and $Ni(OH)_2$ profiles in the passive film formed in different lead solution. The depth profiles show that the presence of lead decreased the metal oxide formation reaction and increased concentration of metal hydroxides in the passive film.

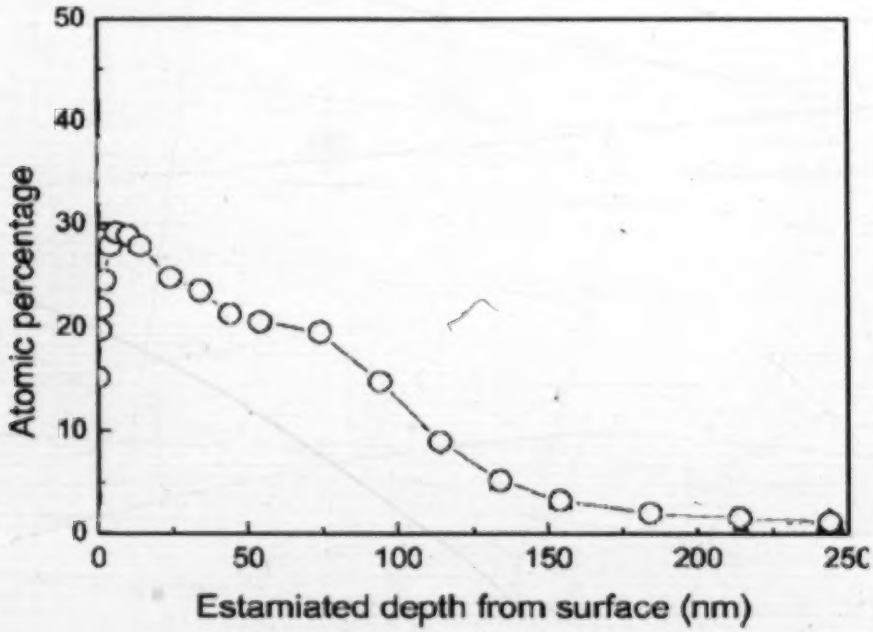

Figure 2-16 Concentration depth profile of Pb in surface layer of sample passivated at 40 OC in SG alkaline crevice chemistry containing 2.2 mM PbO (Reproduced from Lu et al. 2007)

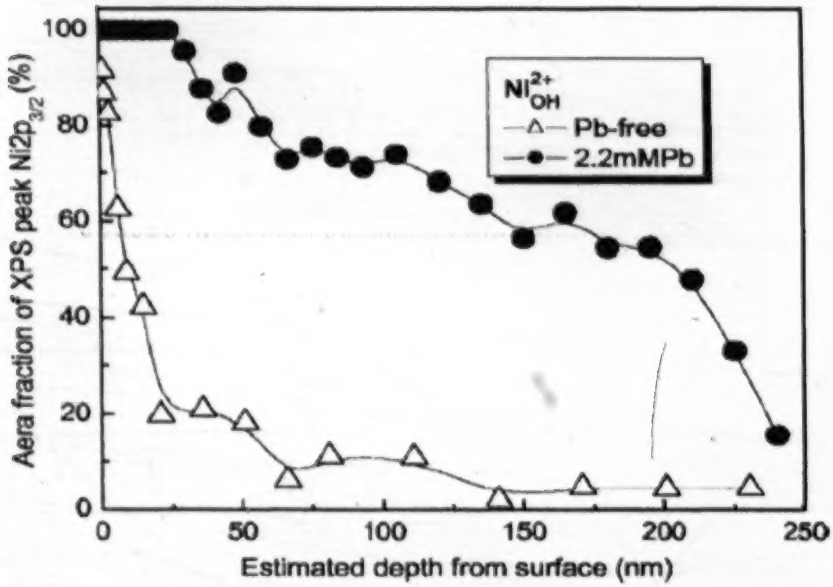

Figure 2-17 Profile of Ni_{OH}^{2+} in passive film formed on UNS N06690 at 40°C (Reproduced from Lu et al. 2007)

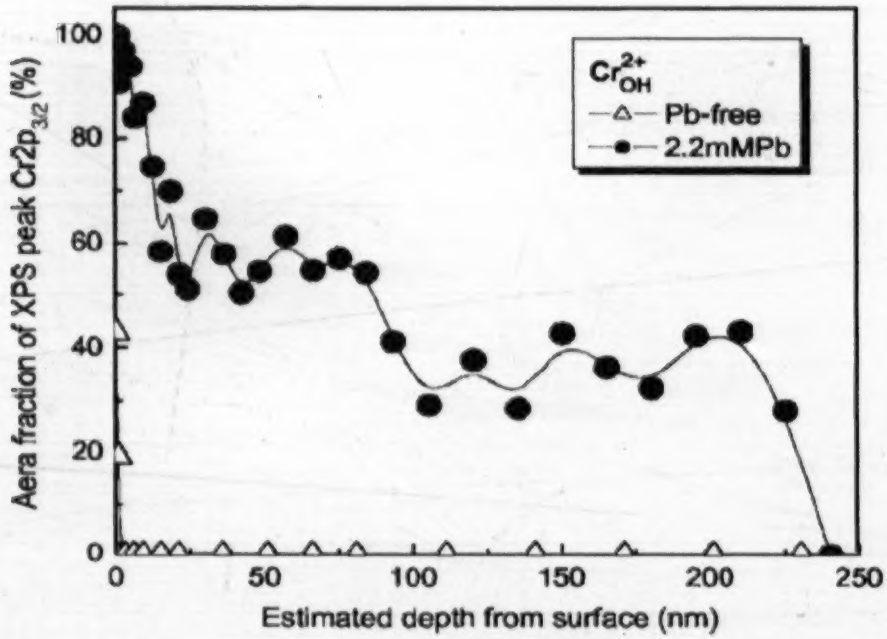

Figure 2-18 Profile of Cr_{OH}^{3+} in passive film formed on UNS N06690 at 40°C (Reproduced from Lu et al. 2007)

2.14 Effect of lead on repassivation

Repassivation of the broken passive film is a most important factor for the material to be less prone to SCC. The models of oxide film formation on the surface were explained earlier section 2.9. Burstin et al. demonstrated that the scratch technique could be used to study the repassivation behavior of the material. Kwon (2000) studied the repassivation kinetics of stainless steel in chloride solution and correlated the repassivation behavior with SCC susceptibility of the material. The repassivation behavior and SCC susceptibility at different passivation potentials in chloride solution were studied by Bernard (2005). When the passivation potential increased the SCC susceptibility increased and repassivation rate decreased. Repassivation kinetics of UNS N06690 in lead contaminated solution was studied by Ahn et al. (2006) using the scratch technique. Fig. 2-19, 2-20 show the current transient plot obtained in acidic and alkaline solutions respectively. Analysis of the transient plot showed that lead decreased the repassivation rate, and that the decrease was higher in alkaline solution compared to acidic solution. Repassivation time (t_r), which is the time taken for attaining predetermined repassivation, shown in current transient plot clearly indicated that lead increased the repassivation time, thereby decreasing repassivation rate. All the results discussed earlier were based on high speed scratch technique and Bosch et al. (2004) showed that slow scratch technique can be used to study repassivation behavior. In slow scratch technique most of the scratched area repassivated before completing the scratch, and it was very difficult to extract the repassivation parameter from the data.

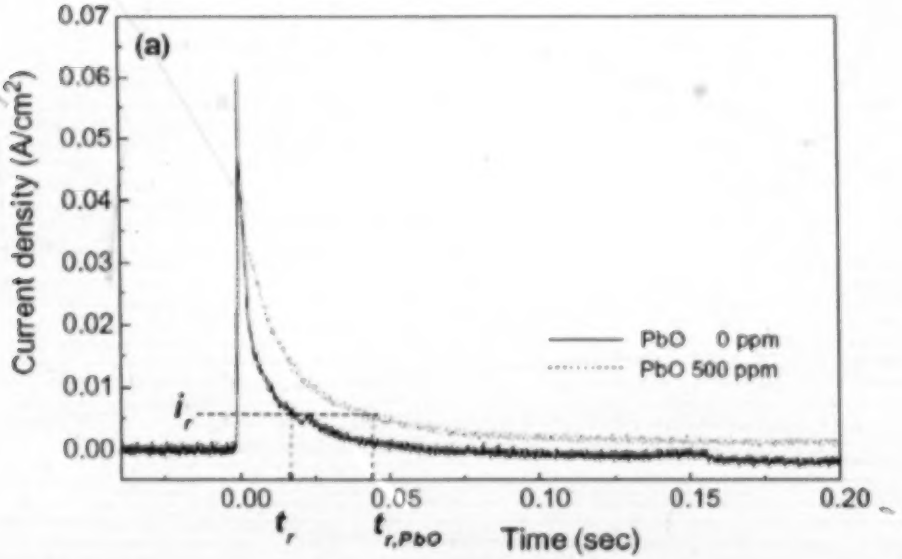

Figure 2-19 Current transient plot of UNS N06690 in 90°C , pH 4 water at an applied potential of -100 mV $_{SCE}$ (Reproduced from Ahn et al. 2006 b)

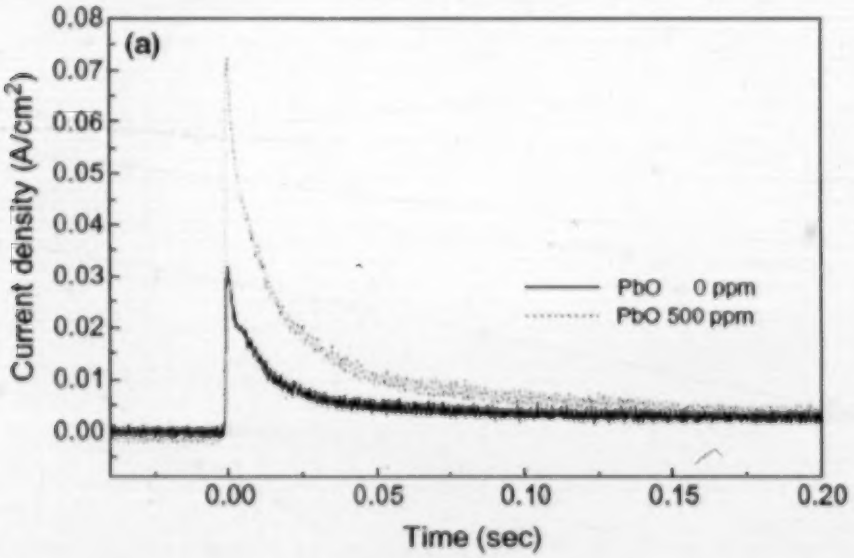

Figure 2-20 Current transient plot of UNS N06690 in 90°C , pH 10 water at an applied potential of -100 mV $_{SCE}$ (Reproduced from Ahn et al. 2006 b)

2.15 Summary

It is very clear that all the SG alloys are susceptible to PbSCC even at very low lead concentrations. Even though feed water lead concentration is in the ppt range, lead accumulates in the heat transfer crevices, leading to PbSCC. Lead induced passivity degradation is considered to be the main reason for these materials susceptibility to PbSCC. There still are many areas of the topic not studied and so PbSCC is not fully understood. In particular, the effect of dissolved ions present in the feed water is not fully elucidated. Sludges from failed tube contain dissolved ions in considerable amounts. Study of the effects of dissolved ions in the feed water on PbSCC is a vast research area. Consequently, for the following study is focused on one topic: effect of magnesium on PbSCC. Two different kinds of studies will be described. In the first part, research focused on the effect of magnesium to calcium ratio on PbSCC at room temperature. The second part of the research focused on the effect of magnesium on PbSCC at 300°C.

Chapter 3- EXPERIMENTAL PROCEDURE

3.1 Test materials

Commercial alloy 800 (UNS N08800), pure iron, nickel and chromium were used in electrochemical experiments. UNS N08800 was received from AECL and three different types of UNS N08800 used in the experiments, namely coupon, small tube (15.88×1.12 mm), and large pipe (200×12 mm). The composition of UNS N08800 is listed in table 3-1. Pure iron, nickel and chromium were received from Good Fellow and had 99.99% purity.

Table 3-1 Compositions of materials used in the experiment

Material	Al	C	Cr	Mn	S	Si	Ti	Cu	P	Co	N	Ni	Fe
UNS N08800 (Coupon) Lot No: J420	0.49	0.07	19.7	0.82	<0.001	0.14	0.57	0.30				31.52	Bal. (46.32)
UNS N08800 (Small tube) Heat No: HH9043A	0.41	0.01	21.7	0.80	0.002	0.10	0.42	0.03	0.009	0.01	0.02	34.11	Bal. (42.41)
UNS N08800 (large pipe) Heat No: 459383	0.21	0.01	20.3	0.70	<0.0005	0.61	0.53	0.01				32.34	Bal. (44.80)

3.2 Solution composition

Solution composition was designed to simulate the prevailing crevice condition in CANDU SG tubes. From the field observation and analysis of the failed tubes, a base composition of the solution was formulated. It contained Na_2SO_4, NaCl, KCl, $CaCl_2$ and NaOH was added for making alkaline solutions and $NaHSO_4$ was added for making acidic solutions. The effects of lead were studied by the addition of 500 ppm (2.2mM) lead oxide (PbO). To study the effect of magnesium in lead contaminated crevice

chemistries, magnesium was added to the base solutions without changing the overall chlorine concentration, as the chlorine concentration plays a vital role in corrosion. The pH of the solution was adjusted by adding NaOH or HCl. For room temperature tests, the solutions were prepared by adding the chemicals together and stirred for minimum of 12 hours. High temperature test solutions were prepared by adding the chemicals in an autoclave and then autoclave was sealed. All the acidic solutions were named A1, A2, A3 and A4 and basic solutions were named B1, B2, B3 and B4 and neutral solutions were named N1, N2, N3 and N4.

To study the effect of the ratio of magnesium to calcium, solutions were prepared by changing the calcium concentration of the base solution. A1 and B1 were the original versions of the acidic/alkaline crevice chemistries that were free of lead contamination. A2 and B2 were solutions made of A1 and B1 but with an addition of 2.2 mMPb (500ppm). A3 and B3 were the revised versions of A2 and B2 where half of the calcium chloride was replaced by magnesium chloride. A4 and B4 were revised version of A2 and B2 where only magnesium chloride was added without changing the calcium chloride concentration. It meant that the ratios of Mg^{2+}:Ca^{2+} in lead-containing solutions were 0 (A2 and B2), 1(A3 and B3) or 0.5(A4 and B4). In all the solutions, the chlorine concentration was kept unchanged. The compositions of acidic and basic solutions were tabulated in table 3-2 and the neutral solutions were tabulated in table 3-3. The ion concentrations were calculated using OLI software.

Table 3-2 Simulated SG crevice acidic and basic solution composition

Condition	NaCl (M)	KCl (M)	Na_2SO_4 (M)	$CaCl_2$ (M)	$MgCl_2$ (M)	HCl (M)	$NaHSO_4$ (M)	NaOH (M)	PbO (mM)	pH at 25 °C	Mg^{2+}: Ca^{2+} ratio
A1	0.3	0.05	0.15	0.15	-	-	0.05	-	-	1.61	0
A2	0.3	0.05	0.15	0.15	-	-	0.05	-	2.2	1.65	0
A3	0.3	0.05	0.15	0.075	0.075	0.01	0.05	-	2.2	1.67	1
A4	0.15	0.05	0.136	0.15	0.075	0.0007	0.014	-	2.2	2.25	0.5
B1	0.3	0.05	0.15	0.15	-	-	-	0.4	-	12.91	0
B2	0.3	0.05	0.15	0.15	-	-	-	0.4	2.2	12.90	0
B3	0.3	0.05	0.15	0.075	0.075	-	-	0.4	2.2	12.90	1
B4	0.15	0.05	0.15	0.15	0.075	-	-	0.549	2.2	12.90	0.5

Table 3-3 Simulated SG crevice neutral solution

Condition	NaCl (M)	KCl (M)	Na_2SO_4 (M)	$CaCl_2$ (M)	$MgCl_2$ (M)	NaOH (M)	PbO (mM)	pH at 300 °C
N 1	0.3	0.05	0.15	0.15	-	-	-	6.1
N 2	0.3	0.05	0.15	0.15	-	-	2.2	6.88
N 3	0.15	0.05	0.15	0.15	0.075	0.1445	2.2	6.1
N 4	-	0.05	0.15	0.15	0.15	0.2945	2.2	6.1

3.3 Sample preparation

3.3.1 Specimen for room temperature measurements

Specimens were cut from coupons with an exposed surface area of 1 cm^2. Specimens were mounted in epoxy using resin and hardener with a ratio of 5:1 and cured for 12 hours at room temperature. The exposed surface of the specimen was ground with SiC

paper of decreasing grit size of 400, 600, 800 and 1200, cleaned with distilled water and then acetone.

3.3.2 Specimen for high temperature measurements

Samples were cut from the small tube and large pipe with a surface area of 2 cm^2 and spot welded with a nickel-chrome wire (80%Cr and 20%Ni). Heat shrinkable teflon tube was used to seal the nickel chromium wire and the connection between the wire and the UNS N08800. Each specimen was ground with silicon carbide paper of grit size 600, cleaned with distilled water and finally acetone.

A slow strain rate test (SSRT) specimen is shown in Fig. 3-1. Specimens with a gauge length of 25.4 mm and a gauge diameter of 3.14mm were used. Each specimen was ground with SiC paper of 600 grit in perpendicular direction to the applied load, so that the residual surface scratch will be in the plane of stress corrosion cracking.

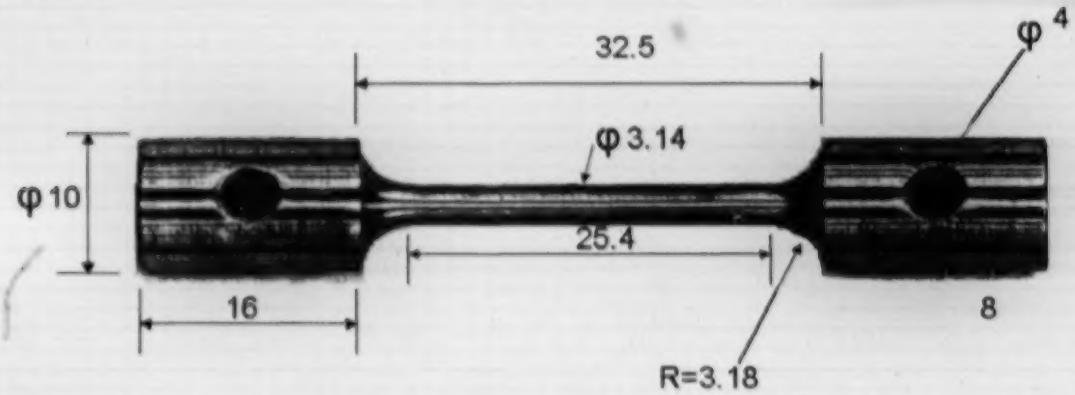

Figure 3-1 Diagram and dimension of SSRT test specimen (All dimensions are in mm)

3.4 Experimental procedure

3.4.1 Electrochemical experiments

A typical three electrode experimental setup was used in the electrochemical experiments. The schematic setup used in the room temperature test is shown in Fig. 3-2. Platinum wire was used as a counter electrode and a saturated calomel electrode (SCE) connected with a salt bridge was used as the reference electrode in room temperature experiment. The tip of the salt bridge was positioned close to the working electrode to minimize solution resistance. All the potentials measured are expressed versus SCE. Initially the solution was purged with nitrogen to remove dissolved oxygen and the sample was preconditioned at -1V $_{VS\ SCE}$ for 5 minutes to remove the passive films formed by air. The potential scan was started at -200 mV below the OCP at the rate of 1 mV/s. A Gamry 3.2 potentiostat was used in the potentiodynamic experiments.

High temperature electrochemical experiments were conducted in an autoclave. Fig. 3-3 shows the schematic electrochemical setup used in the high temperature. Specimen was used as a working electrode, platinum mesh was used as a counter electrode and Ag/AgCl was used as a reference electrode. A home made silver/silver chloride (Ag/AgCl) was used in the high temperature electrochemical test. Silver chloride was melted and deposited on the silver wire on one end. The remaining portion of the sliver wire was covered by heat shrinkable polytetrafluoroethylene (PTFE) tube and the entire silver wire was placed in the PTFE cylinder. The PTFE cylinder was filled with a potassium chloride solution with same molar concentration of chlorine ions as the test solution to avoid migration of chloride ions. Before starting the test, the reference electrode was checked and solution was deaerated by purging nitrogen. Then the

autoclave was sealed and a heater was connected with the controller was used for heating the autoclave. During heating, the specimen was kept in galvanostatic condition at -0.5 mA/cm^2 to avoid passive film formation. Once the temperature stabilized at 300°C, electrochemical experiments were started.

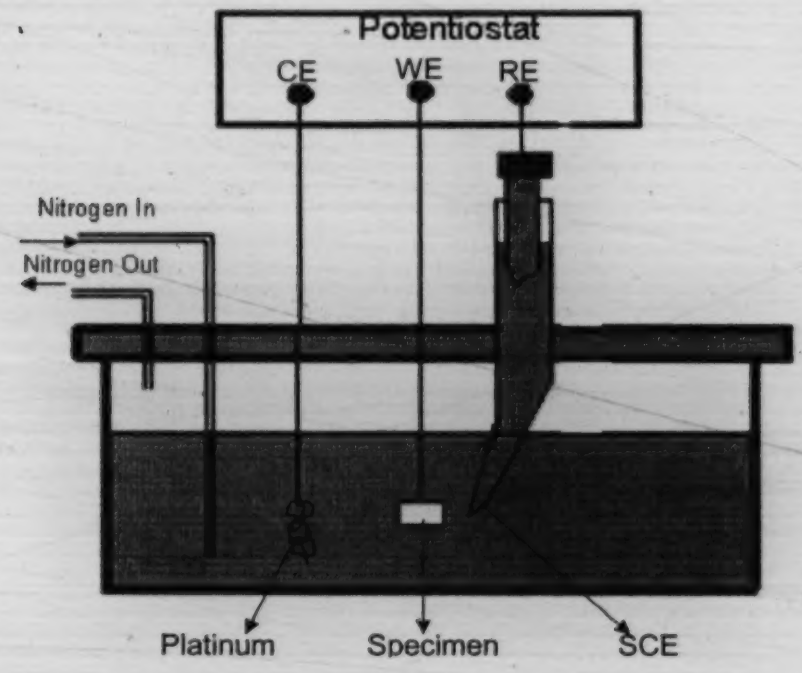

Figure 3-2 Schematic diagram of room temperature electrochemical cell setup

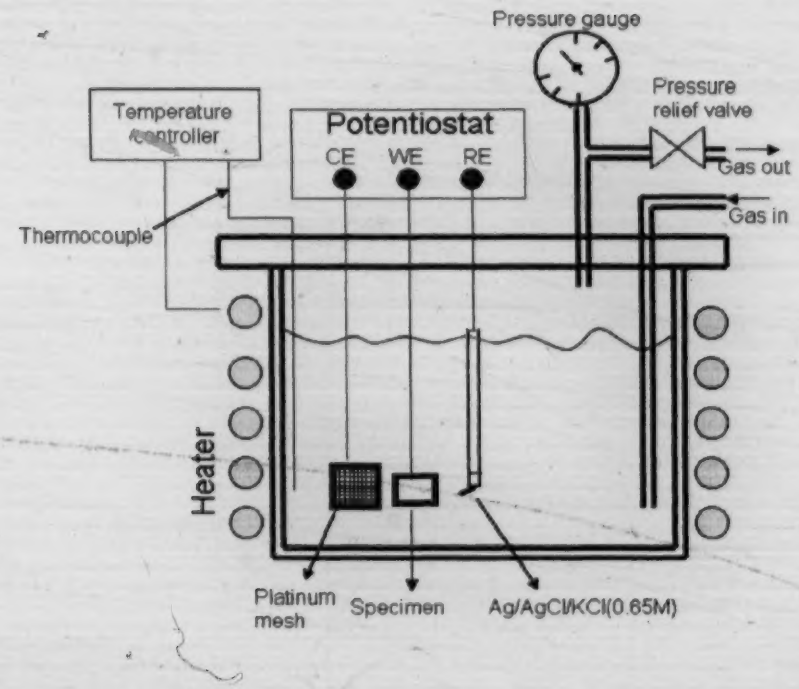

Figure 3-3 Schematic electrochemical cell setup for high temperature experiment

3.4.2 Scratch test

The three electrode cell was modified to measure the repassivation current during the scratch test. A schematic diagram of the scratch cell is shown in Fig. 3-4. The scratch test setup consists of specimen as a working electrode, a platinum wire as the counter electrode and a SCE connected with a salt bridge was used as the reference electrode. The tip of the salt bridge was kept close to the working electrode in order to reduce the ohmic potential drop between working and reference electrode. A scratch was made on the passive film formed on specimen using an alumina tip loaded on a spring. The alumina tip was pulled over the specimen to make a scratch under constant contact stress by an air operated solenoid valve. During the scratch, the potentiostatic condition was maintained and the duration of scratch was less than 1 ms. The repassivation current from the scratch

was measured at 1 ms interval using the Auto lab electrochemical measurement system and the data was processed for further analysis.

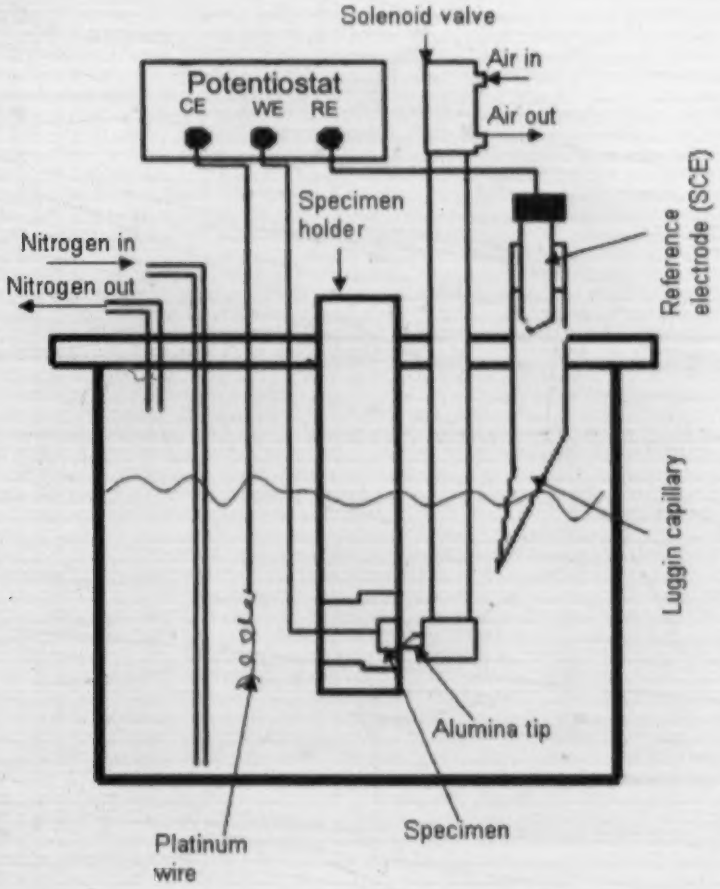

Figure 3-4 Schematic diagram of scratch cell setup

3.4.3 Slow strain rate test (SSRT)

SSRT test was conducted at 300°C in an autoclave and the schematic diagram of the test setup is shown in Fig. 3-5. The specimen was connected to a pressure balancing pull rod and the solution was purged by nitrogen before starting the experiment. The specimen was isolated from the pull rod using a PTFE covered pin, which was used as a

connector for the specimen and the pull rod. The autoclave was sealed before heating and a constant extension of $1.322*10^{-4}$ mm/s was applied once the temperature stabilized at 300°C. During the test the cross head position of the load cell was controlled at a rate of $1.322*10^{-4}$ mm/s. All the tests were conducted at OCP.

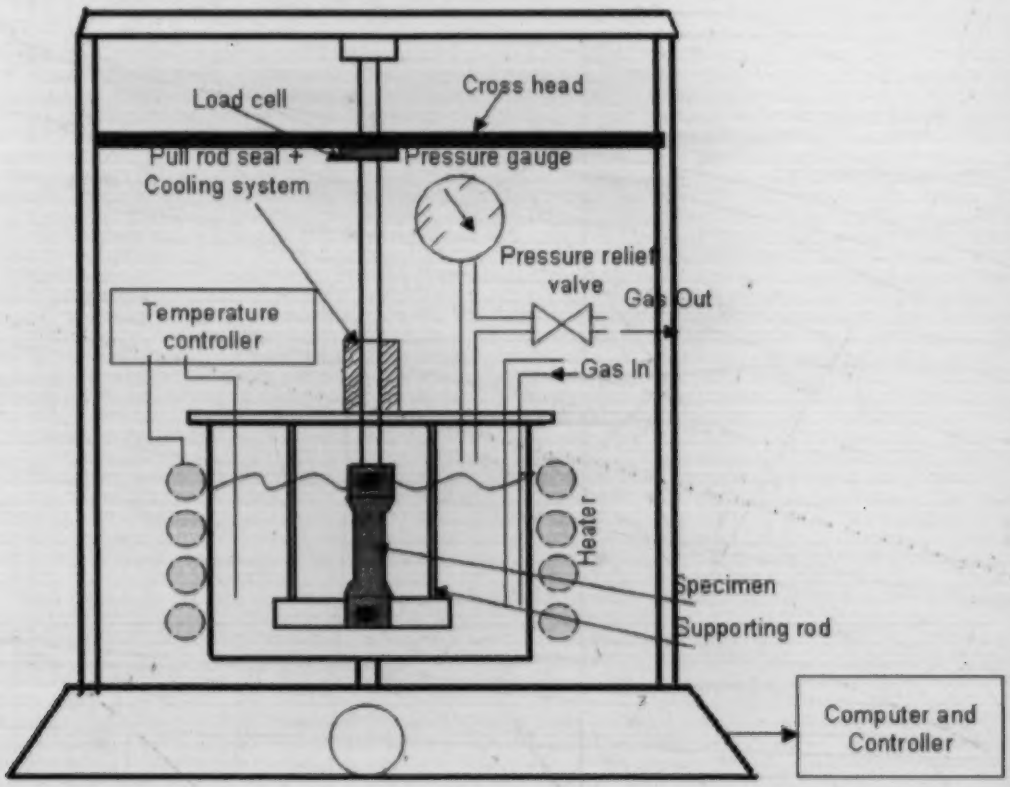

Figure 3-5 Schematic diagram of SSRT test set up

3.4.4 Mott-Schottky test

To analyze the electronic properties of the passive film, Mott-Schottky plots were determined for each of the passive films with a CMS 300 EIS measurement system. The potential was scanned in the anodic direction of the passive range at 5 mV per step and an

AC signal with a frequency of 1,000 Hz and peak-to-peak magnitude of 10 mV were superimposed on the scanning potential. AC impedances were measured as a function of the potential. The capacitance values were calculated from the imaginary part of impedance, assuming an equivalent circuit with resistance and capacitance in series. The impedance of the space charge layer is much smaller than that of the charge transfer resistance of the passive film at 1,000 Hz (Memming)

3.4.5 X-ray diffraction (XRD)

Passive films are characterized using X-Ray diffraction technique which is based on the Bragg equation

$$2d\sin\theta = n\lambda \qquad 3\text{-}1$$

where d is distance between the planes of crystal, θ is angle between X-Ray and sample and λ is wavelength of X-Ray radiation. Thin film analysis was done on the passive film at a small angle of 1θ axis was used to scan entire surface. The peak obtained by this method accounts for top layer of the sample surface which has a thickness around few angstroms. This helped us to get the crystalline phases of the deposited material. X-Ray analysis was done on a rotating anode rigaku ("Rotaflex") X-Ray diffractometers.

Chapter 4- RESULTS AND DISCUSSION

4.1 Effect of magnesium on PbSCC of UNS N08800

PbSCC of SGs was extensively reviewed in Chapter 2. However there was a lack of information regarding the water chemistry on PbSCC. In this section, the effect of magnesium on PbSCC of UNS N08800 was studied at 300°C.

4.1.1 SSRT test results

SSRT test was conducted in neutral crevice chemistry solution at 300°C. Initial study by Copson et al. revealed that PbSCC of UNS N06600 was TGSCC, but subsequent studies refuted this conclusion (Saki et al. 1992, Takamatsu 1997, Hwang et al. 1999, Lumsden et al. 2005). In general UNS N06600 MA sustain IGSCC and UNS N06600 TT, UNS N06690 TT sustain TGSCC (Staehle 2005). However, some works have also reported mixed mode of fracture for UNS N06600 TT. As discussed in Chapter 2, PbSCC depends on pH, potential, alloy composition, alloy microstructure, temperature, solution composition and stress. UNS N08800 is iron based compared to UNS N06600 and UNS N06690 which are nickel based. In duplex stainless steel, the microstructure of steel plays an important role in SCC and the presence of austenitic, ferrite phase can also lead to galvanic corrosion between the phases (Tsai et al.).

The tensile test was carried out in different neutral crevice solutions at 300°C to study the SCC behavior of UNS N08800. Fig. 4-1 shows the stress-strain curve obtained at OCP at 300°C. Fig. 4-2 shows the values of ultimate tensile stress (UTS), reduction area (RA) and fracture strain obtained in four solutions. In lead contaminated solution

(N2), values of UTS, RA and strain fracture reduced sharply when compared to that of lead free solution. The reduction in these parameters clearly indicated that the presence of lead decreased mechanical properties of UNS N08800. The addition of 0.075 M magnesium to the lead contaminated solution (N3) resulted in a significant increase in the values of UTS, RA and fracture strain compared to that of the solution containing only lead. Increasing the magnesium concentration to 0.15 M in lead contaminated solution (N4) led to the increase of UTS, RA and fracture strain value as compared to the solution containing only lead. On the other hand, while comparing lead contaminated solutions containing 0.15 M and 0.075 M of magnesium concentration there were very marginal differences in the UTS, RA and fracture strain value.

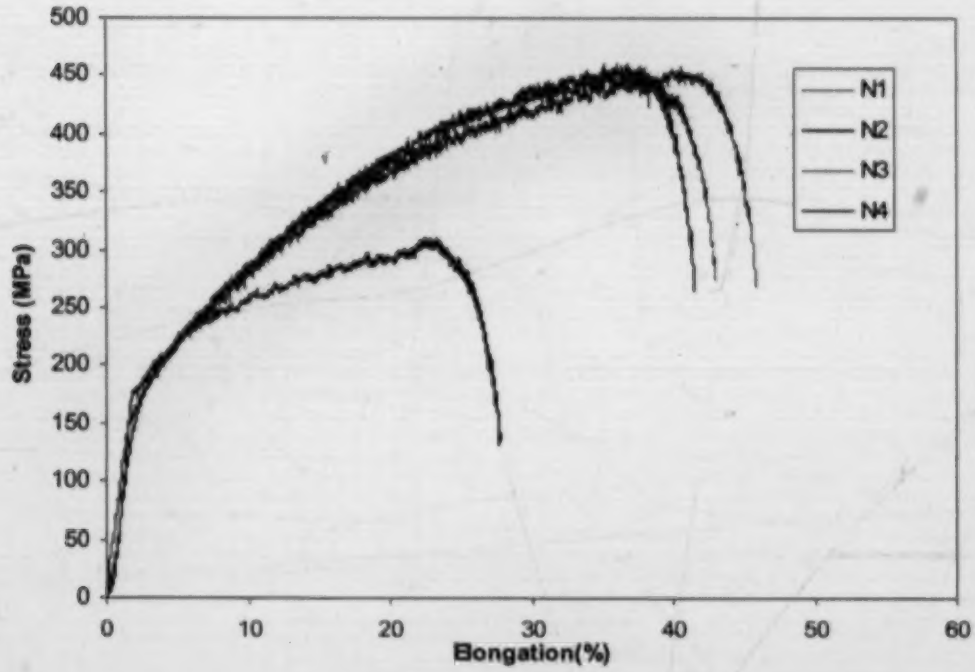

Figure 4-1 Stress-elongation curve of UNS N08800 in neutral crevice solution at 300°C

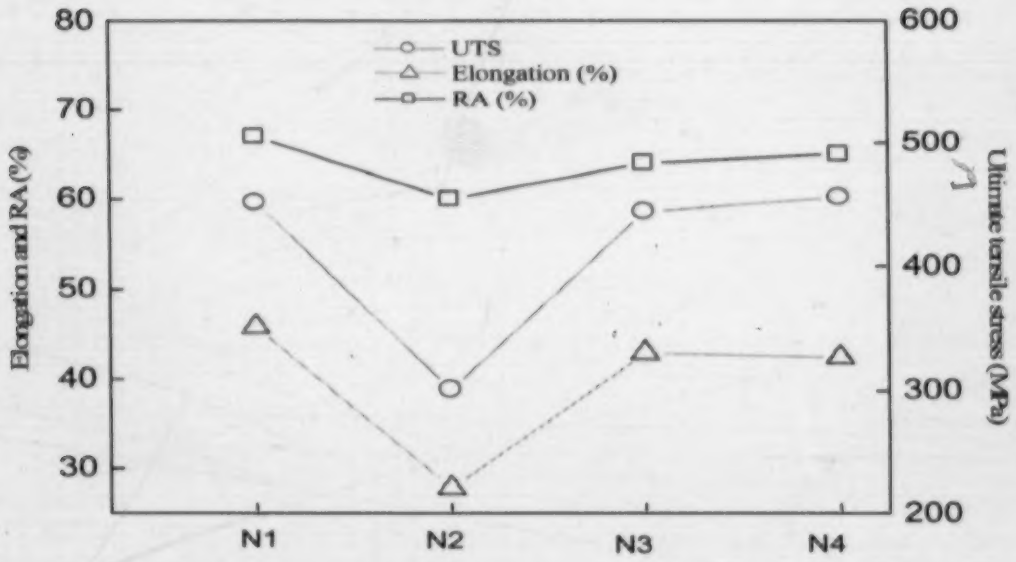

Figure 4-2 Ultimate tensile stress (UTS), reduction area (RA) and elongation of UNS N08800 in neutral crevice solution at 300°C

4.1.2 Side view and fractographic observation

SEM photograph was used as supporting evidence in explaining the fracture morphology on UNS N08800. Fig. 4-3 shows the fracture surface of UNS N08800 in neutral crevice solution at 300°C. The fracture surface in lead free solution (N1) consists of dimple tearing fracture indicating that the fracture was mainly ductile in nature. The fracture surface in lead contaminated solution was mostly brittle and the ratio of ductile to brittle area significantly reduced compared to that of fracture in lead free solution. The ratio of ductile to brittle area measured in lead free and lead contaminated solution were 3.53 and 0.56. It clearly indicated that lead reduces the ductile area on the fracture surface. Cleavage was clearly visible on the fracture surface, which confirmed the brittle

fracture in lead contaminated solution. Addition of 0.075 M magnesium changed the fracture morphology from brittle to ductile in lead contaminated solution and surface contained mostly dimple fracture. As the magnesium concentration increased to 0.15M in lead contaminated solution, the fracture surface was mainly composed of dimples which indicated the fracture was ductile in nature. The ductile to brittle ratio in N3 and N4 solutions were 2.73, 3.00. As the magnesium concentration increased from 0.075M (N3) to 0.15 M (N4), the ductile to brittle ratio also increased but the increase was marginal compared to N3 solution. Fig. 4-4 is a magnified version of Fig. 4-3. It clearly supported the fracture morphology discussed earlier. The dimples tearing fracture were seen in lead free, 0.075 M, 0.15M magnesium containing solution at higher magnification whereas the lead contaminated solution without magnesium did not show any dimple fracture on the surface at higher magnification. Fig. 4-5 shows the side views of the fracture surface obtained in four neutral crevice solutions at 300°C. The side view of fracture in lead free solution showed clear necking on the fracture surface. The fracture side view obtained in lead contaminated solution showed the mixture of necking and cleavage tearing on the fracture surface. In both 0.075M and 0.15M magnesium, necking was clearly visible on the side view of the fracture.

600 micrometers
NT. fracture (SE)

(a)

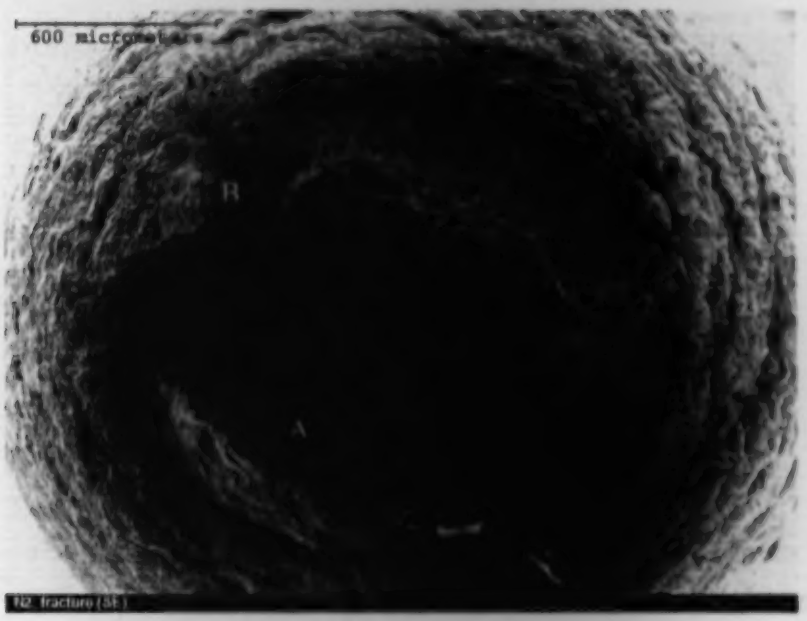
600 micrometers
R
T2: fracture (SE)

(b)

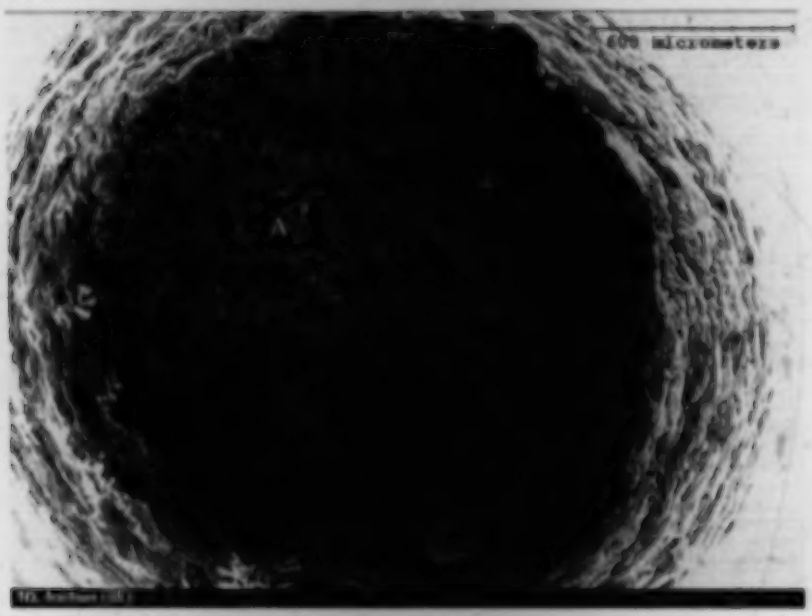

(c)

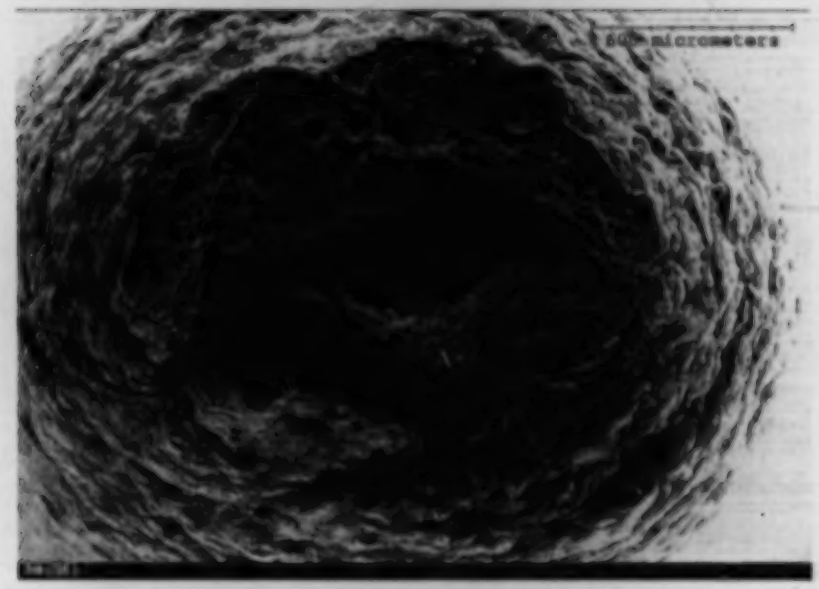

(d)

Figure 4-3 SEM fractrographs of fracture surface after SSRT testing in different neutral crevice solution at 300°C (a) N1, (b) N2, (c) N3 and (d) N4

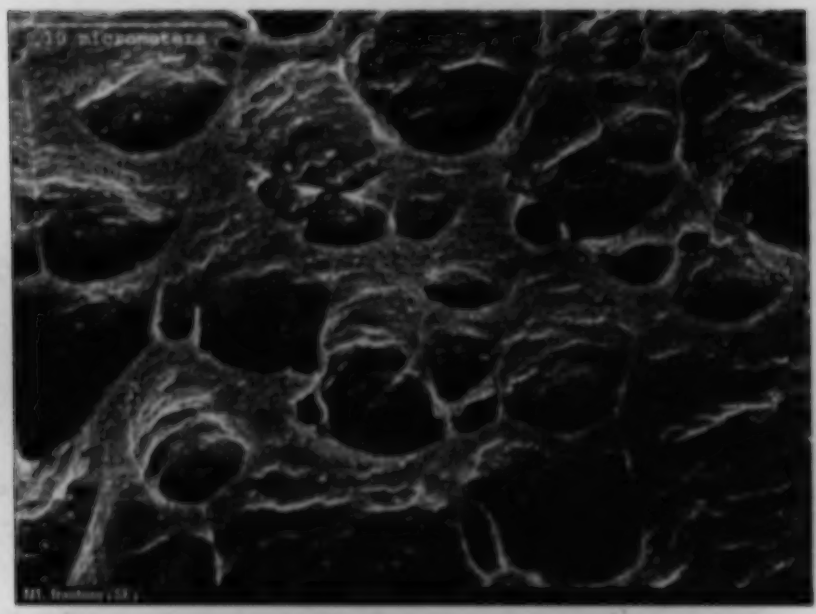

(a)

(b)

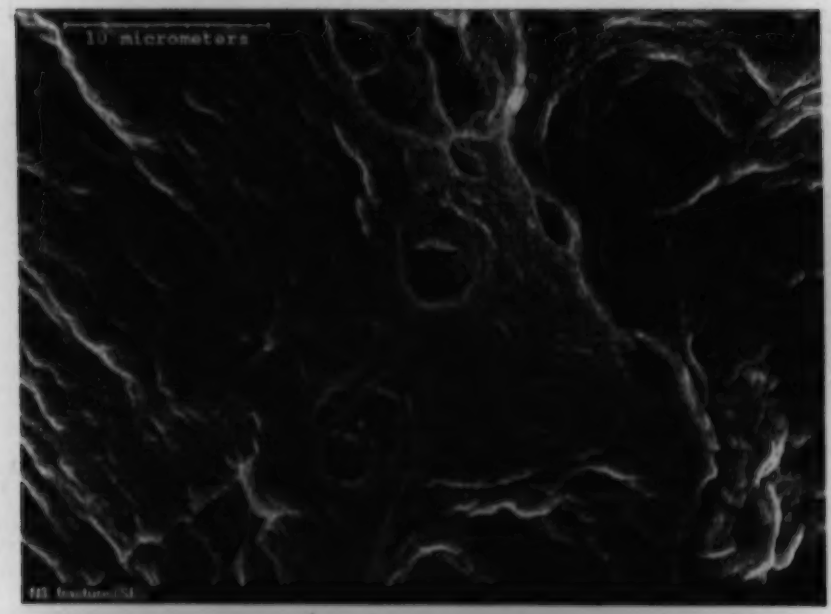

(c)

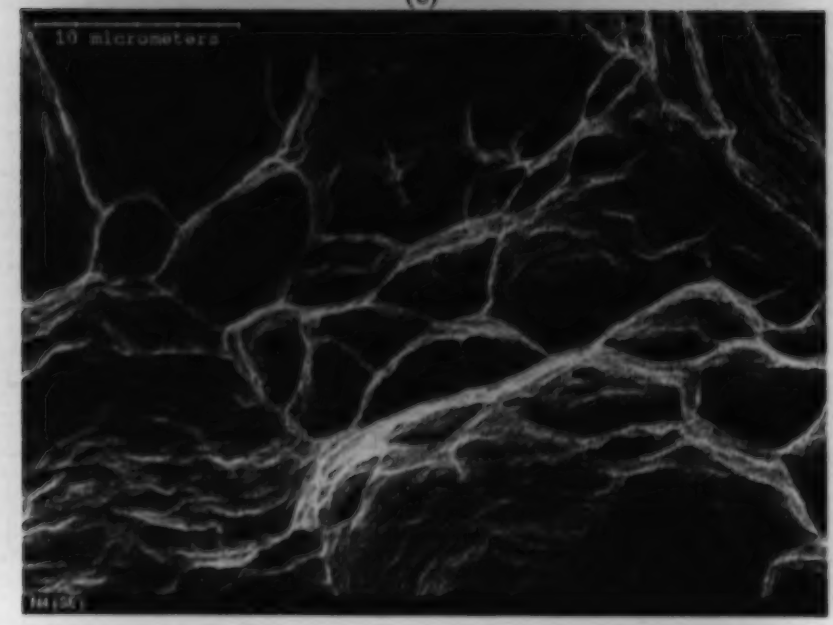

(d)

Figure 4-4 Higher magnification of fracture surface marked as A in Fig. 4-3 (a) N1, (b) N2, (c) N3 and (d) N4

(a)

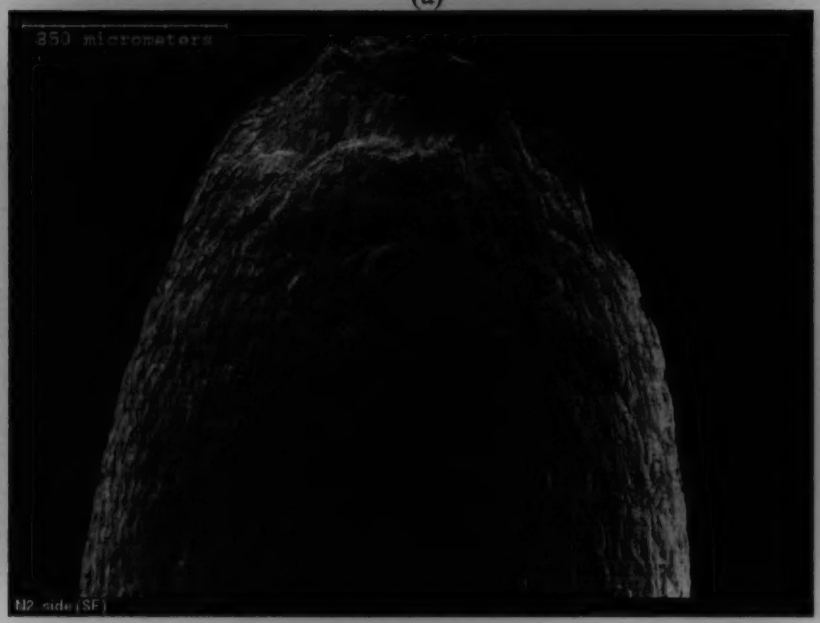

(b)

(c)

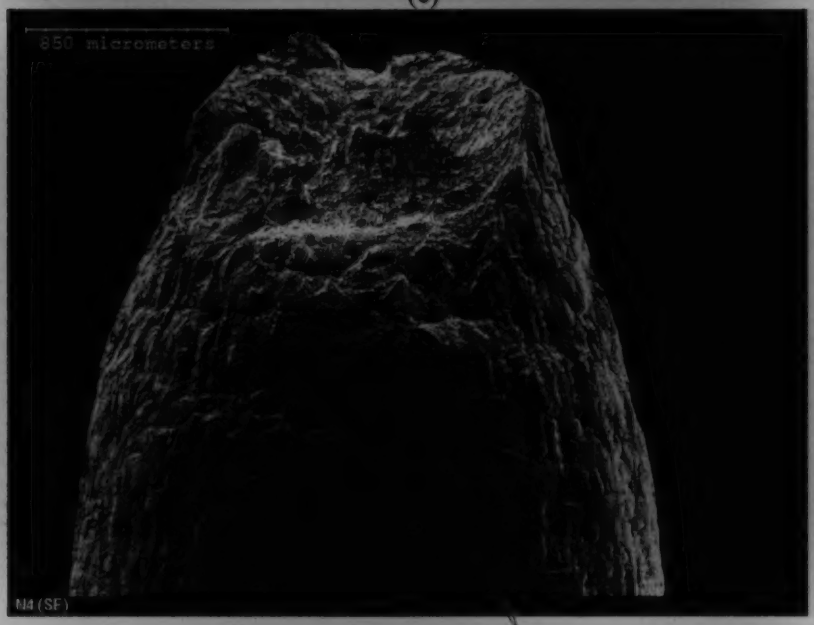

(d)

Figure 4-5 Side view of UNS N08800 after SSRT testing in different neutral crevice solution at 300°C (a) N1, (b) N2, (c) N3 and (d) N4

From Fig. 4-3, no secondary cracks were seen on the fracture surface in N1, N3 and N4 solutions. But in N2 solution secondary crack was seen on the edges of the fracture surface as shown in Fig. 4-6, which was enlarged from the point B in Fig. 4-3 (b). The secondary cracks were not seen on the interior of the fracture surface. The cracks were transgranular and are consistent with the published results (Staehle 2005).

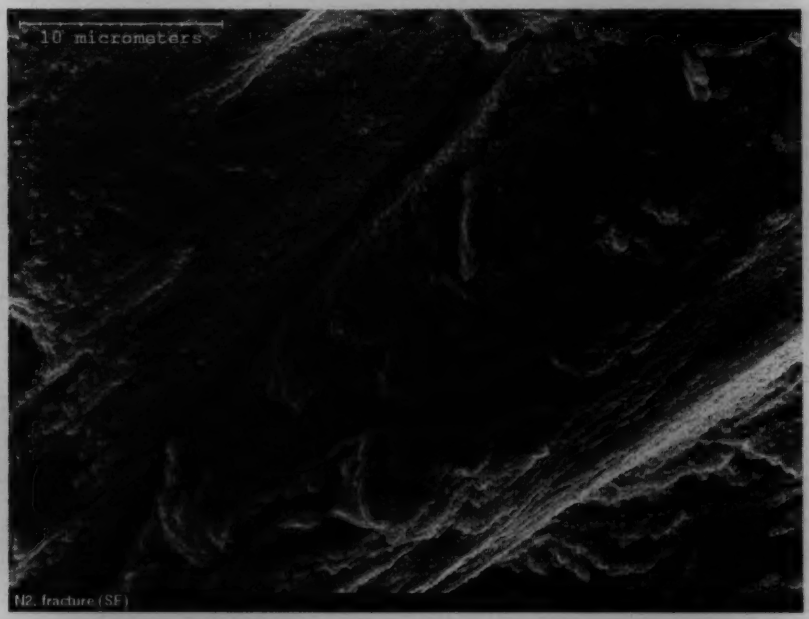

Figure 4-6 Higher magnification of N2 fracture surface marked as B in Fig. 4-3 (b)

4.2 Effect of Mg/Ca ratio and magnesium on lead induced corrosion of UNS N08800

It was believed that lead induced SCC is due to degradation of passive film. In order to understand mechanism of PbSCC and effect of magnesium to calcium ratio on PbSCC, a series of electrochemical tests and scratch tests were conducted at room temperature in

alkaline and acidic crevice solutions. The effect of magnesium on PbSCC was studied at 300°C by electrochemical experiments and surface analysis of the passive films to understand the lead induced passivity degradation. During the growth of passive film, movement of cations and anions in the passive film led to a change in electronic structure of the passive film. Mott-schottky experiment was carried out at room temperature and at 300°C to study the effect of magnesium to calcium ratio and the effect of magnesium on PbSCC of UNS N08800.

4.2.1 Polarization behavior of UNS N08800

4.2.1.1 Effect of magnesium and calcium ratio on the polarization behavior

Fig. 4-7 shows the polarization behavior of UNS N08800 in the acidic crevice chemistries. The results indicated that the effect of the chemical composition of acidic crevice solutions on the passive current density was limited. However, the presence of lead contamination can reduce the pitting potential (A2 vs. A1). When the ratio of Magnesium to calcium was 1 or 0.5 in solution, the detrimental effect of lead species on pitting potential disappeared. The pitting potential was higher in A3 and A4 when compared to that in A2.

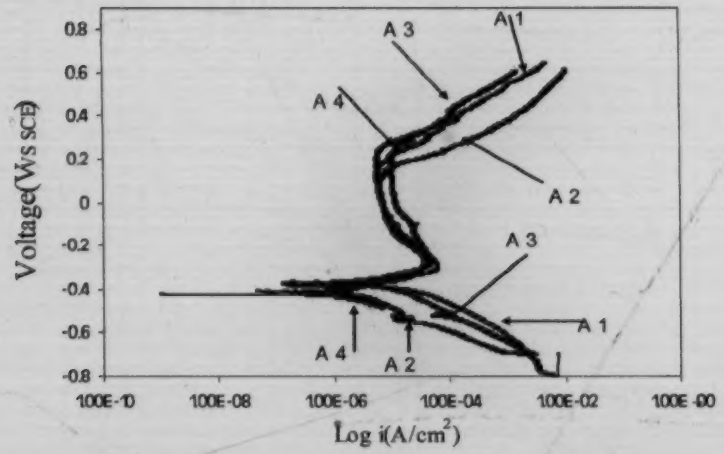

Figure 4-7 Polarization behavior of UNS N08800 in acidic crevice chemistries

The polarization behavior of UNS N08800 in alkaline crevice chemistry was quite different from that in acidic ones (Fig. 4-8). Again, the passive current density was not very sensitive to the addition of PbO. As it was reported earlier, the presence of lead contamination can induce an anodic current peak at a potential of around -0.48 V_{SCE} (B2 vs. B1). This is caused by anodic dissolution of deposited metallic lead formed during the cathodic precondition and probably the lead induced selective dissolution of nickel. (Lu 2005, Lu et al. 2007, Feron et al.). However, when magnesium chloride was added to replace half of the calcium chloride (B3), the anodic current peak disappeared and the passive current density at a potential below -0.55 V_{SCE} was reduced significantly. But in the solution (B4), where magnesium chloride was added without changing the calcium chloride concentration, anodic peak was present. The magnitude of anodic peak was less when compared to that of lead contaminated solution (B2). Fig. 4-8 indicates that the effect of lead, calcium and magnesium species on anodic polarization behavior is difficult to explain in alkaline crevice solutions.

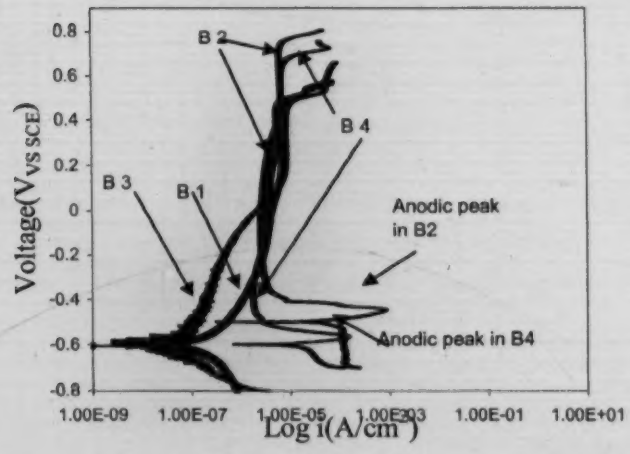

Figure 4-8 Polarization behavior of UNS N08800 in alkaline crevice chemistries

4.2.1.2 Effect of magnesium on polarization behavior at 300°C

Polarization behavior of UNS N08800 in neutral crevice condition is shown in Fig. 4-9. It was observed that presence of lead increased the anodic dissolution, passive current density and decreased the open circuit potential. The polarization results of N1, N2 were comparable with published results (Lu 2005). The increase in anodic peak was due to the dissolution of metallic lead formed during cathodic pretreatment as shown earlier (Hwang et al. 2002, Ahn et al. 2006 b). However the addition of magnesium increased OCP, pitting potential and reduced passive current density compared to that of lead contaminated solution. The magnitude of decrease in passive current density was higher in N4 solution compared to that of N3 solution.

As pointed out by Feron et al., the metallic lead was formed on the surface by following reactions:

$Ni + PbO \rightarrow NiO + Pb$	ΔG: -26.4 KJ/mol	4-1
$3Fe + 4PbO \rightarrow 4Pb + Fe_3O_4$	ΔG: -248 KJ/mol	4-2
$2Cr + 3PbO \rightarrow 3Pb + Cr_2O_3$	ΔG: -474 KJ/mol	4-3

One of the possible mechanisms for the reduction in passive current density is probably the formation of complex ion with magnesium in N3 and N4 solutions and it reduced the availability of lead oxide for reduction through reactions 4-1 to 4-3. The thermodynamic feasibility of magnesium reduction is low and this can be substantiated with EDX analysis of the passive film formed on UNS N08800. EDX survey of passive films formed on UNS N08800 was shown in Fig. 4-10. Lead incorporation observed in the passive film formed in N2 solution. It was reduced substantially for the passive film formed in N3 and N4 solutions. At the same time, magnesium incorporation was not taking place during passive film growth in N3 and N4 solution.

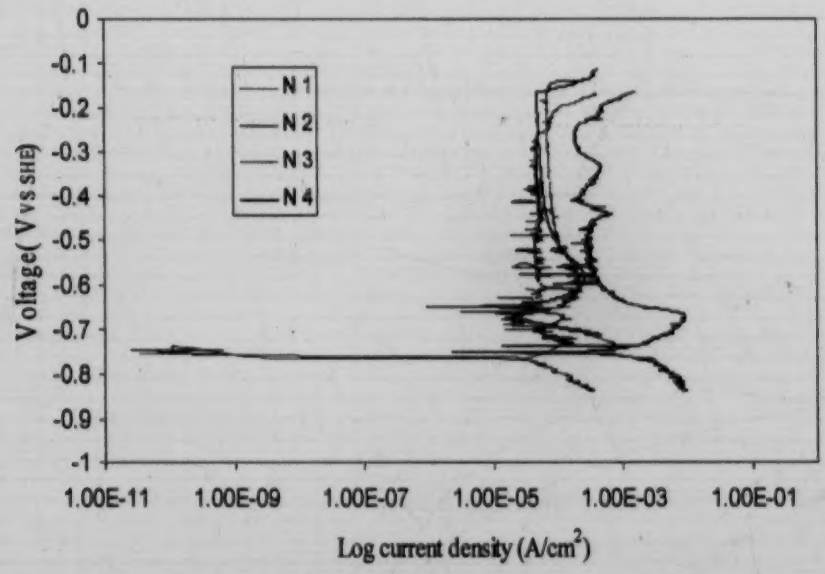

Figure 4-9 Polarization diagram of UNS N08800 at 300°C in neutral crevice solution

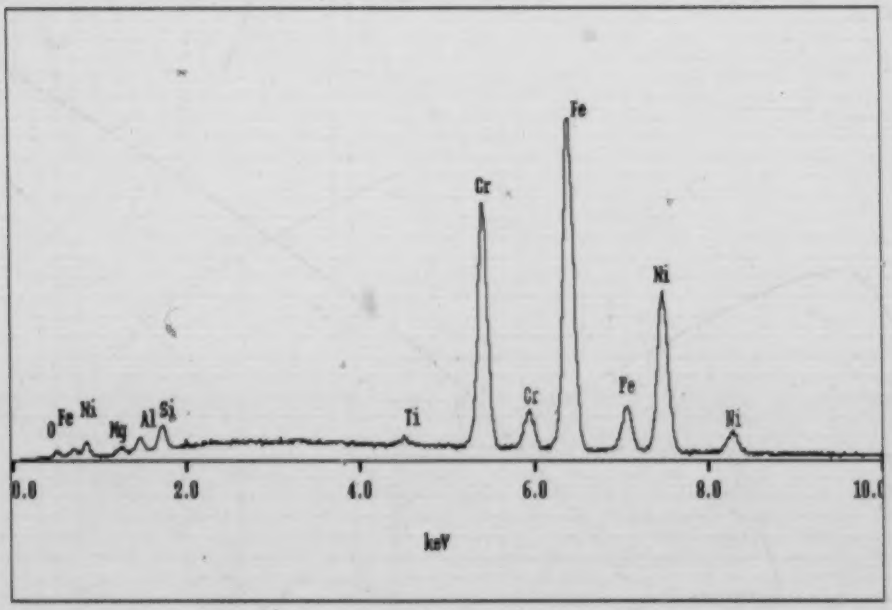
O
Fe
Ni
Mg
Al
Si
Ti
Cr
Fe
Cr
Fe
Ni
Ni
0.0
2.0
4.0
6.0
8.0
keV

(a)

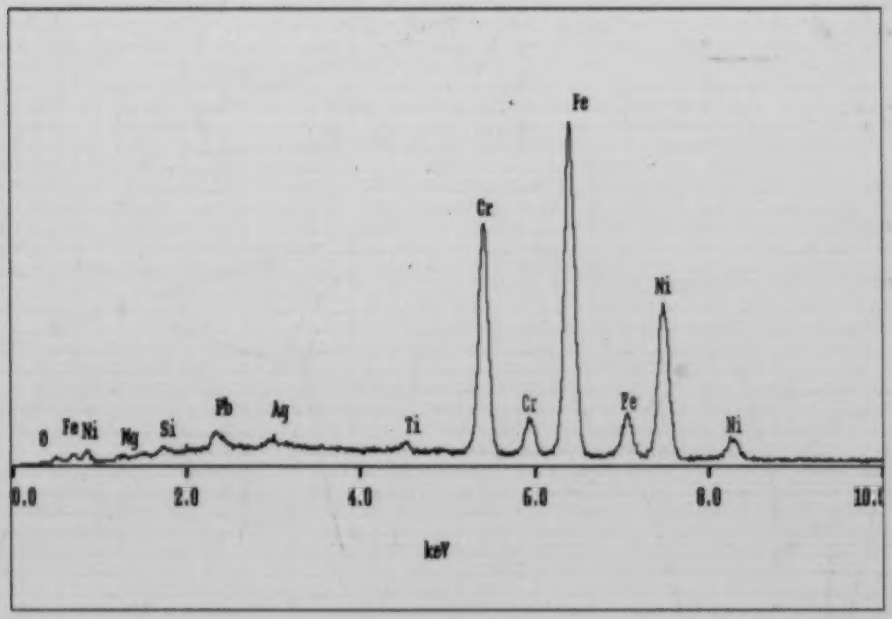
O
Fe
Ni
Mg
Si
Pb
Ag
Ti
Cr
Fe
Cr
Fe
Ni
Ni
0.0
2.0
4.0
6.0
8.0
keV

(b)

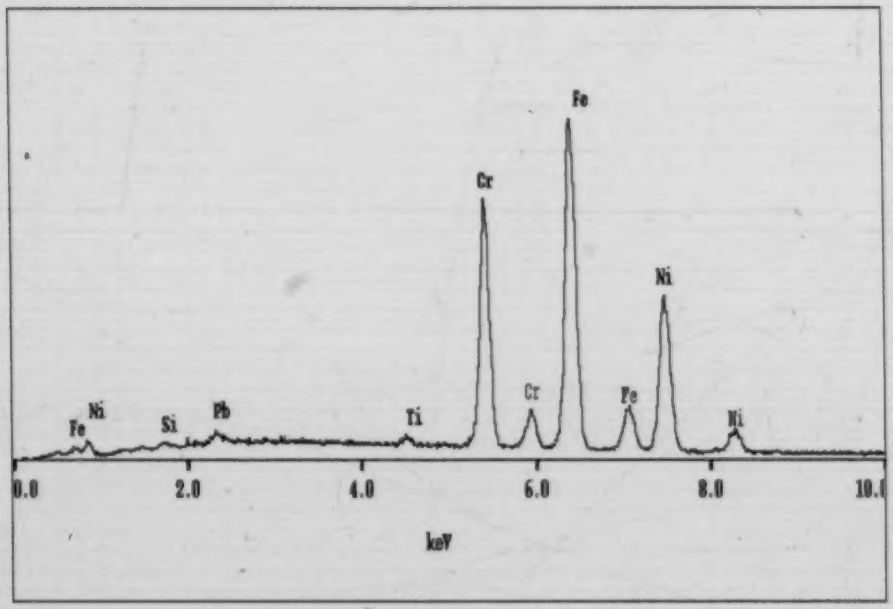

(c)

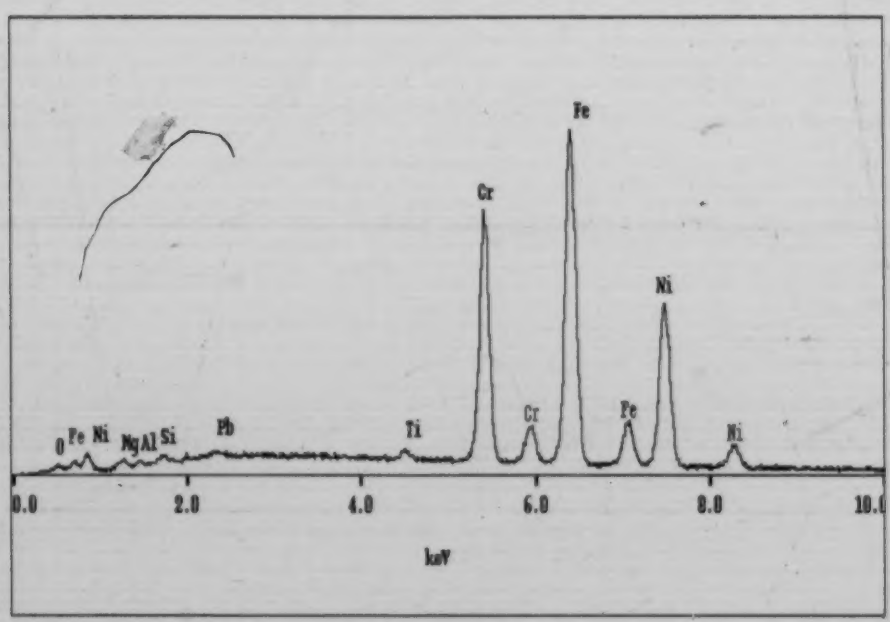

(d)

Figure 4-10 EDX survey of passive film formed on UNS N08800 at 300°C for 24 hours in different neutral crevice solution (a) N 1, (b) N 2, (c) N 3 and (d) N 4

The EDX analysis of passive film formed in N2 condition showed the presence of the silver around 0.4 at.%. This might be due to the dissolution of silver contamination from reference electrode. The lead at.% in the passive film was 0.76, 0.42, 0.2 in N2, N3 and N4 solution respectively. The magnesium peak was not clear in Fig. 4-10, however magnesium was present in the passive film formed in all four solutions in small amount and this might be due to magnesium impurity. The magnesium at.% in the passive film was 1.42, 0.84, 0.78, and 1.26 in N1, N2, N3 and N4 solution respectively. It was indicated from the results shown in Section 4.1 that the magnesium present in the passive film was not detrimental to the SCC.

4.2.2 Effect of magnesium to calcium ratio on semi conducting properties of passive film

Mott-Schottky analysis on the passive film is commonly used to investigate the electronic properties of the passive film. There are two capacitances in series with the electrode/electrolyte interface, a helmholtz layer and a space charge layer. Since the capacitors are in series the total impedance value is the sum of the inverse of the individual capacitance. At a high concentration (>0.001M), capacitance of the helmholtz is very high compared to that of the space charge layer. Since both the capacitance are connected in series, inverse of the helmholtz layer will be much smaller than that of the space charge layer. Under the current test condition, the space charge layer capacitance is much smaller than that of the helmholtz layer; the total measured capacitance is normally related to the capacitance of the space charge layer. The capacitance was calculated by

$$C = \frac{1}{\omega Z''} \qquad 4\text{-}4$$

where ω is the angular frequency and Z'' is the imaginary part of impedance. The capacitance of a space charge layer for a n-type semiconductor can be expressed by the Mott-Schottky relationship (Morrison):

$$\frac{1}{C^2} = \frac{2}{\varepsilon\varepsilon_0 N_D}\left(V - V_{fb} - \frac{kT}{e}\right) \qquad 4\text{-}5$$

where ε is the dielectric constant of the passive film, which is usually 15.6 for most iron-based alloys (Simoes et al.), ε_0 is the permittivity of vacuum, e the electron charge, N_D the donor density, V_{fb} the flat band potential, k the Boltzmann constant and T is the absolute temperature. From Equation 4-5, donor density can be found out from the slope of $1/C^2$ vs. V plot and the flat band potential can be obtained from the extrapolation of the linear portion of the plot to $1/C^2 = 0$.

Fig. 4-11 (a) shows the Mott-Schottky plot obtained for the passive film formed at pH 1.6 in lead free and lead containing solutions. Results showed that the passive film formed on the UNS N08800 was a n-type semiconductor and the findings were consistent with the ones reported by Montemor et al., who studied the electronic properties of passive films formed on 316L at 22°C in borate buffer solution. Donor density was correlated to the defects in the passive film. A passive film with a high donor concentration will have more defects (Macdonald 1992). Therefore its stability can be related to the donor density of the n-type semiconductor. Fig. 4-11 (b) shows Mott-Schottky plots obtained for the passive film formed at pH 12.9. This plot showed similar trend as that of the passive films formed at pH 1.6.

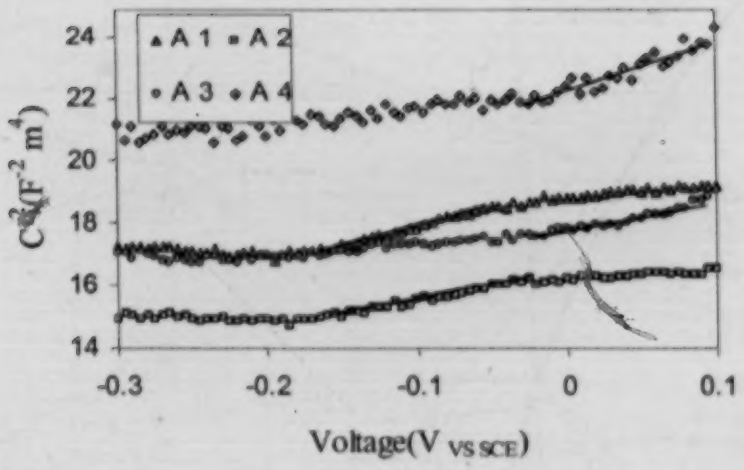

(a)

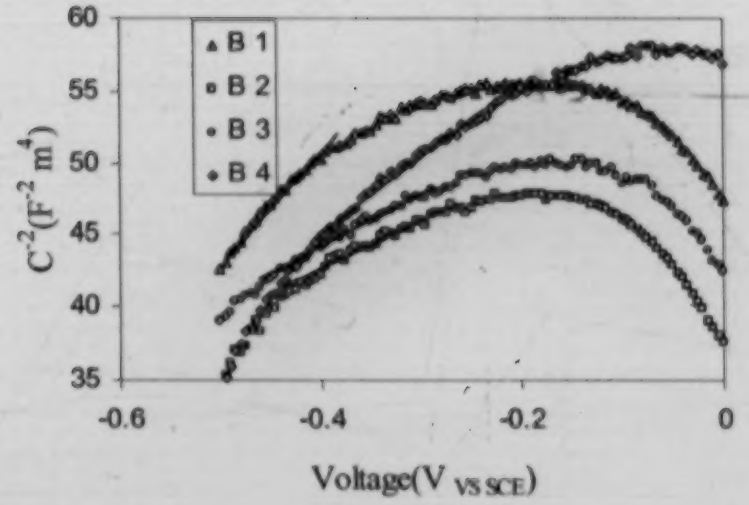

(b)

Figure 4-11 Mott-Schottky plots for passive films formed on UNS N08800 in the solution at (a) pH 1.6, (b) pH 12.9

The donor density of the passive film formed in all the eight solutions were calculated from the linear region of the plot. The results were shown in Fig. 4-12. Initially the

curves were divided into segments and the slope of each segment was calculated using linear regression method. The segment with R^2 value close to one was chosen. In this segment the appropriate potential range was chosen by trial and error method using linear regression. The slope of the linear part was lower in lead containing solutions A2 and B2. Increase in magnesium to calcium ratio in both the solutions increased the corresponding slope. The decrease in slope A2 and B2 might be due to either increased value of dielectric constant or increased donor density of the passive film. The dielectric constant of alloying element oxides are NiO (11.9), Cr2O3 (~12), FeO (14.2) and PbO (25.9) (CRC Handbook 2006). The at.% of lead in the passive film was less than 1 at.%, so the reduced slope was mainly due to the increased donor density of the passive film. The results showed that the defect densities of the passive films formed in lead containing solutions without Mg at pH 1.6 and pH 12.9 had more defects compared to the passive film formed in other solutions. In lead containing solutions with a ratio of magnesium to calcium 0.5 had lower defects compared to the one formed in the solution with ratio 1. Donor density was higher in the passive film formed at pH 1.6 compared to the passive film formed at pH 12.9 in both lead free and lead containing solutions.

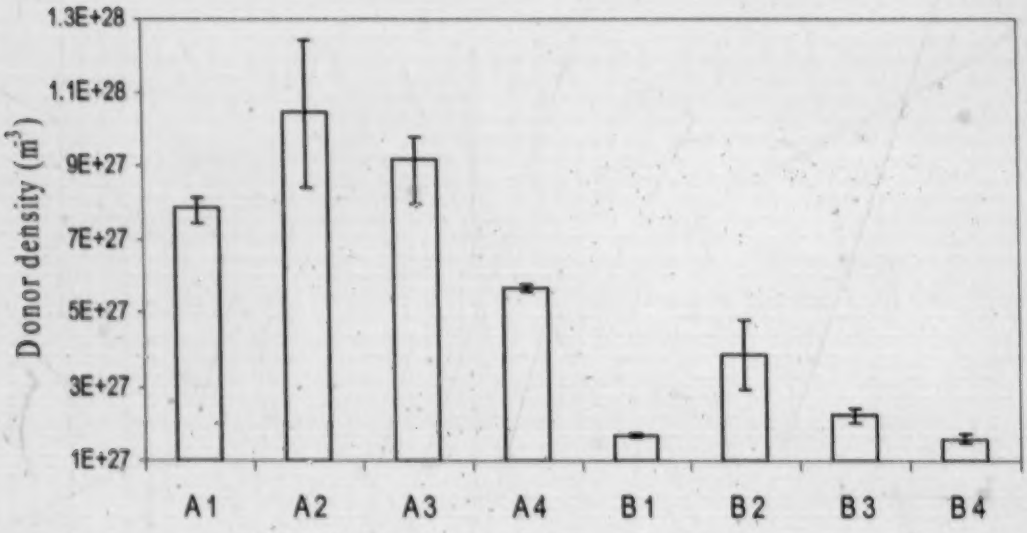

Figure 4-12 Donor density of passive film formed on UNS N08800 at different pH

4.2.3 Effect of magnesium on semi conducting properties of the passive films formed at 300°C

Fig. 4-13 shows Mott-Schottky plots of the passive film formed on UNS N08800 in neutral crevice solutions at 300°C. In all the conditions, -490 mV $_{VS\ SHE}$ was used as a film form potential. As discussed in Section 4.2.2, the passive film formed on UNS N08800 was a n-type semiconductor and the donor density of the passive film can be calculated using Equation 4.5. There exists a linear region in all the plots which were selected using the linear regression method. Donor density of the passive film was calculated using the slope of the linear region. Fig. 4-14 shows the donor density of the passive film formed in different solutions. Donor density was higher in lead containing solution without magnesium addition (N2), whereas it was decreased by the addition of magnesium in lead contaminated solutions (N3, N4). According to the physio-chemical process that takes place in passive film formation, cation vacancies are created in film-

electrolyte interface and anion vacancies are created in metal-film interface. The cation vacancies are created by the following reactions (Macdonald 1992):

$$Ni_{Ni} \rightarrow Ni^{2+} + V_{Ni}^{"} \qquad 4\text{-}6$$

$$Fe_{Fe} \rightarrow Fe^{2+} + V_{Fe}^{"} \qquad 4\text{-}7$$

$$Cr_{Cr} \rightarrow Cr^{3+} + V_{Cr}^{'''} \qquad 4\text{-}8$$

According to PDM, cation vacancies produced at the film/electrolyte interface move towards the metal/film interface and oxygen vacancies move the other way around. The incorporation of lead happens during the growth of passive film as shown in EDX result in Section 4.2.1.2. The incorporation of lead in the passive film takes place through the reaction between the cation vacancies with the lead ions present in the solution (Equation 4-9 to 4-11), leading to dissolution of respective metal elements (Lu et al. 2007).

$$Pb^{2+} + V_{Ni}^{"} \rightarrow Pb_{Ni} \qquad 4\text{-}9$$

$$Pb^{2+} + V_{Fe}^{"} \rightarrow Pb_{Fe} \qquad 4\text{-}10$$

$$Pb^{2+} + V_{Cr}^{'''} \rightarrow Pb_{Cr}^{'} \qquad 4\text{-}11$$

The reaction between trivalent cation vacancy of Cr and Pb will produce oxygen vacancies in the passive film namely electron donors rather than reaction with the divalent cation vacancy, which annihilate the schottky defect pair in the passive film. These electron donors are the majority charge carriers in a n-type semiconductor and this might be the reason for the increase in lead contaminated solution (N2) donor density. When magnesium was added to the solutions (N3, N4), donor density of the passive film

decreased. This might be due to reduced lead ions available for reaction through Equations 4-9 to 4-11. In UNS N08800 inner layers were composed of chromium oxide and outer layers constitute hydroxides of nickel and iron (Alvarez et al.). The propensity of chromium cation vacancy to recombine with lead is high compared to that of nickel cation vacancy and iron cation vacancy. This can be attributed to the low stability of chromium hydroxide (Lu et al. 2007).

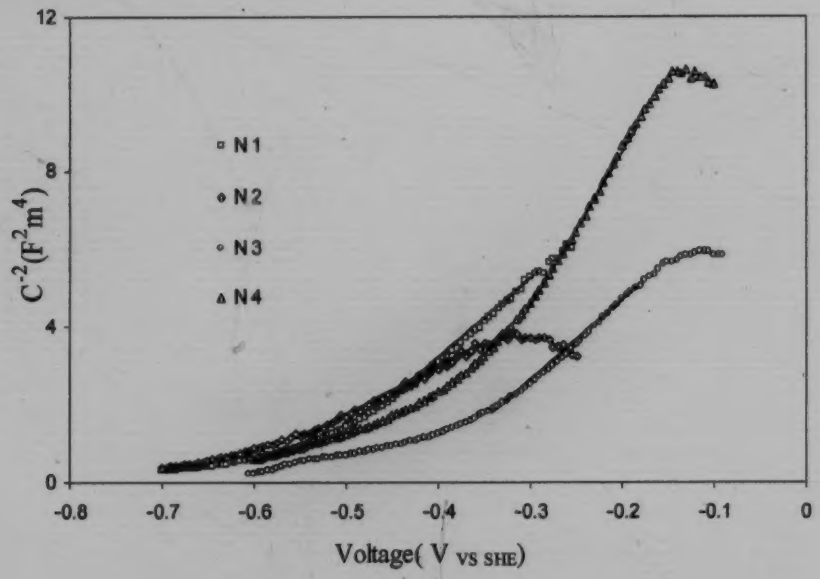

Figure 4-13 Mott-Schottky plots of the passive film formed in neutral crevice solution treated at -490 mV vs SHE for 900 s at 300°C

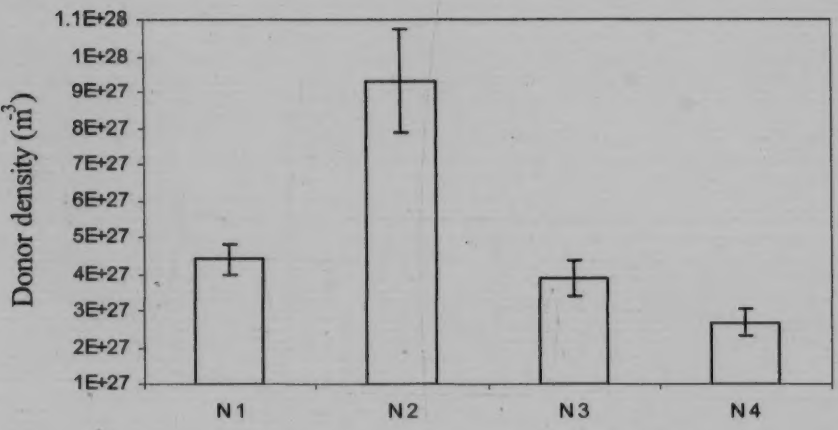

Figure 4-14 Donor density of the passive film formed in neutral crevice solution treated at -490 mV $_{VS\ SHE}$ for 900 s at 300°C

4.2.4 Repassivation kinetics

Synergistic effects of calcium and magnesium on the passive film growth was studied using scratch test. Since the solution chemistry plays a main role in repassivation, it is important to understand the interaction of different metal ions present in the crevice chemistry of PWR SGs during the repassivation processes.

Initially, the passive film was formed on the surface of UNS N08800 samples at -100 mV_{SCE} for 30 minutes. The same potentiostatic condition was maintained during the scratch tests. The passive film was broken by scratching on alumina tip. Scratched surface was observed after scratch tests with an optical microscope. A typical scratch was 1.23 mm in length and 0.11 mm in width.

4.2.4.1 Repassivation behavior in acidic crevice chemistries

Fig. 4-15 (a) shows the typical current transient curve for UNS N08800 at pH 1.6. As soon as the passive film was broken, bare metal surface was exposed to the solution. The current suddenly increased due to the anodic oxidation reaction occurring on the exposed metal surface, and thereafter started to decrease as the repassivation process started.

From Fig. 4-15 (a), the charge density was calculated using the following relationship

$$q(t) = \int (i_{total} - i_{passive})dt \qquad 4\text{-}12$$

where i_{total} is the total current density, $i_{passive}$ is the passive current density. The values of q(t) for the current transients shown in Fig. 4-15 (a) were calculated based on Equation 4-12 and the corresponding log i(t) vs. q(t) and log i(t) vs. 1/q(t) were plotted in Fig. 4-15 (b) and (c) respectively. Fig. 4-15 (b) shows that log i(t) was linearly proportional to q(t) between 2 ms and 20 ms, which follows the place exchange model; while Fig. 4-15(c) shows that log i(t) was linearly proportional to 1/q(t), which follows the high field ion conduction model based on Equation 2.5 between 20 ms and 100 ms. Thereafter the charge density was scattered over a small range. From the above analysis, it was clear that repassivation process can be divided to three different stages. In the first stage, film growth follows the place exchange model and in the second stage it follows the high field ion conduction model. After the second stage, charge density was scattered over small range where the passive film was thick enough to protect the surface. This was called the third stage. The transition of the film growth mechanism from the place exchange model to high field ion conduction model happened due to an increase in activation energy for the rotation of M-O pairs by place exchange process as the film thickens.

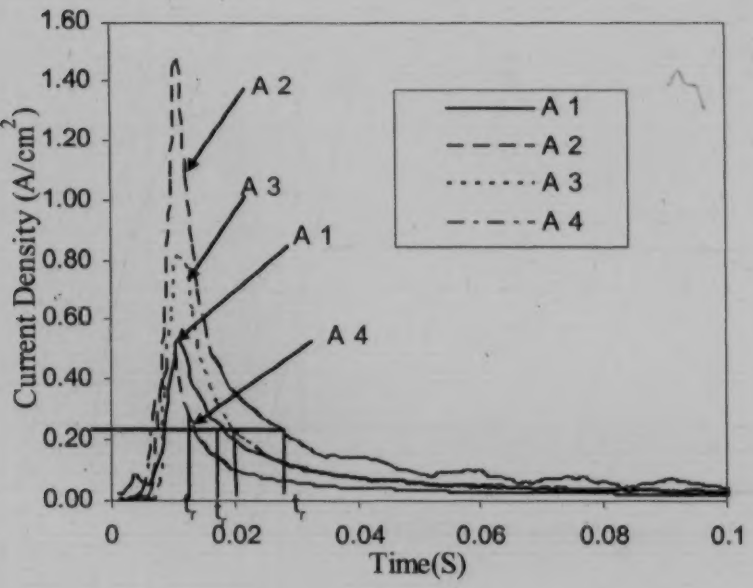
1.60
1.40
1.20
1.00
0.80
0.60
0.40
0.20
0.00
Current Density (A/cm2)
0
0.02
0.04
0.06
0.08
0.1
Time(S)
A 1
A 2
A 3
A 4

(a)

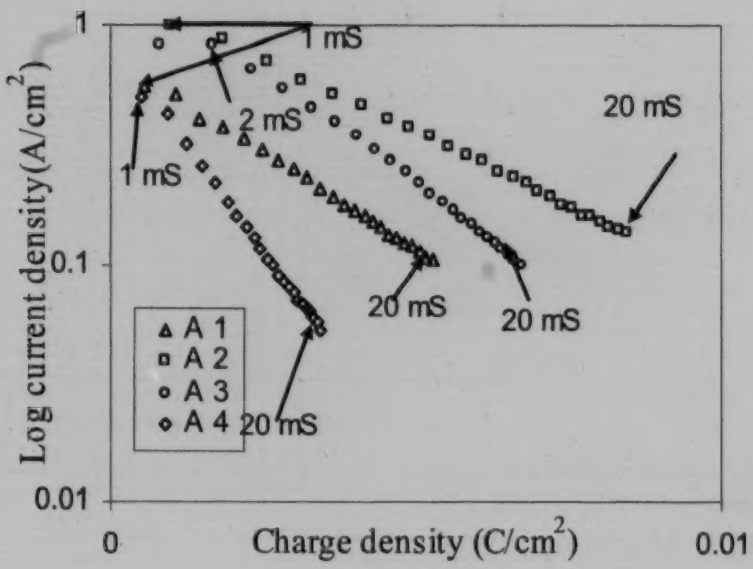
1
0.1
0.01
Log current density(A/cm2)
0
Charge density (C/cm2)
0.01
1 mS
2 mS
20 mS
A 1
A 2
A 3
A 4

(b)

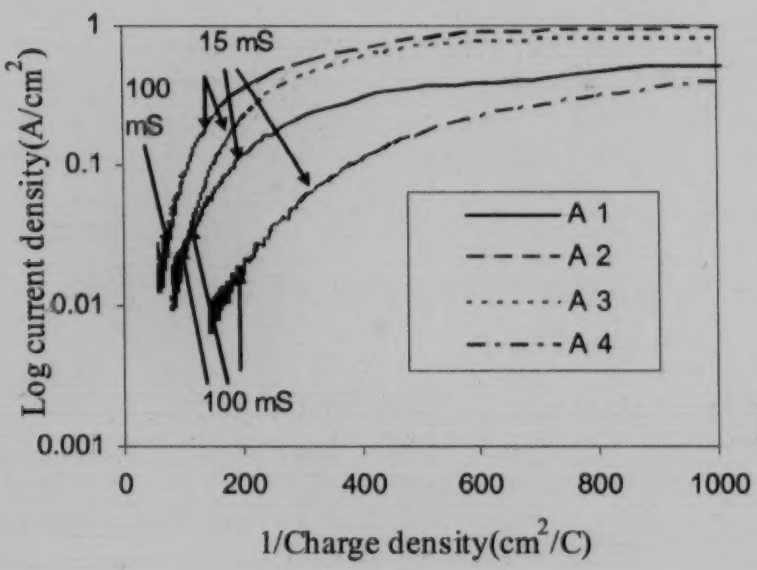

(c)

Figure 4-15 (a) Current transient curves; (b) log i(t) vs. q(t) and (c) log i(t) vs. 1/q(t) plots for the passive films formed on UNS N08800 at pH 1.6

Fig. 4-16 shows the cBV value measured in different solutions at pH 1.6 from the plot of log i(t) versus 1/q(t). In the lead containing solution, the enhanced oxidations of Fe, Cr, Ni induced by lead may be one of the possible reasons for the increase in the cBV value compared to that of lead free solution. In lead free solution, cBV value was lower compared to lead containing solutions with the exception of A4. In lead containing solutions, ratio of magnesium to calcium plays an important role in the lead induced oxidation of the alloy. As the ratio of magnesium to calcium increased to one, the value of cBV was lower compared to that of the lead-containing solutions without magnesium (A2 vs. A3). When the Magnesium to calcium ratio was 0.5, the slope was lower compared to that in the solution where the ratio was 1. The presence of magnesium in the solution suppressed the metal dissolution reaction. In lead containing solutions cBV value

was in the order of A2>A3>A4. It was reported by Cho et al. (2000) that an increase in chlorine concentration increased the cBV value. In Solution A2, the chloride ion concentration was 0.66 M compared to other solutions which were 0.65 M. Since the difference was small, effect of chloride ion concentration was negligible compared to that of magnesium.

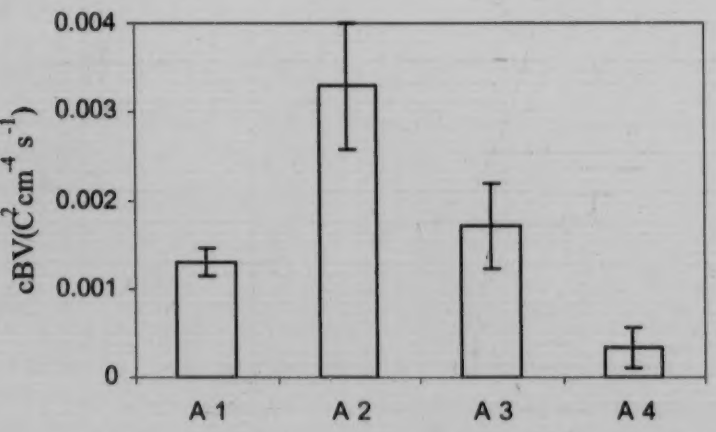

Figure 4-16 cBV value measured in different solutions at pH 1.6

4.2.4.2 Repassivation behavior in alkaline crevice chemistries

Fig. 4-17 shows the current transient curves and the corresponding log i(t) vs. 1/q (t) plots for passive films formed at pH 12.9. Similar to those observed in the acidic chemistry, the lead impurities promoted transient anodic dissolution immediately after the passive film breakdown and retarded the repassivation in the alkaline chemistry. The addition of magnesium chloride can counteract a part of detrimental impact of lead contamination. As shown in Fig. 4-18, cBV values obtained based on the curves in Fig. 4-17 (b) in the alkaline chemistry were higher than those in the acidic chemistry. Again,

the detrimental impact of lead and the beneficial effect of magnesium were clearly demonstrated by the cBV values.

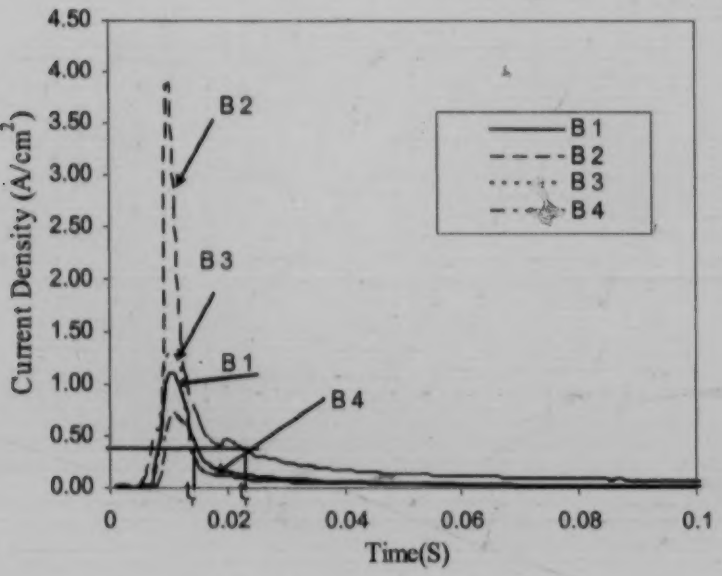

(a)

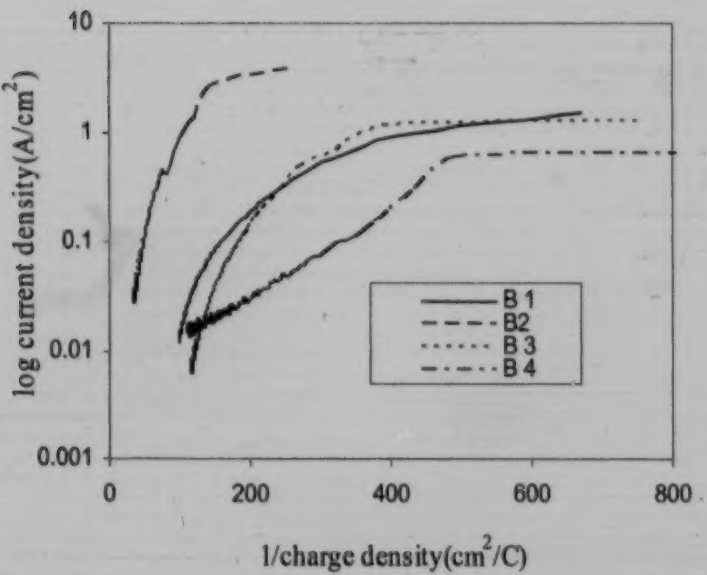

(b)

Figure 4-17 (a) Current transient curves, (b) log i(t) vs. 1/q(t) plots for passive films formed on UNS N08800 at pH 12.9

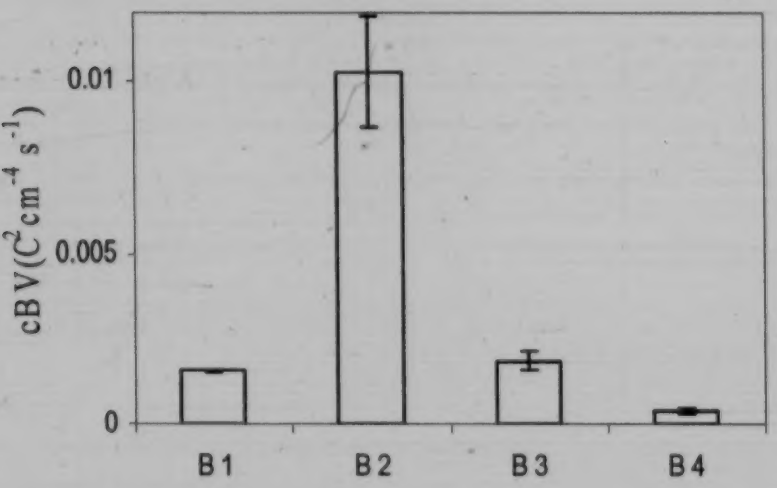

Figure 4-18 cBV values measured in different solutions at pH 12.9

4.2.4.3 Repassivation time

Repassivation behavior of a passive film can also be explained using the repassivation time (t_r) (Ahn et al. 2006 b, Bernard et al.). This was explained using the current transient curve. The shorter the time taken for the predetermined degree of repassivation, faster is the repassivation time under the given condition. Fig. 4-19 shows the repassivation time calculated from Fig. 4-18, 4-20. It was clear that at both pH 1.6 and pH 12.9 solutions the repassivation time was longer in the PbO containing solution compared to that in the lead free solution (A2 vs. A1 and B2 vs. B1). However the repassivation time was shorter in lead containing solutions with magnesium to calcium ratio 1 and 0.5. For the passive films formed in solution containing different magnesium

and calcium ratios, the lead effect on metal dissolution was suppressed compared to that in the solution without magnesium.

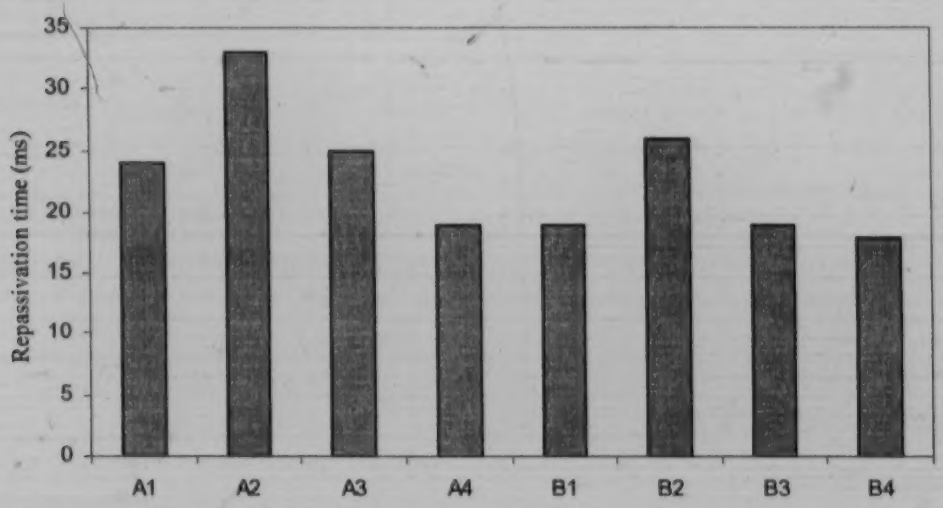

Figure 4-19 Repassivation time calculated from the current transient plot

4.3 Transient dissolution of Fe, Cr and Ni at active dissolution potential

The repassivation rate of UNS N08800 in lead containing alkaline solution was slower compared to the one in acidic crevice chemistry solution. In order to understand which alloying element plays a major role on PbSCC of UNS N08800, scratch test was conducted for Fe, Cr and Ni in alkaline crevice solution. The specimen was passivated in anodic peak potential for 15 minutes in alkaline crevice solution (B1 and B2) and then scratch test was done. Bin studied the effect of lead on pure Fe, Cr and Ni by polarization diagram and found that in lead containing solution these elements showed the anodic peak at -720 mV $_{VS\ SCE}$ and the peak current density was higher in Ni compared to that in Cr and Fe. Polarization behavior of gold in lead containing solution was studied by Bin to

confirm whether the anodic peak was due to deposited lead or due to dissolution of alloying elements. The presence of anodic peak in gold indicated that it was mainly due to the dissolution of deposited lead during cathodic pretreatment. At the same time the anodic peak current density was higher in pure Fe, Cr and Ni compared to that in gold. This indicates increased dissolution of Fe, Cr and Ni.

Fig. 4-20 shows the current transient plots and log i(t) vs. 1/q(t) for Fe. The peak current density and repassivation time was increased by lead. The slope of log i(t) vs. 1/q(t) was increased by the addition of lead. This indicates that the repassivation rate was reduced in lead containing solution. In Cr, lead did not increase the peak current density, in fact repassivation time decreased in lead containing solution as shown in Fig. 4-21. It showed that chromium was resistant to the lead induced corrosion. Fig. 4-22 shows the current transient plots and log i(t) vs. 1/q(t) for Ni. Even though the peak current density was decreased in lead containing solution, repassivation time does not show significant difference. The slope of log i(t) vs. 1/q(t) was decreased in lead containing solution on Cr and Ni. This indicates that lead did not have any influence on the repassivation kinetics of Cr and Ni. Since UNS N08800 is a combination of Fe, Cr and Ni, it is very difficult to correlate the pure elements repassivation to UNS N08800 repassivation behavior. It helps to understand the effect of lead on passive film formation on Fe, Cr and Ni.

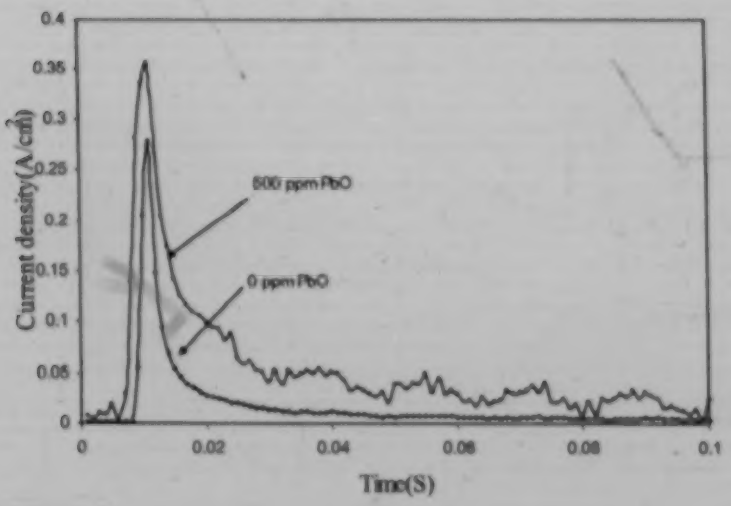

(a)

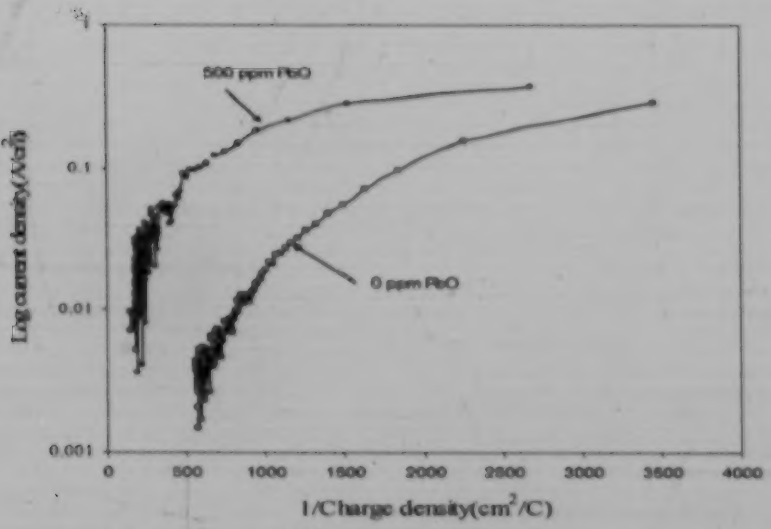

(b)

Figure 4-20 (a) Current transient curves, (b) log i(t) vs. 1/q(t) plots for passive films formed on Fe at pH 12.9

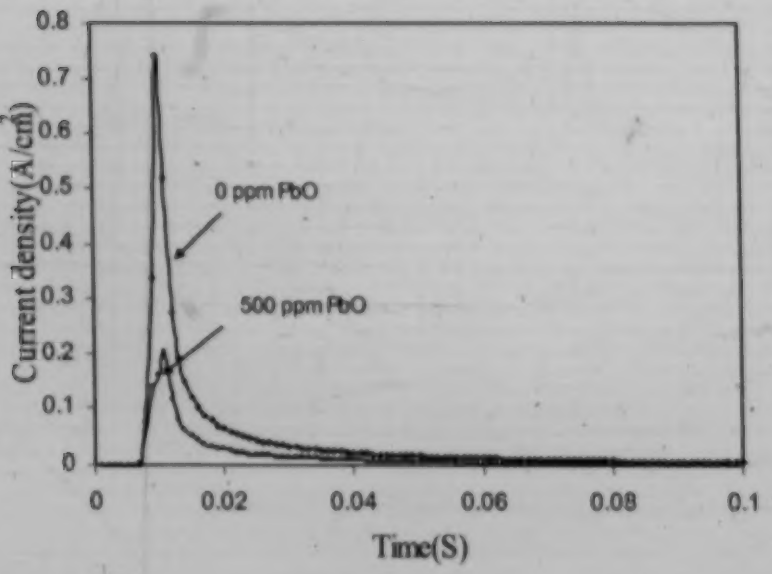

(a)

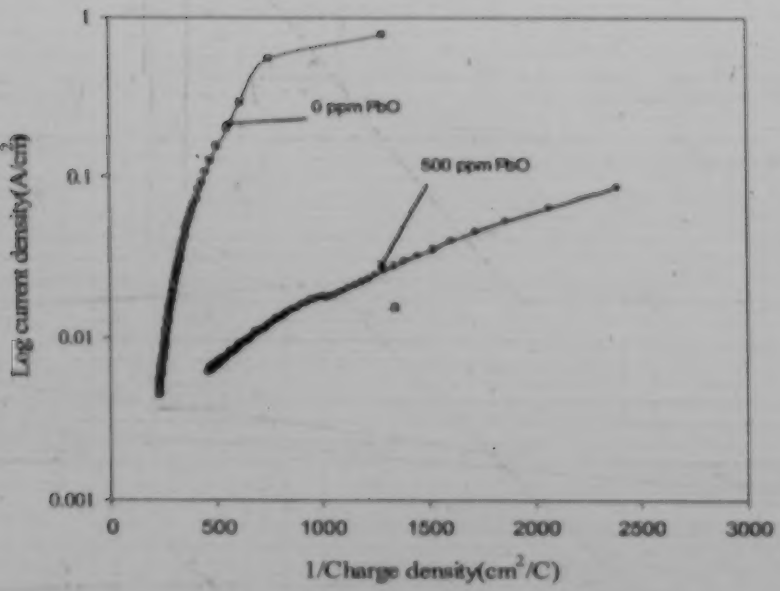

(b)

Figure 4-21 (a) Current transient curves, (b) log i(t) vs. 1/q(t) plots for passive films formed on Cr at pH 12.9

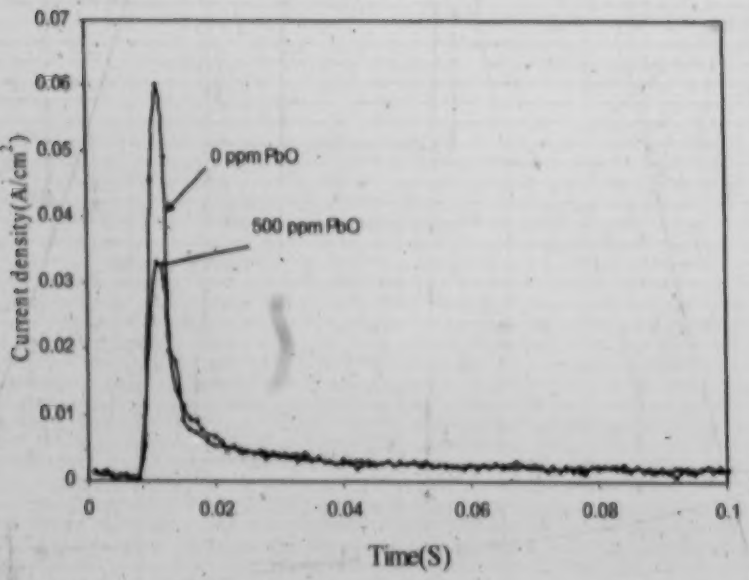

(a)

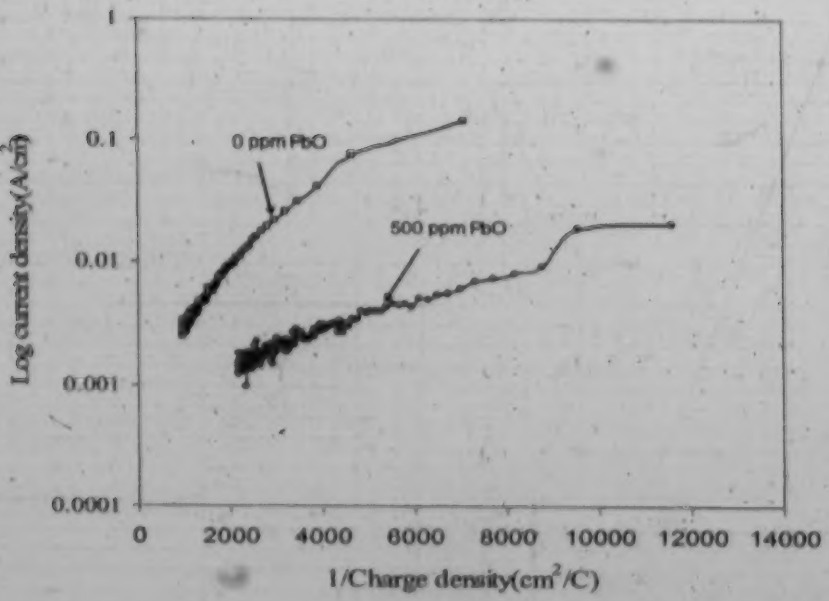

(b)

Figure 4-22 (a) Current transient curves, (b) log i(t) vs. 1/q(t) plots for passive films formed on Ni at pH 12.9

4.4 Effect of passivation potential on lead induced degradation of film rupture ductility

SCC of the stainless steel and nickel based alloys of SG tubes was mainly due to film rupture mechanism (Ford). The average crack propagation rate in SG tubes can be calculated from the following equation (Ford)

$$\bar{V} = \frac{MQ_f \varepsilon_a}{z\rho F \varepsilon_f} \qquad 4\text{-}13$$

where M is atomic weight of the material, ρ is density of the material , Q_f is charge density flown between two ruptures of the passive film, z is number of electrons transfer in rupture reaction, F is faraday constant, ε_a is crack tip creep rate, ε_f is film rupture ductility of the passive film. Film rupture ductility is defined as the resistance of the passive film to rupture. Lu et al. (2008) studied the film rupture ductility of passive film on UNS N08800 at different passivation potentials and reported that increasing the passivation potentials in noble direction decreased the film rupture ductility. Passive film formed in lead containing solution also showed similar trend as lead free solution and film rupture ductility was decreased by the addition of lead (Lu et al. 2008). Here it was mentioned that the film rupture ductility decreases as the passivation potential increases. However, the explanation for the reason behind this phenomenon was not discussed. Composition of passive film studied by Lu et al. (2008) indicated that lead incorporation depends on the passivation potential. Passive film formed at OCP and active-passive region had high lead incorporation, nickel and iron content increased while chromium content decreased. The passive film formed at passive region and below the pitting potential showed reverse trend compared to the passive film formed at OCP. The

transient dissolution of the passive film increased as the passivation potential increased and this might increase the vacancy generation of the passive film. To explore the electronic properties of the passive film formed at different passivation potential and to make correlation with the film rupture ductility, this part of the experiment was conducted. Four different potentials were chosen to explore the donor density of passive film formed at different passivation potentials and the potentials used in this experiment are listed in Table 4.1, which is same as the ones used in Lu et al. (2008). In both lead free and lead contaminated solution, the specimen was treated for 30 minutes at 300°C in different film form potentials as shown in the Table 4.1. After passive film was formed on the surface, Mott-schottky experiments were carried out in the passive potential range.

Table 4-1 Potentials used for passivating the sample at 300°C (data from Lu et al. 2008)

Condition	E1(mV) OCP	E2(mV) Active-Passive region	E3(mV) Passive region	E4(mV) Below pitting potential
N 1 (Pb free)	-760	-650	-490	-300
N 2 (2.2mM Pb)	-770	-650	-490	-300

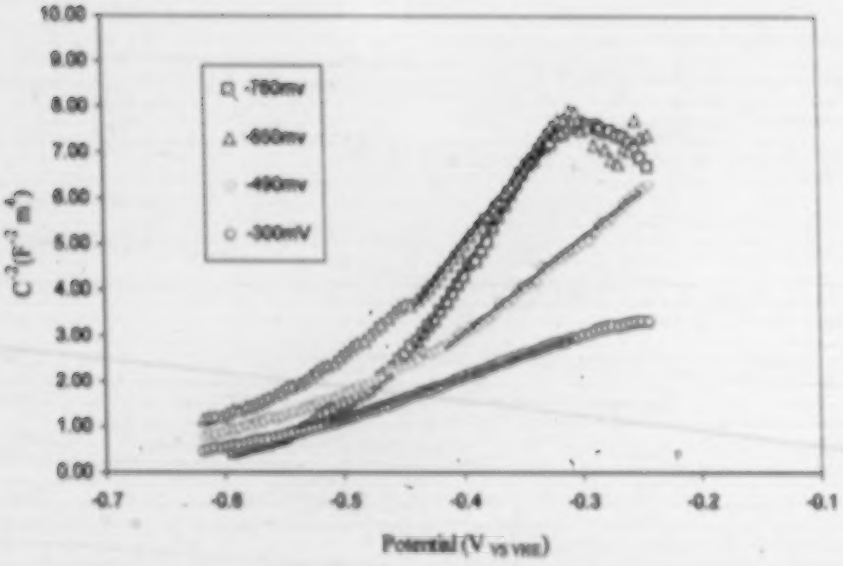

Figure 4-23 Mott-Schottky plots for passive films formed on UNS N08800 at 300°C in neutral lead free solution

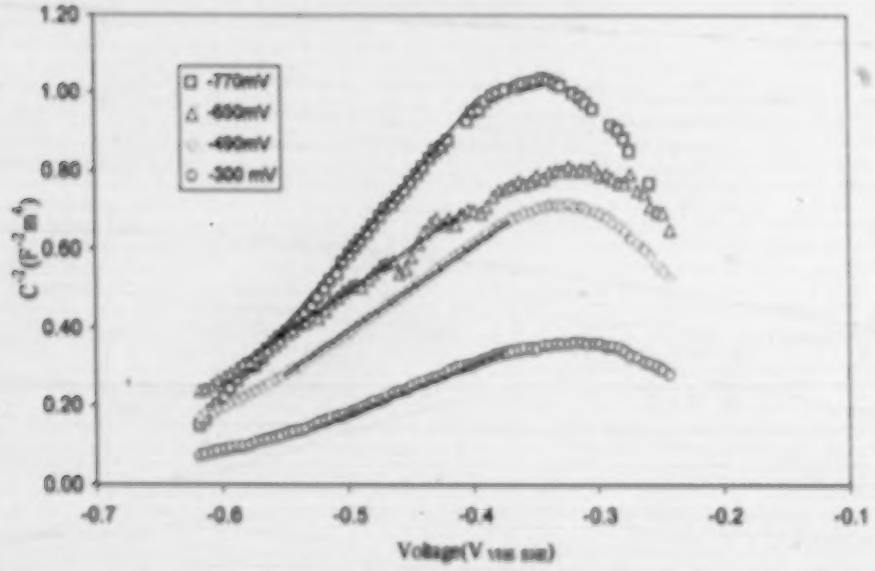

Figure 4-24 Mott-Schottky plots for passive films formed on UNS N08800 at 300°C in neutral lead contaminated solution

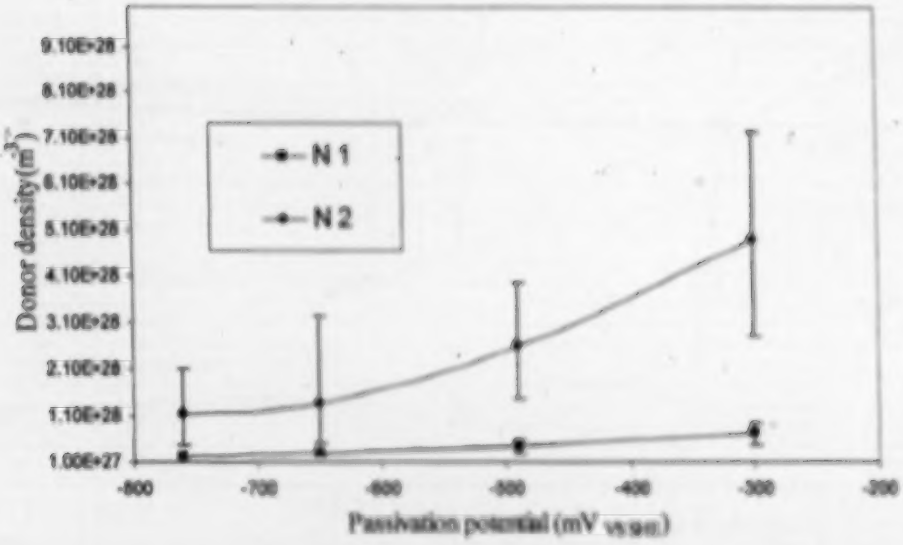

Figure 4-25 Donor densities of the passive films formed on UNS N08800 at 300°C at different film form potentials

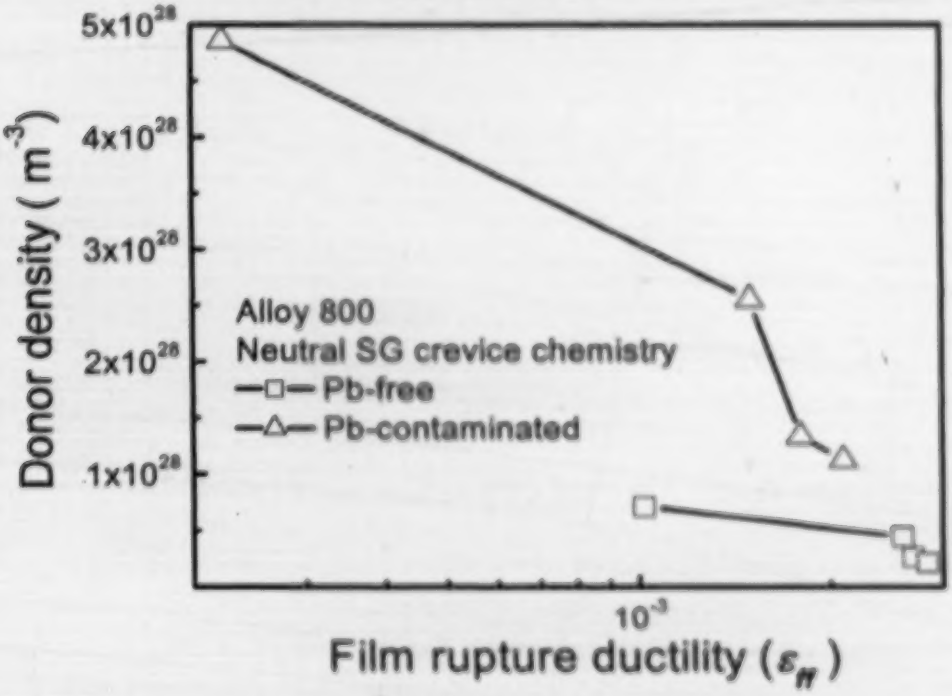

Figure 4-26 Correlation between the donor densities and film rupture ductility for the passive films formed on UNS N08800 at 300°C at different passivation potentials

Fig. 4-23 and 4-24 show the Mott-schottky plot obtained in lead free and lead contaminated solution. As the passivation potential increased, the slope of the linear region decreased in both conditions. Donor densities of the passive film calculated using equation 4-5 were shown in Fig. 4-25. As the passivation potential increased, donor density of the passive film increased in both conditions. Increase of donor density follows an exponential trend in both conditions and donor density of the passive film can be correlated with the film rupture ductility of the passive film as shown in Fig. 4-26. Increase in donor density may be due to the vacancy generation in the passive film. The SCC susceptibility of the materials depend upon the combination of many parameters like transient dissolution after rupture of passive film , creep rate of passive film at crack tip, film rupture ductility and it can also be related to donor density. Increased donor density in lead containing solution may be responsible for the decrease in film rupture ductility.

4.5 Morphology of oxide film

The morphology of the oxide film formed on UNS N08800 at 300°C was shown in Fig. 4-27. The oxide film formed on N1 solutions showed needle like deposit on the surface, whereas the oxide film formed in N2 solution showed spherical precipitation on the surface. The precipitation of spherical particle in lead contaminated solution indicated that a precipitation growth was taking place rather than a particle formation on the surface. Analysis of precipitation by EDX was impossible since the precipitate was very small and hence it was difficult to eliminate the base effect. The oxide film formed in 0.075M magnesium and in 0.15 M magnesium added to lead containing solution did not show any precipitation on the surface. It indicated that oxide film growth was mainly due

to the particle formation on the surface. The particles present on the surface formed in the lead containing solution were not seen in the passive film formed in the magnesium containing solution (N3, N4).

(a)

(b)

(c)

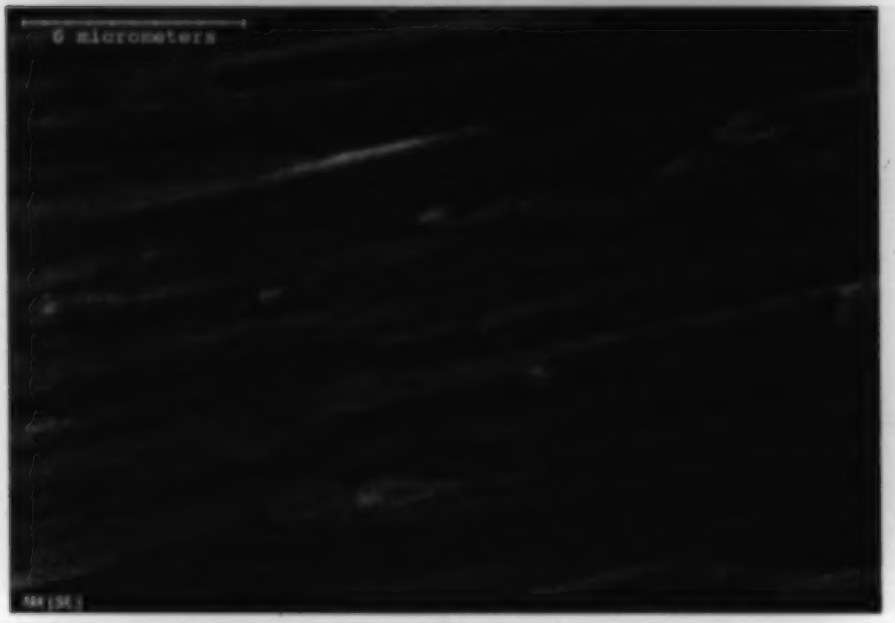

(d)

Figure 4-27 SEM Micrograph of oxide film formed on UNS N08800 at 300°C in different solution (a) N1, (b) N2, (c) N3 and (d) N4

4.6 XRD analysis

Passive film formed on the metal surface by a series of reactions between the alloying elements present on the metal surface and the solution. According to Sato and Cohen (1964), the passive film initially contains mainly M-OH and M-OH_2 bonds. Dehydration or ageing of these bonds led to the formation of M-O bond which is stable and less reactive compared to M-OH bonds.

In neutral crevice solutions Fe, Cr, Ni cations form metal hydroxides and these hydroxides form gel like structure on the surface (Beverskog et al. 1996, 1997 a, 1997b, Pourbaix).

$$Ni^{2+} + 2(OH)^- \rightarrow Ni(OH)_2 \qquad 4\text{-}14$$

$$Fe^{2+} + 2(OH)^- \rightarrow Fe(OH)_2 \qquad 4\text{-}15$$

$$Fe^{3+} + 3(OH)^- \rightarrow Fe(OH)_3 \qquad 4\text{-}16$$

$$Cr^{3+} + 3(OH)^- \rightarrow Cr(OH)_3 \qquad 4\text{-}17$$

These metal hydroxides form metal oxides by dehydration reaction during ageing of the passive film (Okamoto, Yang et al.).

$$2Ni(OH)_2 \rightarrow NiO + H_2O \qquad 4\text{-}18$$

$$Fe(OH)_2 \rightarrow FeO + H_2O \qquad 4\text{-}19$$

$$2Fe(OH)_3 \rightarrow Fe_2O_3 + 3H_2O \qquad 4\text{-}20$$

$$2Cr(OH)_3 \rightarrow Cr_2O_3 + 3H_2O \qquad 4\text{-}21$$

During the dehydration reaction, mixture of oxides with spinel structure was formed. These spinel oxides are highly corrosion resistant (Cubicciotti, Beverskog et al. 1999).

$$Ni(OH)_2 + 2Cr(OH)_3 \rightarrow NiCr_2O_4 + 4H_2O \quad 4\text{-}22$$

$$Ni(OH)_2 + 2Fe(OH)_3 \rightarrow NiFe_2O_4 + 4H_2O \quad 4\text{-}23$$

$$Fe(OH)_2 + 2Cr(OH)_3 \rightarrow FeCr_2O_4 + 4H_2O \quad 4\text{-}24$$

In Ni-Cr-Fe system, the spinel oxides that were formed according to Eqn 4-21 to 4-22 are magnetite (Fe_3O_4), trevorite ($NiFe_2O_4$), chromite ($FeCr_2O_4$) and nichromite ($NiCr_2O_4$) (Cubicciotti, Beverskog et al. 1999). XRD patterns of the passive film formed at 300°C treated at OCP for 24 hours were shown in Fig. 4-28. The patterns showed that lead free solution (N1) led to the spinel oxide mainly trevorite and lead contaminated solution (N2) suppressed the spinel oxide formation. However the addition of magnesium led to the formation of nichromite spinel oxide in both N3 and N4 solutions. It is interesting to note that the magnesium addition leads to the formation of spinel oxide in the lead contaminated solution. Lead is present in the solution in the form of lead hydroxide in neutral crevice chemistry at high temperature and this lead hydroxide is adsorbed on the surface to form the lead doped passive film (Lu et al. 2007) and suppressed the spinel oxide formation in the passive film formed in N2 solution. As Lu et al. (2007) and Zhou (2005) pointed that the lead doped passive film formation by following reaction hinders the spinel oxide formation.

$$Pb(OH)_2 + 2Fe(OH)_2 \rightarrow (OH)Fe-O-Pb-O-Fe(OH) + 2H_2O \quad 4\text{-}25$$

$$Pb(OH)_2 + 2Cr(OH)_3 \rightarrow (OH)_2Cr-O-Pb-O-Cr(OH)_2 + 2H_2O \quad 4\text{-}26$$

$$Pb(OH)_2 + 2Ni(OH)_2 \rightarrow (OH)Ni-O-Pb-O-Ni(OH) + 2H_2O \quad 4\text{-}27$$

In neutral crevice condition magnesium will be in the form of Magnesium hydroxide since magnesium oxide is unstable compound in the aqueous media (Pourbaix)

$$MgCl_2 + 2H_2O \rightarrow Mg(OH)_2 + 2HCl \qquad 4\text{-}28$$

The magnesium hydroxide may hinder the formation of spinel oxide during the growth of passive film. Fig. 4-28 shows that the presence of magnesium in the solution did not hinder the spinel oxide formation. It was very clear from SSRT result, EDX result and XRD result that lead activity was reduced as the magnesium concentration increased in the lead solution. If same amount of lead was available for reaction in magnesium containing solution N3, N4 compared to lead containing solution without magnesium (N2), passive film should not contain any spinel oxides. But the passive films formed in N3, N4 solutions contain spinel oxides. One of the possible mechanisms might be that the magnesium hydroxide reacts with the lead hydroxide, thereby reducing the possibility of lead hydroxide in the solution, which eventually reduces the availability of lead for adsorption on the surface.

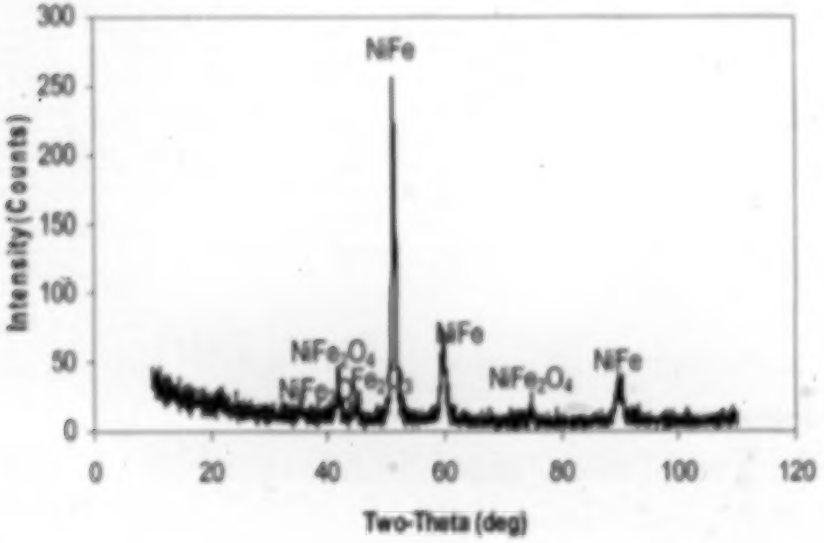

(a)

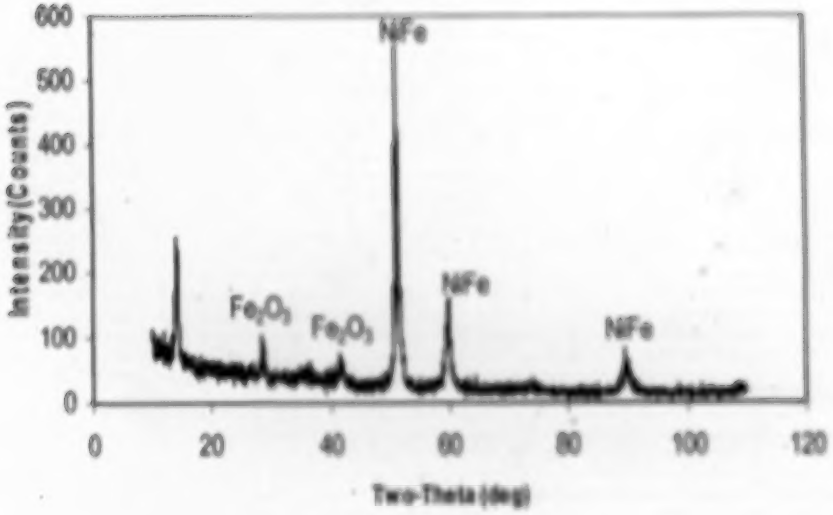
NiFe
Fe_2O_3
Fe_2O_3
NiFe
NiFe
Intensity(Counts)
Two-Theta (deg)
0
100
200
300
400
500
600
0
20
40
60
80
100
120

(b)

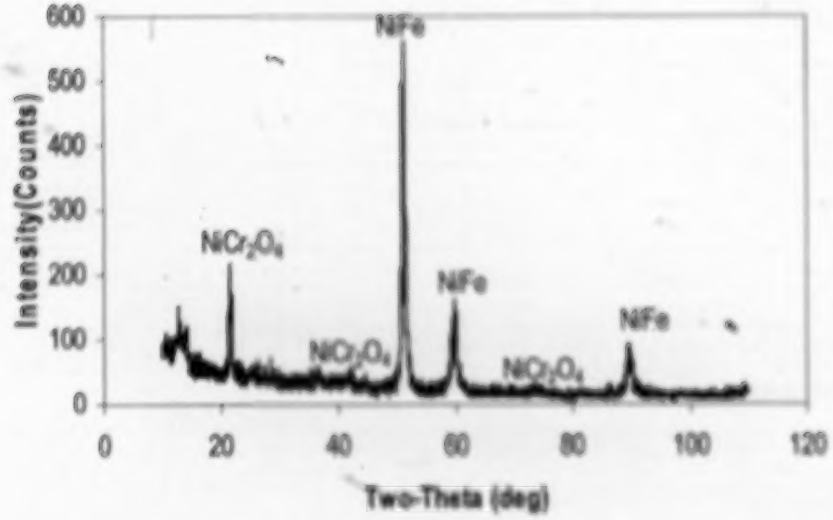
NiFe
$NiCr_2O_4$
$NiCr_2O_4$
NiFe
$NiCr_2O_4$
NiFe
Intensity(Counts)
Two-Theta (deg)
0
100
200
300
400
500
600
0
20
40
60
80
100
120

(c)

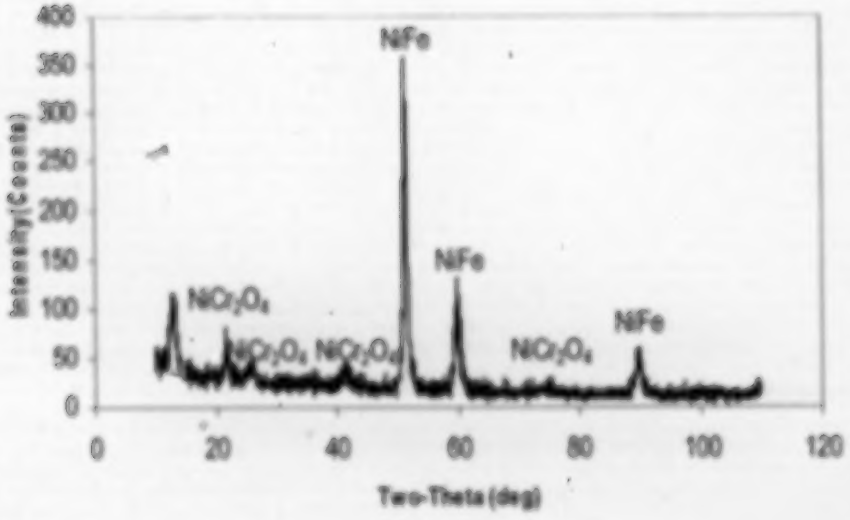

(d)

Figure 4-28 XRD patterns of the passive film formed in neutral solutions at 300°C treated in OCP for 24 h (a) N1, (b) N2, (c) N3 and (d) N4

UNS N08800 susceptibility to PbSCC is reduced by magnesium in lead contaminated is observed from SSRT test results. Lead induced passivity degradation is considered to be the main cause for PbSCC (Lu et al. 2005). Addition of magnesium in lead contaminated solution decreases the lead induced passivity degradation. It can be substantiated by electrochemical and surface analysis results. Polarization experiment results showed that the lead increases passive current density whereas magnesium decreases the passive current density. Donor density of the passive film is reduced by magnesium in lead contaminated solution compared to solution without magnesium. Repassivation of the passive film is increased in magnesium containing solution indicated that the passive film grows faster when localized corrosion takes place on the surface and decreases the dissolution of metal. Since the repassivation is quicker in magnesium

containing solution, the passivity of the material is increased. During the passive film growth, the corrosion resistance of the material increased when spinel oxides present in the passive film. These spinel oxides are highly corrosion resistance and will protect the specimen from environment. XRD results indicated that the passive film formed in lead containing solution devoid of spinel oxides but spinel oxides are formed when magnesium added. All the test results are clearly showed that the presence of magnesium in the solution increases the passive film properties and thereby decreases the lead induced passivity degradation might be the reason for decreased PbSCC susceptibility of UNS N08800 in magnesium containing lead solution.

Chapter 5- CONCLUSIONS AND FUTURE WORK

5.1 Conclusions

1) At room temperature, addition of PbO to acidic crevice solution decreased pitting potential, while the pitting potential increased in both the magnesium to calcium ratios. Addition of PbO to the alkaline crevice solution without magnesium increased the anodic dissolution in the active zone, resulting in an anodic peak.
2) Passive film growth on UNS N08800 initially follows place exchange model up to 20 ms. In this period lead did not have any appreciable impact on the repassivation. Rate determining step for repassivation is from 20 ms to 100 ms follows the high field ion conduction model. During this period the repassivation had decreased in the presence of lead and increased by the addition of magnesium.
3) For the passive films formed in the solutions containing PbO alone at both acidic and alkaline crevice, cBV value was higher when compared to those formed in the lead-free solutions. The cBV value was lower in magnesium containing PbO solution compared to that in the solution containing PbO alone. The values of cBV in the solution with the ratio of magnesium to calcium 0.5 were the lowest among that in all the solutions in both alkaline and acidic crevice solutions. Lead did not affect repassivation rate in pure Cr, Ni but pure Fe repassivation rate was greatly reduced by lead.
4) Mott-Schottky results at room temperature showed that the defects in the passive films formed in acidic solutions were higher compared to those formed in the alkaline solutions. Addition of PbO alone to the solution significantly increases the amount of

defects in the passive films whereas addition of magnesium decreases defects in the passive films in both acidic and basic solutions. The amount of defects was lowest when the ratio of magnesium to calcium was 0.5.

5) As the passivation potential increased in noble direction, donor density increased in both lead free and lead contaminated neutral crevice solution at 300°C. Increase in donor density was higher in lead contaminated solution compared to that in lead free solution. Magnesium addition in lead containing neutral crevice solution at 300°C led to an increase in OCP, pitting potential and a decrease in passive current density compared to that in solution containing lead alone. Donor density of the passive film formed at 300°C in neutral crevice solution was increased by the addition of lead and decreased by addition of magnesium.

6) Lead incorporation in the passive film formed at 300°C in neutral crevice solution was reduced by addition of magnesium. It can be attributed to immobilization of lead in the solution. Spinel oxides were reduced in the passive film formed at 300°C in lead contaminated neutral crevice solution whereas addition of magnesium in the solution increased spinel oxides formation in the passive film.

7) At 300°C in neutral crevice solution, the mechanical properties such as UTS, elongation were reduced drastically by addition of lead. Addition of Magnesium increased the mechanical properties in lead contaminated solution. Fractography of fracture surface showed the ductile and dimple mode in lead free and magnesium containing solution whereas brittle fracture was observed in the solution contaminated by lead alone. Even though 0.75 M magnesium addition decreased the donor density, there was an increase in spinel oxide formation and mechanical properties in lead

contaminated neutral crevice solution at 300°C. However, when magnesium concentration was increased to 0.15M, there was marginal increase in the beneficial activity of magnesium compared to values obtained from 0.075 M solution containing magnesium.

8) SSRT test results clearly indicated that susceptibility of UNS N08800 to PbSCC was reduced by addition of magnesium. This is corroborated by the decreased passive current density, increased repassivation rate, decreased donor density, increased spinel oxide formation and decreased lead incorporation of the passive film formed in magnesium containing lead contaminated solution compared to that in the solution containing lead alone.

5.2 Future work

All the test results indicated that UNS N08800 exhibits better corrosion resistance when magnesium is present in the lead contaminated solution. Future research could be carried out to study the following aspects

1) Film rupture ductility of the passive film formed on UNS N08800 in magnesium containing solution for a better understanding of the magnesium effect on PbSCC.
2) In addition to Mg, Cu and Al were also present in significant quantities in the sludge. Further investigation could be done to study the effect of Cu and Al on PbSCC of UNS N08800.
3) Crack propagation rate can be studied in different solutions by in situ multimeter monitoring system at high temperature to unfold the conundrum of magnesium effect.

References

Ahn S.J., Kim D.Y and Kwon H.S., "Analysis of Repassivation Kinetics of Ti Based on the Point Defect Model," Journal of Electrochemical Society 153 (2006) pp B370-B374. (a)

Ahn S., Rao V.S., Kwon H.S and Kim U.C., "Effects of PbO on the Repassivation Kinetics of Alloy 690," Corrosion Science 48 (2006) pp 1137-1153. (b)

Airey G.P., "The effect of carbon content and thermal treatment on the SCC behavior of Inconel alloy 600 steam generator tubing," Corrosion 35(1979) pp 129-135.

Alvarez M.G., Olmedo A.M and Villegas M., "Corrosion behavior of Alloy 800 in high temperature aqueous solutions: Electrochemical studies", Journal of Nuclear Materials 229 (1996) pp 102-114. (a)

Alvarez M.G., Olmedo A.M and Villegas M., "Corrosion behavior of Alloy 800 in high temperature aqueous solutions: long term autoclave studies", Journal of Nuclear Materials 229 (1996) pp 102-114. (b)

Bernard F., Rao V.S and Kwon H.S., "A study on the Repassivation Kinetics and SCC Behavior of Duplex Stainless Steel in Chloride Solution," Journal of the electrochemical society 152 (2005) pp B425 –B420.

Beverskog B. and Puigdomenech I., "Revised pourbaix diagrams for Iron at 25-300°C," Corrosion Science 38 (1996) pp 2121-2135.

Beverskog B. and Puigdomenech I., "Revised pourbaix diagrams for chromium at 25-300°C," Corrosion Science 39 (1997) pp 43-57. (a)

Beverskog B. and Puigdomenech I., "Revised pourbaix diagrams for nickel at 25-300°C," Corrosion Science 39(1997) pp 969-980. (b)

Beverskog B. and Puigdomenech I., "Pourbaix diagrams for the Ternary system of Iron-Chromium-Nickel", Corrosion 55 (1999) pp 1077-1087.

Bin P., "Passivity degradation of nickel alloy 690 in lead containing environments," M.Sc thesis, University of Alberta (2007).

Bosch R.W., Bogaerts W.F., and Zheng J.H., "Simple and robust external reference electrodes for high-temperature electrochemical measurements," Corrosion, 59(2003) pp 162-171.

Bosch R.W., Schepers B., Vankeerberghen M., "Development of a scratch test in an autoclave for the measurement of repassivation kinetics of stainless steel in high temperature high pressure water," Electrochemica Acta, 49(2004) pp 3029-3038.

Bousier J.M., Dupin M., Gosset P and Rouillon Y., "Secondary side corrosion of French PWR steam generator tubing: Contribution of surface analysis to the understanding of the degradation process," Proceedings of the 9th international symposium on environmental degradation of materials in nuclear power systems-water reactors (1999) pp 555-565.

Bradford S.A., "Corrosion control," Van Nostrand Reinhold Publishing, New York, (1993).

Briceno D.G., Castano M.L and Garcia M.S.," Stress corrosion cracking susceptibility of steam generator tube materials in AVT(all volatile treatment) chemistry contaminated with lead", Nuclear Engineering and Design, Vol. 165(1996) pp 161-169.

Burstein G.T and Marshall P.I., "Growth of Passivating Films on Scratched 304L Stainless Steel in Alkaline Solution," Corrosion Science 23 (1983) pp 125-137.

Cabrera N and. Mott N.F, "Theory of the oxidation of metals," Reports of progress in physics (1948) pp 163-184.

www.canelect.ca (Accessed on June 13, 2008)

Cattant F., Dupin M., Sala B and Gelpi A., "Analyses of deposits and underlying surfaces on the secondary side of pulled out tubes from a French plant," Contribution of materials investigation to the resolution of problems encountered in pressurized water reactors: Proceedings of the international symposium: Fontevraud III, French nuclear society (1994) pp 469-480.

Chen Y.Y., Chou L.B and Shih H.C., "Effect of solution pH on the electrochemical polarization and stress corrosion cracking of Alloy 690 in 5 M NaCl at room temperature", Materials Science and Engineering A , vol 396(2005) pp 129-137.

Chen Y.Y., Chou L.B. and Shih H.C., "Factors affecting the electrochemical behavior and stress corrosion cracking of Alloy 690 in chloride environments", Materials Chemistry and Physics , vol 97(2006) pp 37-49.

Cho E.A., Kim C.K. , Kim J.S and Kwon H.S., "Quantitative Analysis of Repassivation Kinetics of Ferrite Stainless Steels based on the High Field ion Conduction Model," Electrochimica Acta 45 (2000) pp 1933-1942.

Copson H.R and Dean S.W., "Effect of contaminants on resistance to stress corrosion cracking of Ni-Cr alloy 600 in pressurized water," Corrosion 21(1965) pp 1-7.

Costa D., Tahala T., Marcus P., Le calver M and Gelpi A., "Interaction of lead with Nickel-base alloys 600 and 690," Proceedings of the 7th international symposium on

environmental degradation of materials in nuclear power systems-water reactors (1995) pp 199-208.

Craig D.B., "Fundamental aspects of corrosion films in corrosion science," Plenum Press, New York (1991).

CRC Handbook of chemistry and physics, Permittivity of inorganic solids, 87th edition, 2006-2007.

Cubicciotti D., "Potential-pH diagrams for alloy-water systems under LWR conditions," Journal of Nuclear Materials 201(1993) pp 176-183.

Fang Z., "Development and application of the SCC parameter to predicting SCC in the secondary side of steam generators," Proceedings of the 9th international symposium on environmental degradation of materials in nuclear power systems-water reactors (1999) pp 689-694.

Feron D. and Lambert I., "Lead species and lead migration in PWR secondary circuit conditions," Proceedings of the 12th international conference on properties of water and steam (1994) pp 783-790.

Ford, F.P., "Quantitative prediction of environmentally assisted cracking," Corrosion Science 52 (1996) pp 375-395.

Guo H.X., Lu B.T., and Luo J.L., "Study on passivation and erosion-enhanced corrosion resistance by Mott-Schottky analysis," Electrochemica Acta, 52 (2006) pp1108-1116.

Haupt S and Strehblow H.H., "A combined surface analytical and electrochemical study of the formation of passive layers on Fe/Cr alloys in 0.5M H_2SO_4," Corrosion Science 37 (1995) pp 43-54.

Hamm D., Ogle K., Olsson C.O.A., Weber S and Landolt D., "Passivation of Fe-Cr alloys studied with ICP-AES and EQCM," Corrosion Science 44 (2002) pp 1443-1456.

Hwang I.S., Ballinger R.G and Prybylowski J.W., "Electrochemistry of multiphase nickel base alloys in aqueous systems," Journal of Electrochemical Society 136 (1989) pp 1874-1883.

Hwang S.S., Kim H.P., Lee D.H., Kim U.C and Kim J.S., "The mode of stress corrosion cracking in Ni-base alloys in high temperature water containing lead", Journal of Nuclear Materials 275 (1999) pp 28-36.

Hwang S.S. and Kim J.S., "Electrochemical Interaction of Lead with Alloy 600 and Alloy 690 in High-Temperature Water" Corrosion 58 (2002) pp 392-398

Hwang S.S., Kim H.P., Lim Y.S., Kim J.S., and Thomas L., "Transgranular SCC mechanism of thermally treated alloy 600 in alkaline water containing lead," Corrosion Science 49 (2007) pp 3797-3811.

Jabs T., Borthen P and Strehblow H.H., "X-Ray photoelectron spectroscopic examinations of electrochemically formed passive layers on Ni-Cr alloys," Journal of Electrochemical Society 144 (1997) pp 1231-1243.

Jin S., and Atrens A., "ESCA-studies of the structure and composition of the passive film formed on stainless steels by various immersion temperatures in 0.1M NaCl solution," Journal of Applied Physics A 45 (1988) pp83-91.

Jones D.A., "Principles and prevention of corrosion," Prentice Hall, New Jersey (1996).

Jones R.H., and Ricker R.E., "Mechanisms of stress corrosion cracking," Materials performance and evaluation (1992).

Keir J., "Experiments and observations on the dissolution of metals in acids and their precipitations; with an account of a new compound acid menstrum, useful in some technical operations of parting metals," Philosophical Transactions of the Royal Society of London 80 (1790) pp 359-384.

Kelly R.G., Sculy J.R., Shoesmith D.W., and Buchiet R.G., "Electrochemical techniques in corrosion science and engineering," Marcel Dekkar, New York (1993).

Kilian R., "Influence of lead on the SCC behavior of SG tubing materials," IAEA specialists meeting on steam generator problems and replacement, International Atomic Energy Agency (1993) pp137-167.

Kim U.C., Kim K.M and Lee E.H., "Effects of chemical compounds on the stress corrosion cracking of steam generator tubing materials in a caustic solution," Journal of Nuclear Materials 341(2005) 169-174.

King F.G., and Brown J., "Stress corrosion cracking experience in steam generators at Bruce NGS," Proceedings of the 6th international symposium on environmental degradation of materials in nuclear power systems-water reactors (1993) pp 233-240.

Kwon H.S., Cho E.A. and Yeom K.A., "Prediction of Stress Corrosion Cracking Susceptibility of Stainless Steels Based on Repassivation Kinetics," Corrosion Science 56 (2000) pp 32-42.

Lumsden J., "Effects of Pb on SCC of alloy 600 and alloy 690 in prototypical steam generator chemistries," Materials Science Forum Vols. 475-479 (2005) pp 1387-1392.

Lu B.T., Luo J.L. and Lu Y.C., "A Mechanistic study on Lead-Induced Passivity-Degradation of Nickel-Based Alloy", Journal of The Electrochemical Society, 154(2007), C379-389

Lu B.T., Luo J.L. and Lu Y.C., "Correlation between Rupture Ductility-Degradation Of Anodic Film And Stress Corrosion Cracking Susceptibility Of Alloy 800 In Lead-Contaminated Environments," Electrochimica Acta 53 (2008) pp 4122-4136.

Lu Y.C., "Comparative studies on the localized corrosion susceptibility of Alloy 690 and Alloy800 under stimulated steam generator conditions," Proceedings of the 11th International conference on Environmental Degradation of Materials in Nuclear Power System-Water Reactors, Stevenson, Washington (2003).

Lu Y.C., "Effect of lead contamination on steam generator tube degradation," Proceedings of the 12th International conference on Environmental Degradation of Materials in Nuclear Power System-Water Reactors (2005).

Macdonald D.D., "The point defect model for the passive state," Journal of Electrochemical Society 139 (1992) pp 3434-3449.

Macdonald D.D., "Passivity- the key to our metals based civilization," Pure Appl. Chem., 71 (1999) pp 951-978.

Machet A., Galtayries A., Zanna S., Klein L., Maurice V., Jolivet P., Foucault M., Combrade P., Scott P and Marcus P., "XPS and STM study of the growth and structure of passive films in high temperature water on a nickel-base alloy", Electrochimica Acta 49 (2004) pp 3957-3964.

Marcus P., and Maurice V., "The structure of passive film on metals and alloys," Proceedings of 8th international symposium: passivity of metals and semiconductors (2001) pp 30-56.

Marijan D., Vukovic M., Pervan P and Milun M., "Surface modification of inconel-600 by growth of a hydrous oxide film," Journal of applied electrochemistry 28 (1998) pp 96-102.

Max H., "Lead assisted stress corrosion cracking of alloys 600,690 and 800," Proceedings of the 6th international symposium on environmental degradation of materials in nuclear power systems-water reactors (1993) pp 179-188.

Maurice V., Yang W.P. and Marcus P., "X-Ray photoelectron spectroscopy and scanning tunneling microscopy study of passive films formed on (100) Fe-18Cr-13Ni single crystal surfaces," Journal of Electrochemical Society 145 (1998) pp 909-920.

Mcintyre N.S., Davidson R.D., Weisener C.G., Taylor K.R., Gonzalez F.C., Rasile E.M and Brennenstuhl A.M., "SIMS imaging studies of the corrosion of alloy 800 and alloy 600 surfaces under secondary side boiler conditions," Surface and interface analysis 18 (1992) pp 601-603.

Memming R., Philips Res. Repts. 19 (1964) p 323.

Morrison S.R., "Electrochemistry at semiconductor and oxidized metal electrodes," Plenum Press, New York (1980).

Montmor M.F., Ferreira M.G.S, hakiki N.E and Belo M.D., "Chemical composition and electronic structure of the oxide films formed on 316L stainless steel and nickel based alloys in high temperature aqueous environments," Corrosion science 42 (2000) pp 1635-1650.

Okamoto, G., "Passive film of 18-8 stainless steel structure and its function," Corrosion Science 13 (1973) pp 471-489.

Olssson C.O.A., Landolt D., "Passive films on stainless steels-chemistry, structure and growth", Electrochimica Acta 48 (2003) pp 1093-1104.

Olmedo A.M., Villegas M and Alvarez M.G.," Corrosion behavior of Alloy 800 in high temperature aqueous solutions: Electrochemical studies", Journal of Nuclear Materials 229 (1996) pp 102-114.

Psaila-Dombrowski M.J., "Lead assisted stress corrosion cracking of alloy 690," Proceedings of the 9th international symposium on environmental degradation of materials in nuclear power systems-water reactors (1999) pp 703-710.

Pourbaix M., "Atlas of electrochemical equilibrium," Pergamon Press Ltd., London (1966).

Radhakrishnan H., Carcea A.G., and Newman R.C., "Influence of Pb^{++} ions on the dissolution and passivation of nickel and Ni-21Cr in acidic solutions," Corrosion Science 47 (2005) pp 3234-3248.

Raja K.S and Shoji T., "Effect of pre-oxidation and corrosion potential on electronic properties of passive films on Ni-Cr-Fe alloys in pure water at 288 OC," Journal of materials science 39 (2004) pp 1033-1036.

Ries L.A.S., Belo M.D.C, Ferreira M.G.S and Muller I.L., "Chemical composition and electronic properties of passive films formed on alloy 600 in acidic solution," Corrosion Science 50 (2008) pp 676-686.

Sakai T., Aoki K., Shigemitsu T., and Kishi Y., "Effect of lead water chemistry on oxide thin film of alloy 600," Corrosion 48 (1992) pp 745-750.

Sakai T., Nakagomi N., Kikuchi T., and Aoki K, "Mechanism of lead-induced stress corrosion cracking of nickel-based alloys in high temperature water," Corrosion 54 (1998) pp 515-524.

Sato N and Cohen M.,"The kinetics of Anodic Oxidation of Iron in Neutral Solution 1. Steady Growth Region," Journal of Electrochemical Society 111 (1964) pp 512-519.

Sikora E and Macdonald D.D., "Nature of passive film on nickel," Electrochemica Acta 48 (2002) pp 69-77.

Simoes A.M.P., Ferreira M.G.S., Rondot B and Belo M.C. , "Study of passive film formed on AISI 304 stainless steel by impedance measurements and phtoelectrochemistry," Journal of Electrochemical Society 137 (1990) pp 82-87.

Stachle R.W., "Assessment of and proposal for a mechanistic interpretation of the SCC of high nickel alloys in lead containing environments," Proceedings of the 11th international conference on environmental degradation of materials in nuclear power system-water reactorsVol.1 (2003).

Stachle R.W., "Clöes and issues in the SCC of high nickel alloys associated with dissolved lead," Proceedings of the 12th international conference on environmental degradation of materials in nuclear power system-water reactors-(2005) pp 1163-1209.

Stachle R.W and Gorman J.A., "Quantitative Assessment of Sub modes of Stress Corrosion Cracking on the Secondary Side of Steam Generator tubing in Pressurized Water Reactors :Part1," Corrosion 59 (2003) pp 931-993 ; Part2 . Corrosion 60 (2004) pp 931-993; part 3 Corrosion 59 (2003) pp 931-993.

Soustelle. C., "PWSCC of alloy 600: A parametric study of surface film effects," Proceedings of the 9th international symposium on environmental degradation of materials in nuclear power systems-water reactors (1999) pp 105-113.

Takamatsu H., Miglin B.P., Sherburne P.A and Aoki K., "Proceedings of the 8th international symposium on environmental degradation of materials in nuclear power systems-water reactors (1997) pp 216-223.

Tsai W.T., Chou S.L., " Environmentally assisted cracking behavior of duplex stainless steel in concentrated sodium chloride solution" , Corrosion Science 42 (2000) pp 1741-1762.

Uhlig H.H, and Revie R.W., "Corrosion and corrosion control", John Wiley & Sons, New York (1991).

Wright M. D, "Lead-induced SCC propagation rates in alloy 600," Proceedings of the 9th international symposium on environmental degradation of materials in nuclear power systems-water reactors (1999) pp 657-665.

Yang, W.P., Costa, D., and Marcus, P., "Chemical composition, chemical states and resistance to localized corrosion of passive films on an Fe-17%Cr alloy," Journal of Electrochemical Society 141 (1995) pp 111-116.

Zhou Z.Q., "Lead effect on the corrosion and passivation behavior of alloy 600," Ph.D thesis, University of Illonois at Chicago (2005).

Ziemniak S.E. and Hanson M., "Corrosion behavior of NiCrFe Alloy 600 in high temperature, hydrogenated water", Corrosion Science 48 (2006) pp 498-521.